



JIMMA UNIVERSITY
JIMMA INSTITUTE OF TECHNOLOGY
SCHOOL OF GRADUATE STUDIES
FACULTY OF MECHANICAL ENGINEERING
SUSTAINABLE ENERGY ENGINEERING CHAIR

EFFECT OF PYROLYSIS PARAMETERS ON THE BIO-OIL PRODUCTION
YIELD FROM CASSAVA PEELS

A Thesis Submitted to School of Graduate Studies of Jimma University in Partial
Fulfillment of the Requirements for the Degree of Masters of Science in sustainable energy
engineering

By: Pacifique KOSHIKWINJA MATABISHI

Advisor: Prof. Venkata Ramayya (Ph.D.)

Co-Advisor: Mr. Million Merid (MSc Eng)

November 2021
Jimma, Ethiopia

JIMMA UNIVERSITY
JIMMA INSTITUTE OF TECHNOLOGY
SCHOOL OF GRADUATE STUDIES
FACULTY OF MECHANICAL ENGINEERING
SUSTAINABLE ENERGY ENGINEERING CHAIR

EFFECT OF PYROLYSIS PARAMETERS ON THE BIO-OIL PRODUCTION
YIELD FROM CASSAVA PEELS

A Thesis Submitted to School of Graduate Studies of Jimma University in Partial
Fulfillment of the Requirements for the Degree of Masters of Science in sustainable energy
engineering

Advisor: Prof Venkata Ramayya (Ph.D.)

Co-Advisor: Mr Million Merid (MSc Eng)

November 2021
Jimma, Ethiopia

DECLARATION

I declare that this research entitled “*effect of pyrolysis parameters on the bio-oil production yield from cassava peels*” is my original work and has not been submitted as a requirement for the award of any degree in Jimma University or elsewhere.

Name

Pacifique KSHIKWINJA MATABISHI

Signature: _____ Date _____

As research Adviser, I hereby certify that I have read and evaluated this thesis paper prepared under my guidance, by First Father, Grand Father Name entitled “*EFFECT OF PYROLYSIS PARAMETERS ON THE BIO-OIL PRODUCTION YIELD FROM CASSAVA PEELS*” and recommend and would be accepted as a fulfilling requirement

Advisors: Prof Venkata Ramayya (Ph.D.)

Signature: _____ Date _____

Co-Advisor: Mr. Million Merid (MSc Eng.)

Signature: _____ Date _____

November 2021

Jimma, Ethiopia

ABSTRACT

Cassava peels (CP) constitute an important source of energy in the tropical region, are one of the most abundant agricultural residues, and have a high biofuel production potential. This thesis work investigates the effect of pyrolysis parameters on the bio-oil production yield from CP. The two principal objectives were to perform a comparative assessment of empirical methods of fast determination of lignocellulosic composition and predict numerically the pyrolysis byproduct yield using the detailed kinetic model of biomass pyrolysis.

The results show that TGA data can be used for accurate determination of the lignocellulosic composition of biomass, the error between results from the chemical method data and TGA-PKM method ($\pm 7\%$) lies in the range of error obtained from experimental chemical methods ($\pm 10\%$). Additionally, the empirical method of lignocellulosic composition based on elemental composition does not include all biomass samples. Therefore TGA-PKM method is an interesting option to have a good estimation of lignocellulosic fractions content. The quality of the fit between the DTG curves from the experiment and from the model for CP gave an $R^2 = 0.9765$.

The kinetics parameters were obtained by isoconversional methods based on thermal devolatilization behavior for four different heating rates: 5K/min, 15K/min, 20K/min, and 30K/min. The mean value of activation energy using the KAS, FWO, and Friedman method was 224.87kJ/mol, 234.3kJ/mol, and 347.87kJ/mol respectively. Finally, the result from the investigation of pyrolysis conditions on bio-oil yield showed that the maximum bio-oil yield is obtained for the heating rate ranged between 80K/min to 100K/min. tacking into account the secondary reaction of tar, the vapor residence time affect negatively the bio-oil yield. An optimum pyrolysis temperature for maximum bio-oil yield is around 475°C. CP pyrolysis is not significantly affected by the particle size when the latter is less than 0.5mm since the temperature gradient between the surface and the center of the particle is less than 1°C.

Keywords: *Bio-oil, Pyrolysis kinetics, TGA-PKM, Cassava peels, Biomass pyrolysis*

“Theory is when you know everything but nothing works. Practice is when everything works but no one knows why.” (Anonymous)

*“There are two possible outcomes : if the result confirms the hypothesis, then you’ve made a measurement, if the result is contrary to the hypothesis, then you’ve made a discovery”
(Enrico Fermi)*

DEDICATION

To my beloved family for their patience and unconditional support
during my academic journey.

ACKNOWLEDGEMENT

May he who has the primacy in everything and in whom everything subsists and finds meaning, He who governs the universe according to his will and gives us and life, works in us to will and to act in order to fulfill his good purpose, receive the expression of my deepest gratitude.

Next, my heartfelt thanks to Professor Venkata Ramayya who accepted to be the advisor of this thesis work, and for his continued support throughout this tedious work. The constant support and trust he has shown in me have been very motivating and helpful to me in the successful completion of this work. Also, huge thanks to my co-advisor Mr. Million Merid for his input, direction, and knowledge while working on this thesis. You two have shared so much knowledge with me during the elaboration of the present work.

My sincere acknowledgment to MOUNAF project for having financed this master's program. My thanks also go to all the Lecturers and staff of JiT in general and particularly those of the faculty of Mechanical Engineering, especially the Sustainable Energy Engineering chair for the scientific and human training they gave me. May they feel proud of having contributed to the training the man I have become. Moreover, that all who have participated in one way or another in the accomplishment of this work feel flattered by its pages. I am thinking particularly of Jimma Agricultural Research center for providing the cassava sample, Miss Ebise Getacho for chemical characterization of the sample, and Bahir Dar institute of technology for logistic assistance while conduction thermogravimetric analysis.

My heart is overflowing with gratitude for my family, friends, colleagues, and friends, for their constant support and encouragement. May all those who made my stay in Ethiopia pleasant: International students from Jimma University and Addis Ababa University, Missionaries of Charity sisters, and my Ethiopian friends feel gratified by the completion of my training in Sustainable Energy Engineering.

Finally, I thank the members of the jury for reading and evaluating this work.

Pacifique KOSHIKWINJA MATABISHI

TABLE OF CONTENT

DECLARATION.....	i
ABSTRACT	ii
DEDICATION	iv
ACKNOWLEDGEMENT.....	v
TABLE OF CONTENT	vi
LIST OF FIGURES.....	ix
ACRONYMS AND ABBREVIATIONS	x
CHAPTER 1. INTRODUCTION.....	1
1.1. Background	1
1.2. Problem statement	2
1.3. Aims and Objectives	3
1.4. Scope of the study	3
1.5. Significance of the Study	3
1.7. Methodology	4
1.8. Organization of the work.....	5
CHAPTER 2. LITERATURE REVIEW.....	6
2.1. Introduction	6
2.2. Biomass composition and characterization	7
2.2.1 Proximate Composition (Ash, Fixed Carbon, and Volatiles).....	8
2.2.2 Elemental Chemical Composition.....	8
2.2.3 Chemical Composition	9
2.3. Biomass valorization and conversion.....	11
2.3.1 Biomass conversion pathways.....	11
2.3.2 Thermochemical conversion of biomass	13
2.4. Biomass pyrolysis.....	19
2.4.1 Conceptual pyrolysis process design.....	19
2.4.2. Kinetic models of biomass pyrolysis.....	21
2.4.3 Influence of minerals on biomass pyrolysis mechanisms	23
2.5. Critical Literature review	24
2.5.1. Research gaps on cassava waste pyrolysis	28
CHAPTER 3. RESEARCH METHODOLOGY	29
3.1. Materials.....	29
3.2. Material characterization.....	29
3.2.2. Thermogravimetric analysis (TGA)	30
3.3. Lignocelulosique composition.....	30

3.3.1. Analytical/chemical method	30
3.3.2. Empirical method based on elemental composition	32
3.3.3. Based on TGA-PKM method [25]	34
3.4. Kinetics of CP pyrolysis	37
3.5. Detailed multistep kinetic scheme of biomass pyrolysis	40
3.6. Heat transfer model	43
3.7. Solution Strategy	44
3.7.1. Chemical reactions	44
CHAPTER 4. RESULT AND DISCUSSION.....	46
4.1 Proximate and elemental composition.....	46
4.2 Thermal degradation process.....	47
4.3 Lignocellulosic composition	48
4.3.1. Analytical/chemical Method	48
4.3.2 Prediction based on elemental composition	49
4.2.3 TGA-PKM method.....	51
4.4 Isoconversional kinetic model of CP.....	56
4.5 Thermodynamics of CP.....	58
4.6 Effect of pyrolysis parameters on released products	61
4.6.1 Effect of the heating rate	63
4.6.2 Effect of vapor residence time and pyrolysis temperature.	65
CHAPTER 5. GENERAL CONCLUSION AND RECOMMENDATIONS	69
REFERENCES.....	72
APPENDIX	77
Appendix A: TGA data (after smoothing and reduction).....	77
Appendix B: Detailed pyrolysis kinetics data	78
B.1. Species properties	78
B.2. Kinetics Matrix	79
Appendix C: Matlab Codes	81
C.1. TGA data smoothing and reduction.....	81
C.2.TGA-PKM method code.....	84
C.3. Kinetic parameters by Isoconversional method.....	87
C.4. Heat Transfer in the particle	91
C.5. Byproduct yield prediction	92
Appendix D : Thermochemical properties of Cassava Rhizome and Cassava Stalk (source Pattiya et al. 2011 [21]).....	94

LIST OF TABLES

Table 1.1. Research methodology matrix.....	4
Table 2.1. An overview of kinetic data for different pyrolysis models.....	22
Table 2.2. Literature review on cassava waste pyrolysis	26
Table 3.1. Multistep Kinetic Scheme of Biomass Pyrolysis.....	40
Table 4.1. Main characteristic of cassava peels sample.....	46
Table 4.2. Lignocellulosic composition of Cassava peels, experimental result on DAF basis.....	49
Table 4.3. Mass composition for the seven reference species of Cassava Peels.....	51
Table 4.4. Minimum number of components for each biomass fraction.....	52
Table 4.6. Initial kinetic parameters of the pseudocomponents (PC).....	53
Table 4.7. Lower bounds of the pseudocomponents (PC).....	53
Table 4.8. Upper bounds of the pseudocomponents (PC).....	53
Table 4.9. Kinetic parameters of the pseudocomponents.....	53
Table 4.10. Kinetic parameters from other studies.....	54
Table 4.11. Comparison between the experiment and thermogravimetric analysis pseudocomponent kinetic model (TGA-PKM) results.....	56
Table 4.12. Kinetics parameters of cassava peels at different degree of conversion.....	57
Table 4.13. Comparison between code developed in this study and CRECK software results.....	63
Table 4.14. Effect of heating rate on the CP pyrolysis released product.....	64

LIST OF FIGURES

Figure 2.1: Photosynthesis phenomenon.....	7
Figure 2.2. Typical biochemical compositions of four biomass samples.....	8
Figure 2.3. General structure of lignocellulosic biomass.....	9
Figure 2.4. Reference species for biomass characterization.....	11
Figure 2.5. The different transformation pathways of lignocellulosic biomass.....	13
Figure 2.6. Biomass combustion route.....	14
Figure 2.7. Example of reactors used in biomass gasification.....	15
Figure 2.8. Stages of pyrolysis process.....	17
Figure 2.9. Schematic of torrefaction machine.....	18
Figure 2.10. Representative schematic of continuous SCWG reactor.....	19
Figure 2.11. The superstructure of fast pyrolysis technologies.....	20
Figure 2.12. Multistep kinetic mechanism of cellulose and hemicellulose pyrolysis.....	23
Figure 2.13. Multistep kinetic mechanism of pyrolysis of the three reference lignins.....	23
Figure 3.1. a) cassava from the field; b) sun-drying of cassava peels; c) dried cassava peels before grinding; d) ground cassava peels.....	29
Figure 3.2. Extended biomass characterization. H% vs C% plot of biomass samples along with their reference species.....	34
Figure 3.3. Decision tree of the calculation procedure.....	37
Figure 3.4. Steps involved in finding activation energy through isoconversional method.....	40
Figure 4.1. TG and DTG curves of CP pyrolysis. a) X curves; b) DTG curves; c) α curves; d) Temperature vs time curves.....	48
Figure 4.2. Biomass characterization. Reference species and Cassava Peel sample in the H% vs C% plot.....	50
Figure 4.3. TGA and DTG curves of biomass components.....	52
Figure 4.4. Model fitted to the experimental DTG curve.....	54
Figure 4.5. Model-free kinetics. a) KAS model. b) FWO model. c) Friedman model.....	58
Figure 4.6. Thermodynamic parameters of CP at different conversion and heating rates. a) Activation energy. b) Enthalpy. c) \log_{10} (Arrhenius exponential factor). d) Entropy. For b), c), and d), we present only result from Friedman method.....	61
Figure 4.7. Temperature gradient between the surface and the center of the particle (HR=100K/min).....	62
Figure 4.8. Temperature profile as function of reaction time, position at 100K/min.....	62
Figure 4.9. Effect of vapor residence time on bio-oil yield at 800K, $\beta=100\text{K}/\text{min}$	66
Figure 4.10. Effect of pyrolysis temperature on a) bio-oil yield; b) gas yield.....	67
Figure 4.11. Comparison with experimental data, RT=0.93s.....	68

ACRONYMS AND ABBREVIATIONS

1G:	First Generation
2G:	Second Generation
3G:	Third Generation
AF:	Ash Free
ASTM:	American Society of Testing and Materials
CELL:	Cellulose
CP:	cassava peels
CPFD:	Computational Particle Fluid Dynamic
CR:	Cassava Rhizome
CS:	Cassava Stalk
DAEM:	distributed activation energy model
DAF:	Dry Ash Free
DTG:	Derivative TG
FWO:	Flynn-Wall-Ozawa
GC-MS:	Gas Chromatography- Mass Spectrometry
GDP:	Gross Domestic Product
GHG:	Green House Gases
GPC:	Gel Permeation Chromatography
HCELL:	Hemicellulose
HR:	Heating Rate
KSA:	Kissenger-Akahira Sunose
LIG:	Lignin
LIG-C:	Carbon-rich lignin
LIG-H:	Hydrogen-rich Lignin
LIG-O:	Oxygen-rich Lignin
MPPIC:	Multi-Phase Particle In Cell
MS:	Mass Spectroscopy
RM:	Reference Mixture
RT	Residence Time
SCWG:	Supercritical water gasification
TANN:	Condensed tannins
TAPPI:	technical Association of the Pulp and Paper Industry
TCD:	Thermal Conductivity Detector
TG:	Thermogravimetry
TG-MS	Thermogravimetry Mass Spectrometry
TGA:	Thermogravimetric Analysis
TGA-PKM:	Thermogravimetric Analysis and Pseudocomponent Kinetic Model
TGL:	Triglycerides
UN:	United Nations
UV:	Ultraviolet Radiation
XRD:	X-ray Diffraction

CHAPTER 1. INTRODUCTION

1.1. Background

The world economy continues to grow at a rate of 3.25% and has been estimated to grow at a faster rate in Asia and Africa. Significant energy sources are also required to meet the desired economic development. The total energy demand is expected to increase worldwide by 28% by 2040[1]. Shortage of fossil fuels and global warming issues required an alternative way of meeting energy demand without affecting negatively the environment.

Renewable energy development is the best solution for a sustainable and green world, but due to the fluctuating behaviors of most renewable energy, storage still constitutes a big challenge. However, biofuel produced from biomass and waste is one of the very promising ways for the energy transition toward the decarbonized economy. It presents considerable socio-economic benefits and it is environmentally friendly [2]. From the literature, it is proven that thermochemical conversion of biomass constitutes an efficient way of producing liquid biofuel from biomass; indeed, liquid biofuel is preferable in the transportation sector due to its high energy density and ease of handling [3]. Pyrolysis is an efficient technology for bio-oil production among thermochemical conversion technics [4].

Number of researches have been conducted to improve the yield and quality of bio-oil production from biomass pyrolysis while producing biochar as well. Biochar is one of the byproducts of pyrolysis which has much application in agricultural soil amendment and fertilization[5]. Apart from the agricultural benefit of biochar, Slezak et al demonstrated that the addition of charcoal to coal improves the gasification efficiency [6]. The main objective of biomass pyrolysis is to produce liquid biofuel [7]. Many previous researches were focused on the parametric sensitivity of pyrolysis on bio-oil yield and properties[8]. Different biomass feedstocks have different kinetics parameters, different optimum pyrolysis process parameters for a maximum bio-oil yield[9]–[12].

Cassava residues constitute one of the most abundant agricultural waste in the tropical region and their biofuel production from pyrolysis has been proved by many researchers [13]. The valorization of cassava residue for biofuel production is one of the best ways of cassava waste management and reduce environmental footprint, indeed untreated cassava residue can pollute the agricultural soil due to its high cyanide content, this is even the reason why is not mostly used as livestock application [14].

1.2. Problem statement

The UN 2030 agenda for sustainable development has set energy access as a fundamental goal to achieve a full energy transition, one that is sustainable, equitable, and universal [15]. With renewable electricity, fossil fuels can be replaced in many applications but not in all of them such as in certain industrial and transport applications. Moreover, the shortage of fossil fuel coupled with the global warming issue pushed humanity to search for alternative fuels to sustain the energy demand which is still increasing. Waste and Biomass constitute a promising alternative solution for an energy transition towards a decarbonized economy since they are carbon neutral.

Biomass is very abundant on earth but due to its low energy density, the harvestmen and transportation of a big amount of biomass constitute its main drawback. Thermochemical conversion is one of the ways of converting biomass into a more valuable biofuel that can be easily handled, stored, transported, and used in different applications: power generation, industrial plants, and transportation sector (road vehicles, maritime shipping ...). In tropical regions, cassava residues constitute one of the abundant agricultural waste, and contrary to many agricultural wastes, cassava waste due to its high cyanide content is not mostly used for soil enrichment or livestock feed.

Many researches have been conducted on thermochemical conversion of biomass for biofuel production, but the technology is yet not mature enough and still has many gaps to fill. When it comes to pyrolysis, studies are still needed on emerging pyrolysis technologies and process design, understanding and modeling of catalytic pyrolysis process, fast techniques of pyrolysis byproduct characterization as well as the impact of reactor modeling on the multi-scale process design, etc. [3], [16]–[19]. Moreover, the properties and the yield of bio-oil from pyrolysis need to be improved to meet the standard of commercial fuels. The biofuel production from cassava residues pyrolysis has been investigated Pattiya et al. [20], [21], Zhang et al.[22] and Ong Lu et al. [10], and from their result, it has proven that cassava residue has a high potential of bio-oil production through pyrolysis.

The contribution through this research was the evaluation through experiment and theoretical analysis of the best kinetics parameters of cassava peel pyrolysis, and determination by numerical investigation, the optimum parameters of pyrolysis possess for maximum bio-oil production. Additional information on cassava peels was also provided such as elemental and lignocellulosic composition. These data are still missing in the literature.

1.3. Aims and Objectives

The main objective of this thesis work is to investigate the effect of pyrolysis parameters on the bio-oil yield, and thus, determine the optimum operating conditions for maximum bio-oil production. A multidisciplinary approach was used to achieve this objective; the following specific objectives were addressed:

- Physical characterization of cassava peels
- Thermochemical characterization of cassava peels
- Determination of the kinetics parameters for cassava peel pyrolysis
- Numerical determination of optimum pyrolysis parameters for maximum bio-oil yield.

1.4. Scope of the study

The scope of this study consists of the characterization of cassava peels by conducting the following laboratory experiments: Proximate, Ultimate and Thermogravimetric analysis (TGA). Data collected from the experiment will help us to determine the simple kinetics parameters of the pyrolysis process. Furthermore, since the byproduct composition from pyrolysis depends on the lignocellulose composition of biomass, first, the composition was determined analytically by chemical method, then a comparison assessment was conducted using the elemental composition of our feedstock and TGA data to predict the composition. The detailed pyrolysis kinetics parameters were used to investigate numerically the effect of pyrolysis operating parameters on the pyrolysis product yield. An original Matlab code was developed for this purpose.

Characterization of the byproducts (bio-oil, gas, and char) is beyond the scope of this study.

1.5. Significance of the Study

The industrialization and commercialization of biomass pyrolysis technologies required detailed and reliable data on the pyrolysis process for both the biomass feedstock and the reactor behavior. This work will try to determine the parameters of the one-step kinetics model which fits well with experimental data of cassava peels pyrolysis, then optimum pyrolysis parameters were numerically investigated for maximum bio-oil production. The expected parameters to be investigated are operating temperature, heating rate, and vapor residence time.

Therefore, this work will contribute to providing **new information and data** regarding the characteristics, composition, and pyrolysis kinetics parameters of cassava peels. The result from

the effect of pyrolysis operating parameters on the byproduct yield will also be useful for further research and development such as reactor design etc.

1.7. Methodology

The general methodology of this thesis work is based on a numerical investigation of the effect of pyrolysis parameters on the byproduct yield and composition from cassava peels. A detailed multistep kinetics model and parameters proposed by Ranzi et al. [23], [24] were used. The characterization of cassava peels was done both analytically using chemical method and numerically based on experimental data from Thermogravimetric analysis and Ultimate analysis. This will allow us to determine the distribution of cellulose, hemicellulose, lignin, and extractives in cassava peels. An innovative method called Thermogravimetric Analysis and Pseudocomponent Kinetic Model (TGA-PKM Method) [25], was used for the determination of Hemicellulose, Cellulose, Lignin and Extractives content in this feedstock. The synthesis of the methodology used in this thesis work is presented in Table 1.1.

Table 1.1. Research methodology matrix

	Description	Inputs	Tools and Techniques	Outputs
1	Literature Review	<ul style="list-style-type: none"> - Topic - Research question - Keywords 	<ul style="list-style-type: none"> - Google Scholar - Scopus - Web of Science 	<ul style="list-style-type: none"> - Relevant papers, articles, books, and documents - State of the knowledge - State of the art - Gaps
2	Sample collection and preparation	Feedstock specification: Cassava peels	<ul style="list-style-type: none"> - Harvesting Cassava tubes - Peeling cassava tubes - Sun-drying cassava peels - Oven drying - Grinding - Sieving 	Homogeneous sample with particle size equal to or less than 0.5mm
3	Characterization	<ul style="list-style-type: none"> - Homogeneous sample with particle size equal to or less than 0.5mm - Chemicals 	<ul style="list-style-type: none"> - Oven - Furnace - TGA - Ultimate analysis - Chemical reactors and apparatus 	<ul style="list-style-type: none"> - Moisture content - Volatile matter - Fixed carbon - TGA data - Elemental composition - Lignocellulose Composition
4	Kinetics and thermodynamic study	<ul style="list-style-type: none"> - TGA data - Elemental composition 	<ul style="list-style-type: none"> - Friedman, FWO, and KSA methods - TGA-PKM method - MATLAB 	<ul style="list-style-type: none"> - Kinetic parameters - Predicted Lignocellulose Composition - Thermodynamic parameters

5	Modeling and simulation	<ul style="list-style-type: none"> - Detailed kinetics models and parameters - Pyrolysis process parameters 	<ul style="list-style-type: none"> - MATLAB - Excel 	<ul style="list-style-type: none"> - Pyrolysis byproduct yield and composition and the effect of pyrolysis parameters.
---	-------------------------	---	---	---

1.8. Organization of the work

The present thesis is subdivided into five main chapters as described below.

The first chapter concerns the general introduction of the thesis work by providing the background of the topic under study, defining the problems statement, presenting aims and objectives, the scope and significance of the study, and finally briefs the methodology used to achieve the thesis objectives.

The second chapter presents the review of the literature related to biomass conversion in general and more specifically biomass pyrolysis. The chapter presents the general composition of biomass and characterization methods and techniques; it provides an explanation about biomass valorization and conversion technologies such as biochemical and thermochemical conversion. Finally, the chapter also describes the pyrolysis process design, discusses the existing pyrolysis kinetic models and the influence of the mineral contained in the ash on the pyrolysis process.

The third chapter describes the research methodology, material, and techniques, defines material collection and preparation, experimental procedures, and techniques and algorithms used for cassava peel characterization. The chapter discusses also in a detailed manner the simple and detailed kinetics models, and modeling and numerical procedure for pyrolysis byproduct prediction.

The fourth chapter presents the findings of this study and discusses the results. Firstly, the cassava peels characterization results are presented. Secondly, after presenting the result of the kinetics parameters determination, findings on the investigation of pyrolysis parameters on the bio-oil yield and composition are discussed.

Finally, the fifth chapter presents the general conclusion, and recommendations while suggesting potential future works.

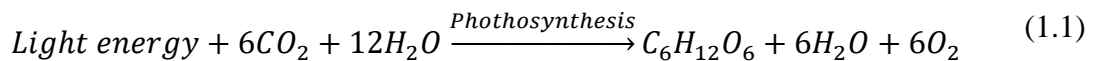
CHAPTER 2. LITERATURE REVIEW

2.1. Introduction

Energy sources may be categorized as being renewable or nonrenewable. Nonrenewable resources are considered those whose regeneration rate is much smaller than their consumption rate, it is the case of fossil fuels such as coal, oil, or natural gas. These resources are still the main sources of energy despite their negative effect on the environment and their unsustainability. Renewable natural resources are those who keep steadily in nature since their regeneration rate is greater than their consumption is used sustainably [26]. The plants and animals, water, and arable land, among others, are renewable resources. Other features, like air, sunlight, or wind, are available on an ongoing basis regardless of consumption. Today, renewable alternatives as sources of energy are needed for the development of a decarbonized and sustainable economy and society. It will therefore be necessary to ensure the achievement of alternative energy that reduces the environmental impact on the biosphere. In this respect, biomass can be very useful because, in its processing, the carbon footprint is neutral.

Energy sources can be primary when coming from nature (sun, wind, rivers, tides, etc.) or secondary when suffering some conversion process (alcohol, charcoal, oil products, etc.). The energy conversion takes place to have a final energy form that meets a specific demand as heat or light, which is defined as useful energy. Energy conversions express the ways in which energy is presented in nature.

Biomass is a primary and renewable source of chemical energy able to be converted into other energy forms, both directly on the wood-burning for heat generation, and indirectly via thermochemical or biochemical conversion. Biomass is the product of the conversion of light energy into chemical energy through photosynthesis reaction [27]:



Photosynthesis is the fundamental process for energy conversion. This reaction provides a power supply to a whole range of organisms. However, it is a process of low efficiency seen that the total solar energy absorbed by the leaves only 20% is converted into chemical energy, which determines a theoretical efficiency of 4% for photosynthesis [27]. The energy recovery of this reaction can be accomplished in four different ways according to the final chemical product.

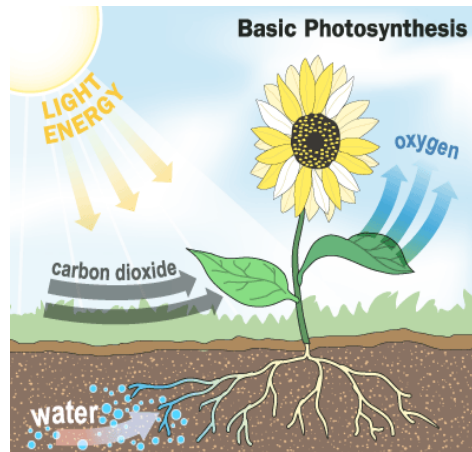


Figure 2.1: Photosynthesis phenomenon

Biomass feedstocks are subdivided into three main generations: first-generation (1G) food crops, second-generation (2G) lignocellulosic biomass (nonfood biomass), and third-generation (3G) algae and various wastes (agricultural wastes, food waste, etc.).

2.2. Biomass composition and characterization

Biomass composition varies depending on different factors such as geographical location, climate condition, type of soil, and part of the plant (roots, stems, branches, leaves). Compared to coal, biomass density and heating value are low. Therefore, the higher heating value of bio-oils typically ranges between 15 and 20 MJ/kg, which is only 40–50% of conventional petroleum fuels (42–45 MJ/kg). This is due to high oxygen content, which is usually in the range of 35–40 on a dry basis weight. Cellulose (30–55 wt %), hemicellulose (13–35 wt %), and lignin (14–36 wt %) are the major components of woody biomass, whereas extractives are usually lower than 15–20% [28].

The composition of the biomass can be determined by proximate analysis (moisture, volatiles, ash content, fixed carbon content), elemental chemical analysis (carbon, hydrogen, nitrogen, and oxygen), and chemical analysis in terms of lignin, cellulose, hemicellulose, and sometimes extractives and proteins. Figure 2.2 shows the relative concentration of several carbohydrates, lignin, extractives, and ash in different biomass samples.

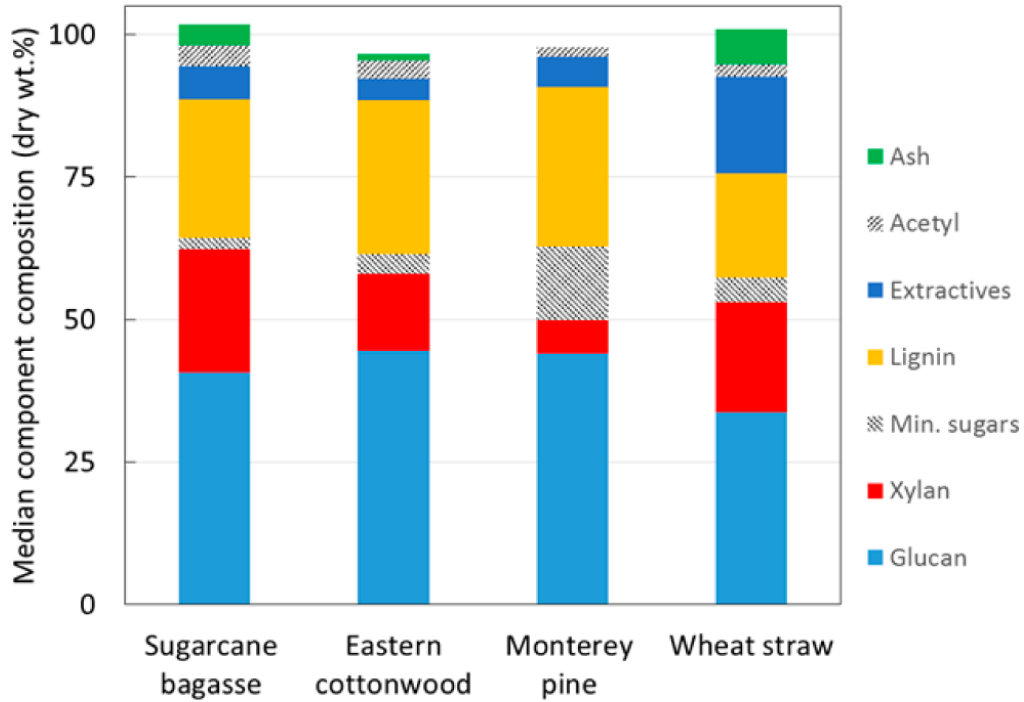


Figure 2.2. Typical biochemical compositions of four biomass samples [23]

2.2.1 Proximate Composition (Ash, Fixed Carbon, and Volatiles)

The proximate analysis of a given fuel provides the percentage of the material that burns in a gaseous state (volatile matter), in the solid-state (fixed carbon), and the percentage of inorganic waste material (ash) and water content (moisture), and is therefore of fundamental importance for biomass energy use [29]. The charcoal yield is mostly proportional to the percentage of fixed carbon while the volatile content and ash relate negatively with charcoal yield. Thus, it is expected biomass with high volatile matter content lead to greater gas production instead of the solid phase. Volatile matters in biomass typically span between 60 and 80%, with a fixed carbon in the range of 10–20% [30].

2.2.2 Elemental Chemical Composition

Biomass elemental composition varies with the species. For woody biomass, it can be assumed that it contains about 50% carbon, 6% hydrogen, 44% oxygen, and between 0.1% and 0.5% nitrogen [29]. However, for agricultural residues, such composition may vary, mainly due to the influence of the ash, since biomass with higher hemicellulose and ash content, as is the case with grasses, have a higher oxygen-carbon ratio than wood [31]. The chemical composition is the basis for the analysis of combustion processes and is useful for the calculation of the volumes of air, gases, and enthalpy, and the determination of the calorific power of the fuel.

2.2.3 Chemical Composition

Lignocellulosic biomasses are renewable and complex products, they are mainly constituted by a combination of polysaccharides, which can be generally grouped into holocellulose (cellulose and hemicellulose) and lignin species. Moisture, together with other components such as acetyl groups, extractives, and minerals are also present. Cellulose microfibril represents the important element surrounded by hemicellulose and pectin, which act as ligand and embed lignin materials (see Figure 2.3).

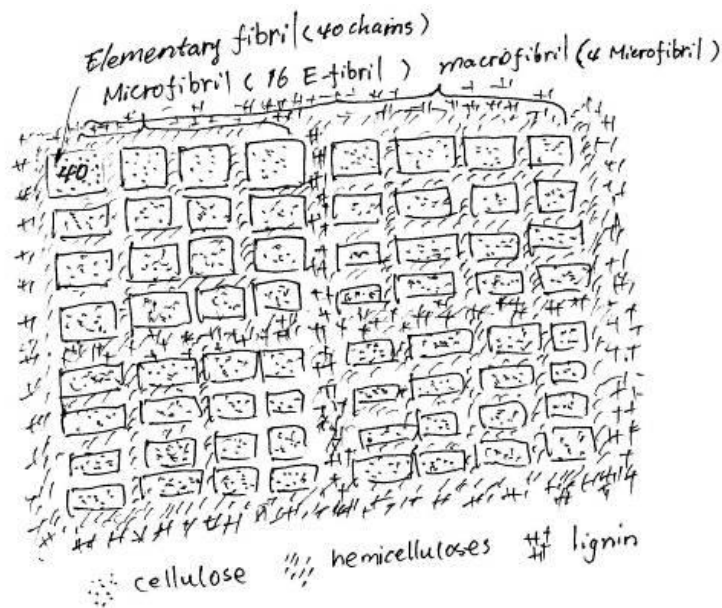


Figure 2.3. General structure of lignocellulosic biomass

Cellulose: cellulose, the most abundant structural polysaccharide in cell walls, comprises 15–50% of the dry weight of plant biomass. It can be summarized as $(C_6H_{10}O_5)_n$, so that mass elemental composition is C = 44.4%, H = 6.2%, and O = 49.4%. The presence of several strong hydrogen bonds explains the recalcitrance of cellulose toward hydrolysis and enzyme activity. Cellulose crystallization is directly related to the formation of these intermolecular hydrogen bonds. Hemicelluloses and pectins are closely associated with the surface of cellulose fibrils with noncovalent linkages forming a microfibril network. Cell walls are further reinforced by lignin, a three-dimensional polymer of phenylpropanoid units, which is covalently linked to hemicellulose.

Hemicellulose: Hemicellulose is a second structural polymer; it is a mixture of sugars (hexoses and pentoses), mainly xylose, mannose, galactose, and arabinose. Different from cellulose, it has a shorter chain and a much more amorphous structure, because of its irregular composition and the branches present on the chain. It is present in biomasses in amounts ranging from 10%

to 40% (dry), rarely in quantities greater than cellulose. It is also common to refer to the combination of cellulose and hemicellulose as “holocellulose”.

Lignin: Lignin is a racemic polymer composed of monomeric units of aromatic alcohols (coniferyl, sinapyl, and p-coumaryl alcohol), whose composition changes widely inside the entire range of biomasses, making its characterization a hard task to accomplish. It is present in biomasses in amounts ranging from 15% to 45%.

Extractives: usually, cellulose, hemicellulose, and lignin account for more than 90% of the entire biomass; thus, extractives are usually <10%. Thousands of different extractives can be identified and they present a great variety of composition, structure, and biological functions, also depending on the different seasons. They are also distributed in different ways among the organs of the plant, being more abundant in leaves and barks. Because of the large variety of extractive species, water solubility is used to classify the main extractive components. Hydrophilic extractives are the soluble molecules in high-polarity solvents, such as ethanol and water, while hydrophobic extractives are only soluble in low-polarity solvents, such as hexane and ether.

- **Hydrophobic extractives:** Softwood plants contain hydrophobic extractives or resins that can reach up to 15% of the total sample mass. Oleo-resins, which are composed of terpenes and fatty acids (free or esterified), are the most abundant. Hardwood samples, with extractives (usually <2%), mostly contain wood resin and are mainly constituted by fatty acids. Triglycerides, with a high presence of linoleic acid, are the most common hydrophobic extractives; these are found in many different plant sources. On this basis, a new reference component (TGL: $C_{57}H_{100}O_7$), with a very high C and H content, represents hydrophobic extractives.
- **Hydrophilic extractives:** they are typically phenolic compounds with antioxidant properties, thereby serving a protective role in plants, and they are mainly present in the external organs (bark and leaves). They can be sorted into flavonoids and nonflavonoids, the second group being the most abundant and including phenolic acids and tannins. In particular, during the plant aging process, the condensed tannins are the result of flavonoids polymerization. In order to describe these phenolic species, a new lumped reference component (TANN, $C_{15}H_{12}O_7$), with a low H content is used, It is well-represented by a polymer of gallicocatechin.

Figures 2.4 shows the structures of the seven reference species considered here to describe the pyrolysis behavior of the different biomasses.

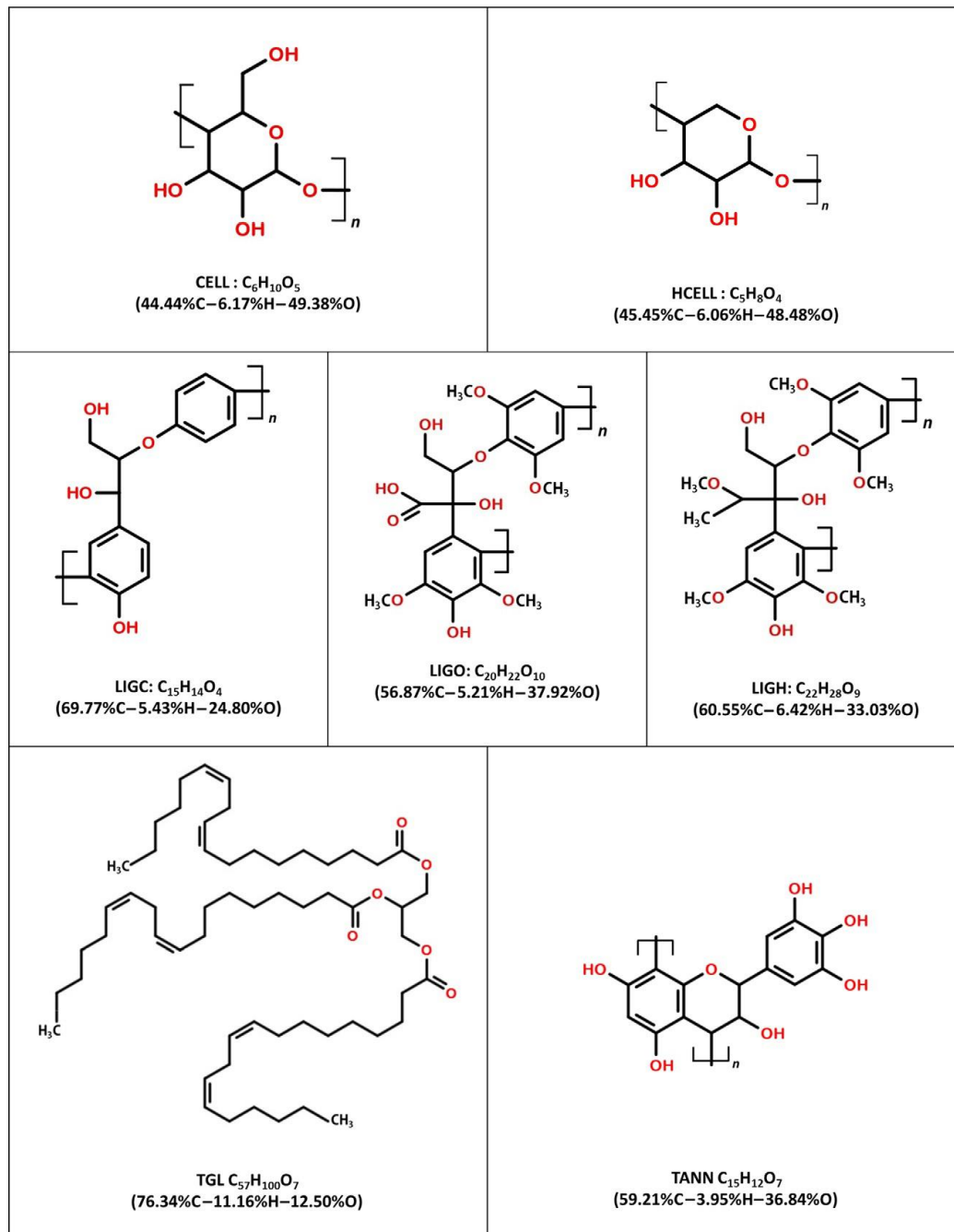


Figure 2.4. Reference species for biomass characterization [28].

2.3. Biomass valorization and conversion

2.3.1 Biomass conversion pathways

Biomass from agricultural residues, forest residues, industrial waste, and municipal solid waste are currently used as the main raw materials for the production of electricity, biofuels, and heat.

Biomass is seen as one of the key options for slowing GHG emissions and replacing fossil fuels [26]. Biomass is also an atypical source due to its diversity and interrelations with many technological and political areas. From the point of view of the slowdown in climate change, the use of biomass in a given sector depends on the competitiveness and availability of biomass potential compared to other renewable options. From the society's point of view, the biomass market creates a number of economic advantages, such as:

- Security of energy supply;
- Regional growth;
- Balance of the regional trade balance;
- Export potential;
- Increased competitiveness;
- Employment;
- Creation of income and wealth;
- Induced investment.
- Economic growth through business expansion (profit) and employment;
- Import substitution (direct and indirect effects on GDP);
- Security and diversification of energy supply.

Lignocellulosic biomass remains a stock of carbonaceous material that can be valorized by biochemical or by thermochemical methods (Figure 2.5) into energy (heat, electricity), fuels (eg: bio-oils, biogas), or chemical molecules with high added value.

Biochemical conversion requires a pre-treatment in order to make the material "digestible" by microorganisms or attackable by chemical or enzymatic agents in order to transform the lignocellulosic material into liquid fuel (ex: ethanol) or gaseous (ex: hydrogen). This conversion can also provide so-called bio-sourced chemical products which can be used in various fields (composites, plastics, etc.). In the case of thermochemical conversion, biomass can be converted into electricity, heat, fuels, or chemical compounds by four main processes: pyrolysis, gasification, liquefaction, and combustion.

It is important to optimize the purity and the nature of the products formed (charcoals, bio-oils, and gases). These advances will make it possible to obtain better energy efficiency for the production of energy (electricity, heat) and production of bioproducts (materials, food additives, etc.) that are more competitive and less harmful to the environment.

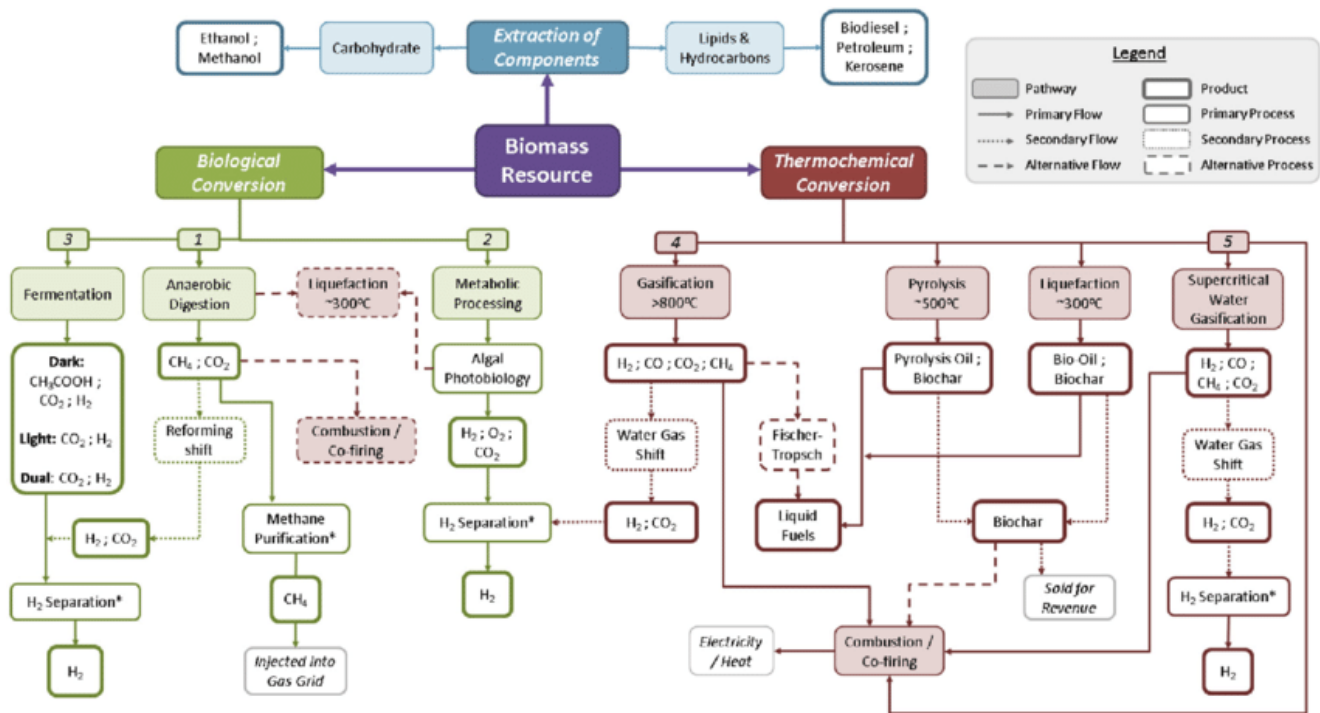


Figure 2.5. The different transformation pathways of lignocellulosic biomass

2.3.2 Thermochemical conversion of biomass

There are various thermochemical conversion processes that can use biomass as a feedstock to produce valuable products[32]. These methods are proven to have many environmental advantages, including waste minimization, pollution reduction, and energy recovery [33].

2.3.2.1 Combustion

Combustion is the simplest process for transforming biomass into heat, and/or electricity. This process consists of heating the biomass in an oxidizing atmosphere (O_2) in order to produce heat. The products mainly formed are gases (CO_2 , CO) and coal. Combustion is currently the most widely used commercially, thanks in particular to its low investment cost. It corresponds to 97% of bioenergy production in the world.

The use of the heat produced during the reaction can be utilized, as in the case of a steam boiler, where heat can be recovered by condensation of water. Complete combustion requires high temperatures between 800 and 1000°C. In addition to the large heat input needed, the biomass used for this process should be dry, since this process does not accept more than 50% moisture content in the biomass. Therefore, before it can be used it will have to undergo a pre-drying process. Furthermore, the biomass must be addressed to achieve an appropriate particle size, making the overall costs of the process are incremented by the initial treatment of the biomass to suit the reaction conditions [34].

The properties of the biomass that most affect the combustion can be divided into physical, chemical, or thermal factors. Within physical factors include the density, porosity, and specific surface of the particles, while chemical factors affect the calorific value and the value of elemental analysis. Moreover, the thermal characteristics that affect the combustion are the specific heat, conductivity, and moisture [34].

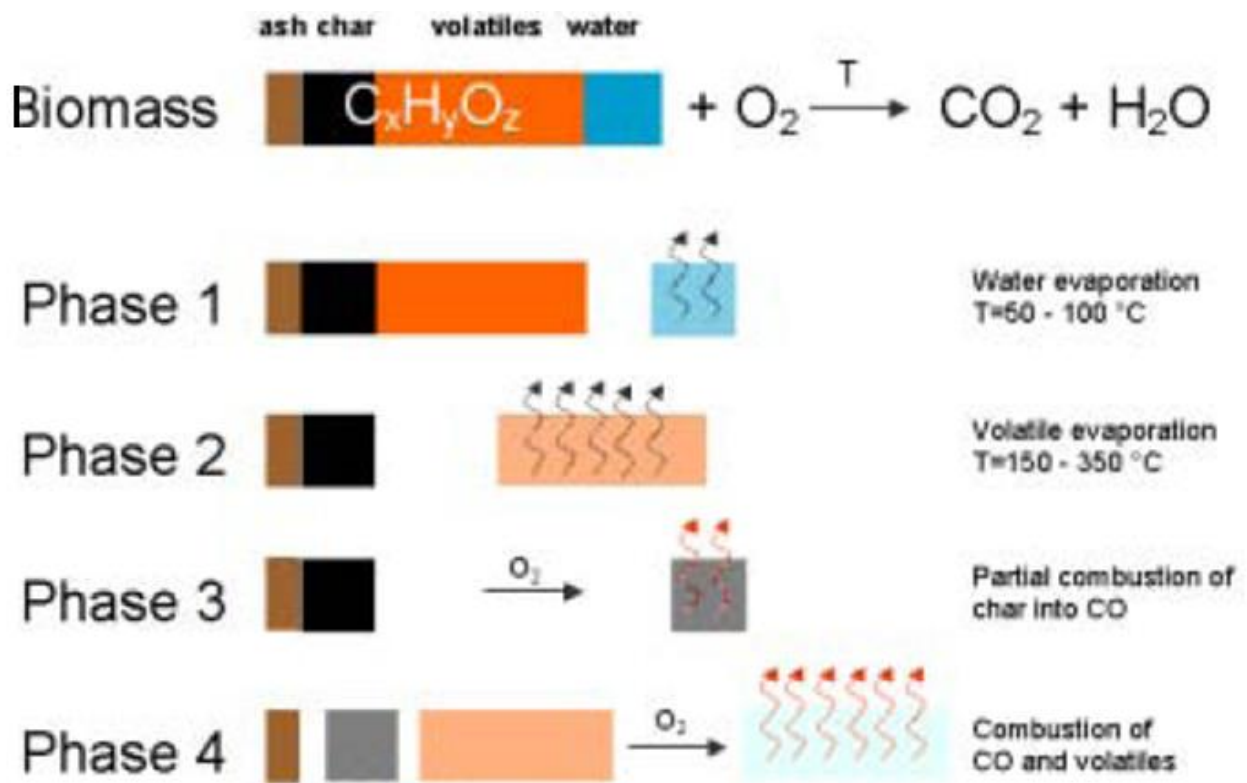


Figure 2.6. Biomass combustion route

2.3.2.2 Gasification

Gasification is a partial oxidation process at temperatures between 800 and 1200°C, depending on the type of gasifier and the application for which the gas produced is intended. It can take place in the presence of air, oxygen, or water vapor following different technologies: fixed beds, fluidized beds, and open beds. The difference between gasification and combustion is that a large part of the energy produced during gasification, is not used directly as heat but rather, is captured in the form of chemical energy in the form of gaseous fuel, the “syngas” (H₂ + CO). This gas can be used in combustion to produce electricity and heat, but also in the production of liquid fuels (such as Fischer Tropsch synthesis), CH₄ (by methanization), or hydrogen. The gasification process also produces condensable vapors (tars, mainly composed of aromatics, water, and other gases (CH₄, CO₂, C₂H₄, etc.). The quality of the "syngas" product depends on the technology used as well as the characteristics of the gasified biomass (water content,

minerals, chemical composition, etc.). Many gasification processes have been developed over the last decades; current research is focused in particular on the means of purification and treatment of tars with the aim of optimizing the production of fuels (alcohols, gas oils) and the combustion of gases in thermal engines.

The gasification process requires the execution of an initial pretreatment of the biomass to be used. The process of gasification is the conditioning of wet biomass, which must have a water percentage of less than 30%. Upper amounts of water considerably reduce the calorific value and retard inflammation, thus that reducing the temperature in the reactor, resulting in incomplete cracking of the hydrocarbons, forming a greater quantity of coke [35]. The resulting reaction yields of the gasification process are 85% gaseous and volatile products and the rest are composed of coke and non-volatile products [26].

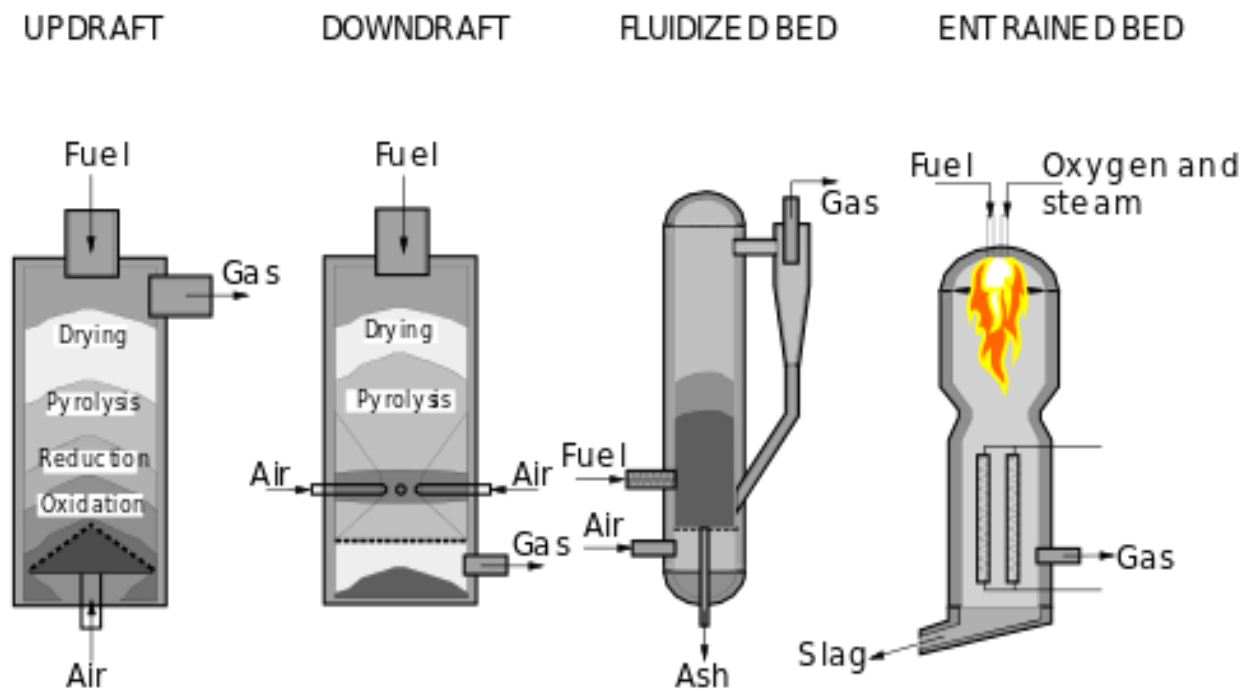


Figure 2.7. Example of reactors used in biomass gasification.

2.3.2.3 Liquefaction

Liquefaction is a process that takes place under a pressurized environment (20-240 bars) in the presence of a solvent. The final goal is to obtain weakly oxygenated bio-oils which after refining (hydrodeoxygenation) can be used as fuels or as chemical compounds. The advantage of liquefaction processes is that they are directly applicable to lignocellulosic biomass without a drying step for a wide temperature range of 180 to 600 ° C. The solvent used for liquefaction varies depending on different parameters, but water is frequently used because of the low cost

and the possibility of converting the raw material with a moisture content of more than 90% by weight. As with the pyrolysis product, the liquefaction of the product also requires further processing. This process of converting woody biomass directly in a liquid is far from being technically and economically feasible and is not yet present at a laboratory-scale production capacity [26].

2.3.2.4 Pyrolysis

Pyrolysis is the heating of organic materials in the absence of oxygen [36], the process takes place at temperatures between 300-600°C. Three main products result from the pyrolysis process: a carbon-rich solid product called biochar, volatile liquids(bio-oil), and gases. The gases mainly consist of carbon monoxide (CO), carbon dioxide (CO₂), hydrogen (H₂), methane (CH₄), and higher hydrocarbons. Depending on the temperature, reaction time, and heating rate, pyrolysis can be subdivided into four categories: slow, fast, flash, and intermediate, where slow and fast are the most common types. The yield of solid char depends on these factors.

The difference between fast and slow pyrolysis is the time and temperature. In fast pyrolysis, the temperature and heating rates are high. The process can be done in seconds and the resulting product consists mainly of bio-oils [37]. In slow pyrolysis, the process can go on for hours and the heating rate and temperature are lower; a temperature under 450°C is common. The purpose of slow pyrolysis is mainly to produce biochar. It's estimated that fast pyrolysis produces 60-75% of bio-oil, 15-25% biochar, and 10-20% gases [38], while slow pyrolysis produces about 35% biochar, 30% bio-oils, and 35% gases [39]. The products in both fast and slow pyrolysis can be further processed and to produce higher-quality fuels [40]. Further processed bio-oil could for instance be utilized as raw material for petrochemical production, biochar could be made into briquettes which can be used for cooking and the gas produced can be burned as energy or a source for heat supply in the pyrolysis process.

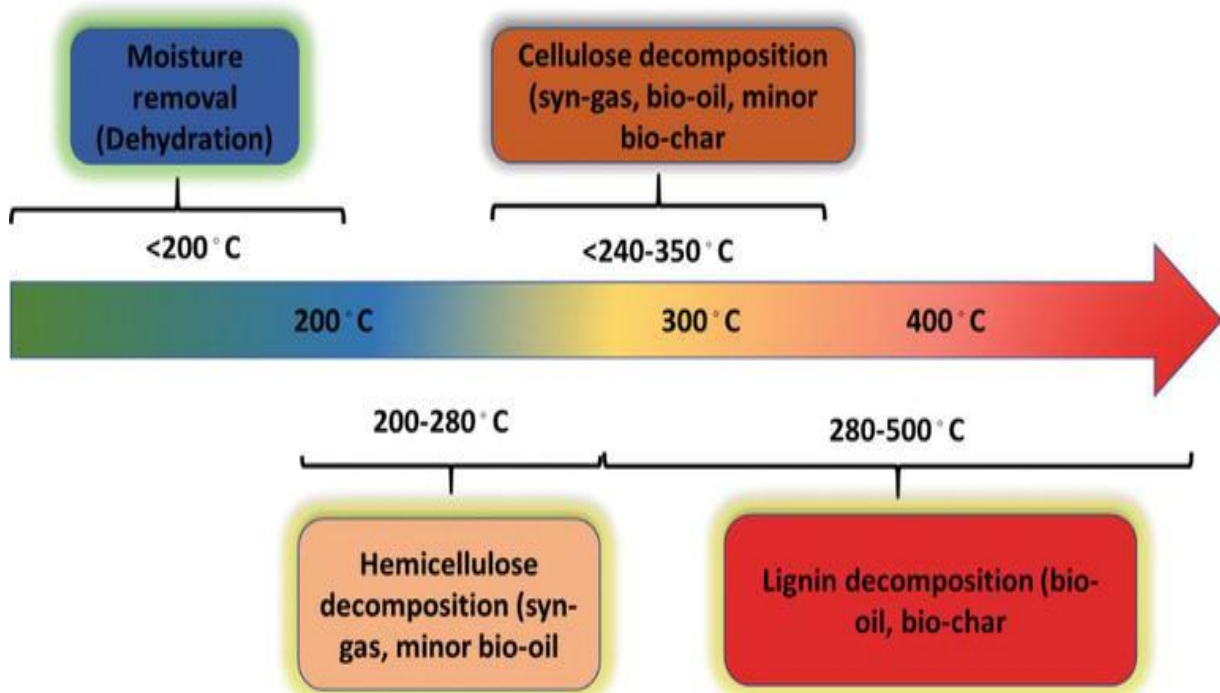


Figure 2.8. Stages of pyrolysis process

2.3.2.5 Torrefaction

The torrefaction of biomass is a process of refinement and heat preprocessing which currently attracts much interest and attention. This process uses temperatures between 200 and 350°C and is much like the coffee roasting process. The resulting torrefied biomass is excellent solid fuel shape, and an intermediate between conventional biomass and charcoal, presenting several advantages in terms of improvement of the intrinsic characteristics of the material [41].

Typically, the process increases heating value, water resistance, friability, and grindability. Thereafter, torrefied products can be densified into pellets or briquettes to obtain higher energy density or even ground to the desired end-use [42]. With the thermal process, biological presence is destroyed, reducing the risk of degradation, spontaneous combustion, as well as the possibility of spreading invasive and nonnative species. The final biomass powder resembles the pulverized coal regarding the supply and its behavior in the combustion process, potentially facilitating the use of biomass in the thermal conversion units, new or already existing, and using technologies that support pulverized fuel on a large scale. The problems associated with the production of ash in the combustion can be significantly reduced through the use of well-studied mixtures as well as the separation of chlorine during torrefaction. Thus, torrefaction is a process of pretreatment of biomass, which is well suited for use initially as possible in the

supply chain of biomass conversion systems to maximize logistics benefits and handling systems [43].

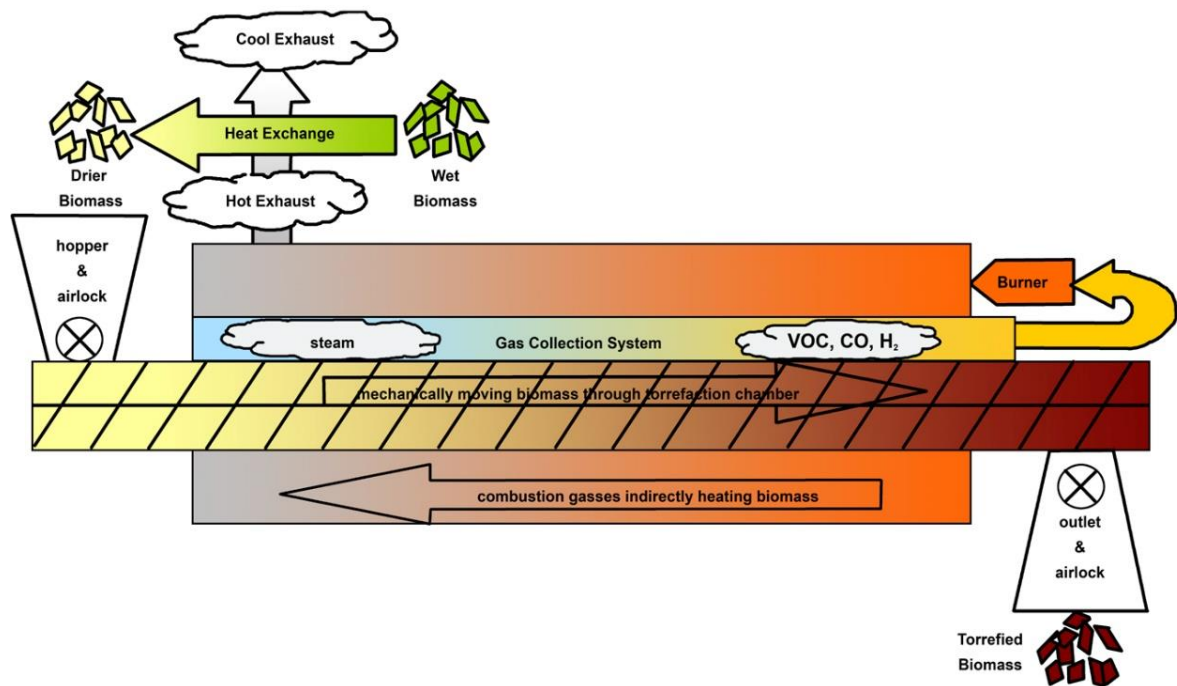


Figure 2.9. Schematic of torrefaction machine

2.3.2.6 Supercritical water gasification (SCWG) of biomass

SCWG is a promising thermochemical technology that can be used to convert high moisture content biomass to syngas. The water reaches supercritical conditions at 374.12°C and 221.2 bar above its critical point, at which the distinct liquid and gas phases do not exist. Supercritical water combines both the dissolution of liquid water and the diffusion of its gaseous phase. It is also characterized by high sensitivity towards changes in temperature, pressure, and low dielectric constant, which make supercritical water act as a solvent or catalyst depending on the conditions. Temperature, pressure, feedstock concentration (biomass-to-water ratio), and residence time are the key parameters that affect the H₂ yield of the SCWG process. The operating temperature ranges from 350°C to 700°C depending on the feedstock type, reactor configuration, catalyst, and desired outputs [44]. SCWG offers several advantages over thermochemical gasification. Biomass with high moisture content can be gasified without drying and hence reduces feedstock drying cost. High reaction rate, high H₂, and low CO yields, and low char and tar formation are other advantages of SCWG. Unlike other thermochemical gasification techniques, water is used as a gasification reaction medium and catalyst in SCWG. Hydrolysis, steam reforming, water–gas shift reaction, methanization, and hydrogenation are

some of the subreactions in the SCWG process. In steam reforming, the main biomass feedstocks and intermediate products from hydrolysis lignin such as phenolics are broken down to CO, CO₂, and H₂. The water-gas shift reaction in H₂ production is between CO and water. Methanization and hydrogenation are secondary reactions that consume CO, CO₂, and H₂ to produce CH₄. There are different reactor configurations for SCWG, i.e. batch, continuous stirred tank, tubular, fluidized bed, and diamond anvil cell. Cellulosic, hemicellulosic, and ligneous feedstock are among the widely investigated model compounds for SCWG.

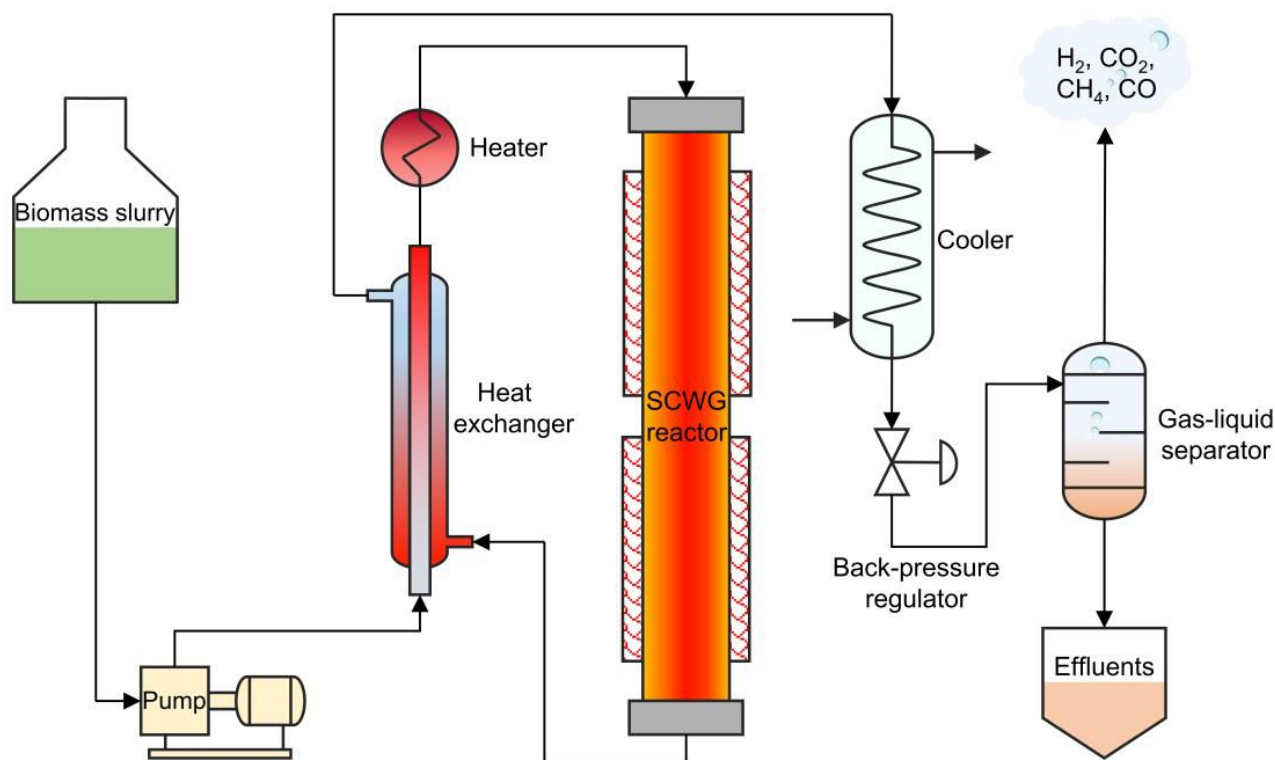


Figure 2.10. Representative schematic of continuous SCWG reactor.

2.4. Biomass pyrolysis

2.4.1 Conceptual pyrolysis process design

Conceptual process design is inherently a multi-scale paradigm and captures all the constituents of pyrolysis technologies and their interactions all through the temporal and spatial scales from pretreatment to the pyrolysis reactor, followed by upgrading and separation of products. According to Figure 2.11, a pyrolysis process is mainly comprised of three main stages: (1) feedstock reception, storage, handling, preparation, and pretreatment; (2) pyrolysis conversion, consisting of initial moisture evaporation and primary decomposition followed by secondary reactions (*e.g.* oil cracking and repolymerization [45], [46]); and (3) upgrading and refining the reactor effluents to marketable products [47].

Figure 2.11 suggests that pyrolysis technologies are highly adaptable to various feedstocks. Pretreatment technologies enable optimization of product yield and composition, and minimization of undesirable by-products. The pyrolysis reactions can be promoted catalytically or non-catalytically. The former is also referred to as *in-situ* catalytic pyrolysis. In the non-catalytic configuration, the primary pyrolysis vapors may be immediately upgraded in a catalytic reactor (known as *ex-situ* catalytic pyrolysis) or are firstly condensed and phase-separated, and then the liquid phase undergoes upgrading processes.

In general, fluidized bed reactors incur higher capital and operational costs but are regarded as a suitable technology for large-scale pyrolysis including catalytic pyrolysis. Entrained flow reactors are expected to be more economically efficient but deliver lower carbon efficiency than fluidized bed systems. Ablative reactors and auger reactors are considered to be suitable for small-scale operations and distributed systems [48]. Other types of reactors in development include microwave-assisted reactors [49], [50], and solar reactors [51], [52].

The optimum operational parameters (*e.g.* particle size, reaction pressure, carrier gas, temperature, heating rate, and vapor residence time) for different types of pyrolysis reactors vary significantly. The system performance under various process configurations can be projected using process simulation models.

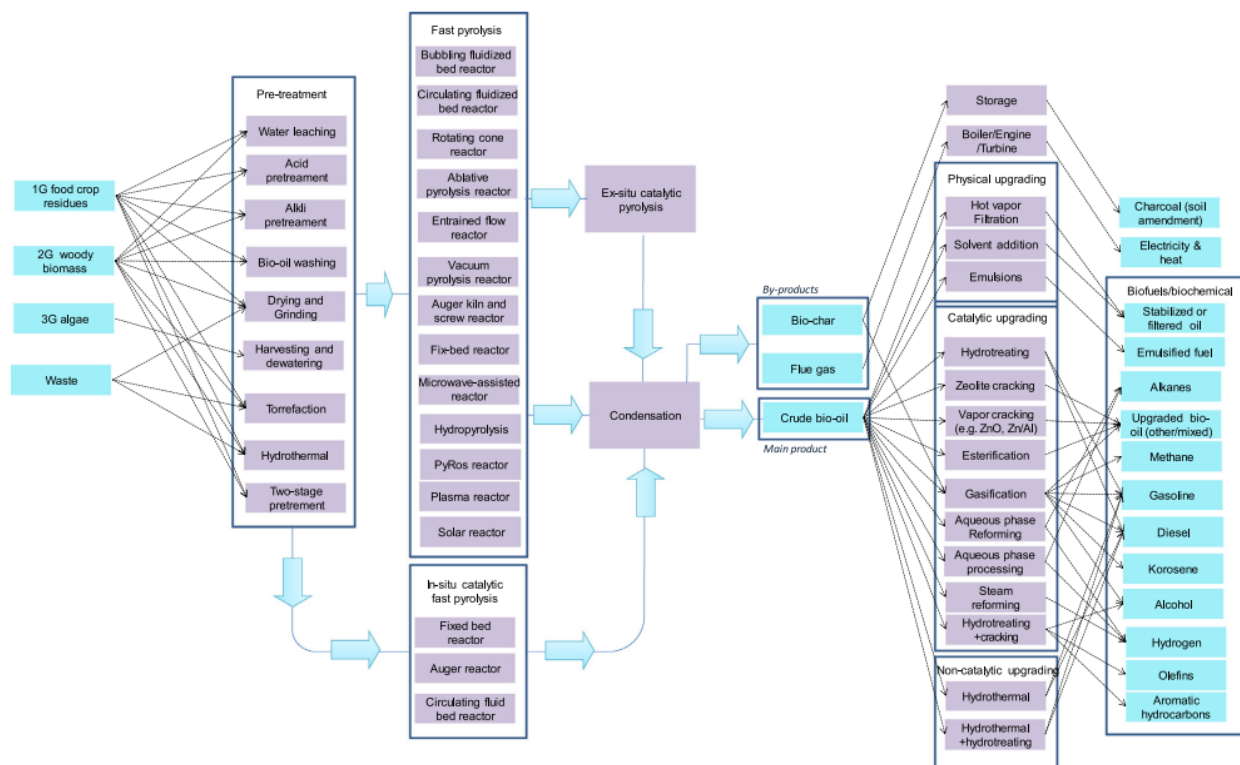


Figure 2.11. The superstructure of fast pyrolysis technologies.

2.4.2. Kinetic models of biomass pyrolysis

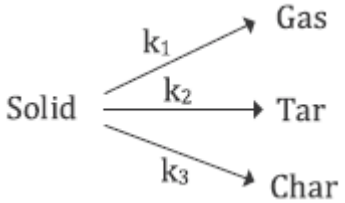
Chemical kinetics play a key role in explaining the characteristics of pyrolysis reactions and developing mathematical models. There have been extensive studies on biomass pyrolysis kinetics in the past decades for developing various kinetic models [18]. Most of the kinetic models are considered lumped models because the kinetics are based on the yields of lumped products (i.e. char, tar, and gas). The recent advances in kinetic models have been well reviewed in the literature [18], [53]–[55].

Kinetic models typically include one-step global kinetic model, parallel and competitive reactions model, models with secondary tar cracking, detailed lumped kinetic model, distributed activation energy model (DAEM), and nucleation growth, model. Some typical models with respective reaction mechanisms are presented in Table 2.1, together with kinetic data (first-order) for different reaction schemes determined experimentally and validated through modeling.

One-step global kinetic models are the simplest models available which represent the conversion of biomass to the volatiles and char as a first-order single-step reaction. Since pyrolysis products only consist of char and volatiles [56], most of the researchers have used the global reaction model coupled with appropriate heat transfer and volume reaction models [18]. Kinetic parameters of these models can be estimated either experimentally or using different models such as the Friedman model, Kissinger Model, Kissinger-Akahira Sunose (KAS), and Flynn-Wall-Ozawa (FWO) [57].

However, global kinetic models have certain limitations as they do not include elaborate reaction mechanisms and only consider the primary reactions. Hence, other kinetic models were later formulated to include secondary reactions [58]. The formation of gases from tar decomposition and the conversion of tar to char by polymerization were included in the kinetic model as secondary reactions [59]. Shafizadeh and Bradbury's model [60] included both primary and secondary decomposition reactions. In this model, cellulose was first converted to active cellulose, which is further decomposed into other secondary products. This model gave good predictions for the product yield, but the determination of activation energy was difficult for this model as the composition of the active material was unknown. This model has been used extensively by researchers in its original form as well as extended forms [61], [62].

Table 2.1. An overview of kinetic data for different pyrolysis models [18]

Model	Reaction mechanism	Feed	Analysis technique	Activation energy, kJ/mol	Frequency factor s ⁻¹
One-step kinetic model	$\text{Biomass} \xrightarrow{k} \text{Volatile gases} + \text{Char}$	Cellulose	TGA-MS	E=221	A=1.47 × 10 ⁷
Three parallel reactions model	$\text{Biomass} (x\text{Cellulose} + y\text{Hemicellulose} + z\text{Lignin}) \xrightarrow{k} \text{Volatiles} + \text{Char}$	Biomass	TGA, DTG	E1=184-192 E2=129-133 E3=64-87	A1=1.14 × 10 ⁶ A2=2.69 × 10 ⁴ A3=2.22 × 10 ¹
Six independent first-order reactions	$S_{v1} \xrightarrow{k_1} G \uparrow$ $S_{v2} \xrightarrow{k_2} G \uparrow$ $S_{v3} \xrightarrow{k_3} G \uparrow$ $S_{v4} \xrightarrow{k_4} G \uparrow$ $S_{v5} \xrightarrow{k_5} G \uparrow$ $S_{v6} \xrightarrow{k_6} G \uparrow$	Pinewood	Steel reactor	E1=83 E2=146 E3=77 E4=60 E5=139 E6=130	A1=0.70 × 10 ⁵ A2=0.20 × 10 ¹⁰ A3=0.43 × 10 ⁴ A4=0.29 × 10 ² A5=0.51 × 10 ⁷ A6=0.32 × 10 ⁶
Competitive reactions model		Cellulose, Wood	Pyrex reactor	E1=140 E2=133 E3=121	A1=1.3 × 10 ⁸ A2=2.0 × 10 ⁸ A3=1.08 × 10 ⁷
Mechanism with secondary interaction (Tar cracking)	$\text{Cellulose} \xrightarrow{k_1} \text{Active cellulose}$ $\text{Active cellulose} \begin{cases} \xrightarrow{k_2} \text{Tar} \xrightarrow{k_4} \text{Gas} \\ \xrightarrow{k_3} \text{Char} + \text{Gas} \end{cases}$	Cellulose	Pyrolysis reactor	E1=58 E2=47 E3=36 E4=108	A1=1.7 × 10 ²¹ A2=1.9 × 10 ¹⁶ A3=7.9 × 10 ¹¹ A4=4.28 × 10 ⁶

Multistep Kinetic Model of Biomass Pyrolysis

A detailed lumped kinetic model for biomass pyrolysis was proposed by Ranzi et al. [63] and generalized by Cuoci et al. [64]. This mechanism included 15 reactions with 30 lumped species. Ranzi et al. [28] extended this mechanistic model to describe the biomass pyrolysis, devolatilization, and gas-phase reaction of the released gas species from the three reference components of biomass. The generalized form of this model for cellulose, hemicellulose, and lignin is presented in Figures 2.12 and 2.13, respectively. The detailed mechanism proposed can be found in the Table 3.1.

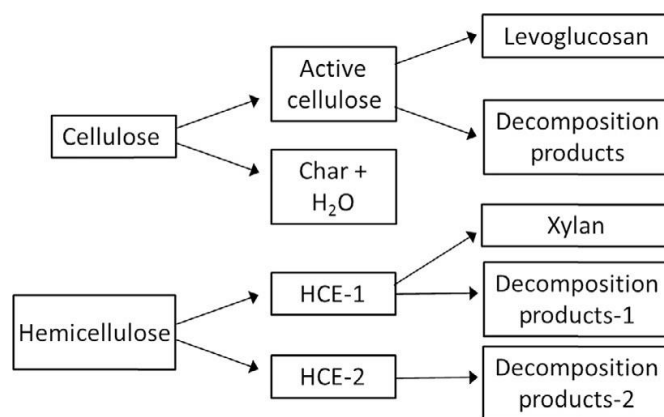


Figure 2.12. Multistep kinetic mechanism of cellulose and hemicellulose pyrolysis.[28]

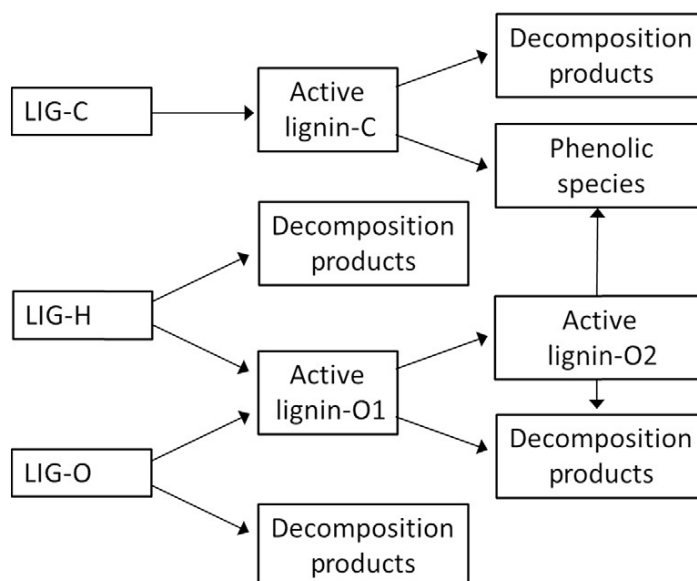


Figure 2.13. Multistep kinetic mechanism of pyrolysis of the three reference lignins.[28]

2.4.3 Influence of minerals on biomass pyrolysis mechanisms

The presence of inorganic elements such as potassium, sodium, calcium, and magnesium in the biomass is seen as having an important influence on the mechanisms of pyrolysis thus modifying the distribution and the composition of the products. The presence of these elements also causes problems in thermochemical transformation processes such as the reduction in the quality of the products obtained (bio-oils, synthesis gas), the increase in corrosion, and agglomeration problems in combustion processes or gasification.

According to thermogravimetric analysis, the conversion of biomass is initiated at a lower temperature when inorganic elements are present within the lignocellulosic matrix. In the case of cellulose, the yield of levoglucosan is considerably reduced and the formation of carbon and gas is favored as well as the formation of furan compounds. Alkali and alkaline earth metals are described as being able to inhibit the mechanism of transglycosylation and thus promote

dehydration and fragmentation reactions. The influence of inorganics on hemicelluloses studied by thermogravimetry experiments after impregnations with different alkali salts does not seem very marked. However, it is important to note that commercial hemicelluloses may contain inorganics because these polysaccharides are naturally rich in minerals and purification techniques do not completely remove these elements. This phenomenon could explain the reason why studies carried out on impregnations of hemicelluloses do not allow the visualization of the effect of minerals. However, even after demineralization, the pyrolysis of commercial hemicelluloses (800°C) seems to give very high carbon yields (20% for xylan, 30% for glucomannan) [30].

The investigations carried out on impregnated lignin samples do not make it possible to distinguish significant variations in the yields of products. However, it has been proven that alkaline inorganics promote certain chemical degradation mechanisms such as demethoxylation, demethylation, condensation reactions.

Knowledge of the influence of minerals on the chemical mechanisms of pyrolysis is essential because the most biomass likely to be used in thermochemical transformation processes present high inorganic levels (herbaceous plants and forest residues). The models of prediction of pyrolysis products do not take into account the influence of inorganics which has a consequence of reducing their effectiveness.

2.5. Critical Literature review

Biofuel production from biomass has got a strong interest and many researches have been conducted either on biochemical conversion or thermochemical conversions to produce valuable solid, liquid, and gaseous biofuels[1]. A wide range of biomass can be converted efficiently into biofuels by thermochemical conversion, carbonization, pyrolysis, or gasification [32]. Pyrolysis presents a big advantage of having high-energy efficiency and high liquid byproduct yield among all thermochemical conversion technologies[7]. Liquid biofuels present the advantage of being handled easily, storage, transportation et usage with existing technologies, however bio-oil properties from biomass pyrolysis still need to meet the requirement of standard liquid fuels and many researches are still needed[65].

Number of researches have been conducted to improve the yield and quality of bio-oil production from biomass pyrolysis while producing biochar as well. Biochar is one of the byproducts of pyrolysis which has much application in agricultural soil fertilization[5]. Slezak et al. [6] demonstrated that the addition of charcoal to coal improves the gasification efficiency.

The main objective of biomass pyrolysis is to produce liquid biofuel [7], many previous researches were focused on the parametric sensitivity of pyrolysis on bio-oil yield and properties [8]. Different studies demonstrate that different types of biomass have different kinetics models, different optimum pyrolysis properties for a maximum bio-oil yield [9]–[12].

To improve the quality of byproducts from biomass pyrolysis and pyrolysis efficiency, different methods have been developed. Solar pyrolysis of corn Stover has been investigated to reduce the dependency of the process on electricity [12] while Green et al. [4] investigated the effectiveness of using solar energy as an energy source for thermochemical conversion and found that pyrolysis is the lesser in terms of energy consumption. Ellison et al. [66] worked on a microwave to explore the pyrolysis effect on the bio-oil quality and were able to reach high pyrolysis temperature and got water-free bio-oil. Furthermore, Parvez et al. [50] found the charcoal heating value was greatly improved by microwave pyrolysis. Additional researches were generally focused on the impact of different catalysts on byproduct distribution and process efficiency. It has been proven that the pretreatment of biomass feedstock with Ferric sulfate [67], acid/alkali [22], and zeolite [68] can greatly enhance the bio-product yield, improve its quality and increase pyrolysis efficiency.

Due to its complex structural constituent, cassava residue is very attractive as a biomass resource for alternative energy and valuable chemical production via thermochemical transformation [13]. Recent researches conducted on cassava residue pyrolysis were mostly oriented on the evaluation of its potentiality for bio-oil production and distribution yield of pyrolysis byproduct. Pattiya et al. [20] investigated the optimum pyrolysis temperature for cassava residues in a free-fall reactor, their result gave 450°C as the optimal temperature for maximum bio-oil yield. For a fixed-bed pyrolysis reactor, the experiment conducted by Ki Ong Lu et al. [69] gave 525°C as optimal temperature while Okekunle et al. [70] found a maximum bio-oil yield at 700°C when the sample was dried at 60°C before pyrolysis.

Further researches are still needed to define strong and detailed kinetic model parameters for cassava residues pyrolysis, investigate the influence of other parameters such as temperature, heating rate, residence time, particle size on the byproduct distribution yield, and bio-oil properties. To accomplish this, the present work aims to determine the parameters of the kinetics model that fits well with experimental data of cassava peels pyrolysis, and then optimum pyrolysis conditions were numerically investigated for maximum bio-oil production.

Table 2.2. Literature review on cassava waste pyrolysis

N°	Ref	Feedstock	Main Objectives	Methods and Technics	Main Findings	Gaps
1	[69]	Cassava Peels	<ul style="list-style-type: none"> - Effect of temperature on bio-oil yield - Bio-oil characterization Experimental investigation	<ul style="list-style-type: none"> - Fixed Bed pyrolysis reactor - GC-MS - One component kinetic model 	<ul style="list-style-type: none"> - Maximum bio-oil yield of 51.2% at 525°C - GCV of bio-oil of 27.43MJ/kg 	<ul style="list-style-type: none"> - Thermochemical characterization - Kinetic parameters - Effect of heating rate, HR, RT - Prediction through detailed kinetics - Lignocellulosic composition
2	[22]	Cassava residues	<ul style="list-style-type: none"> - Effect of acid/alkali pretreated cassava residues on fast pyrolysis behavior: thermal decomposition and kinetics 	<ul style="list-style-type: none"> - Chemical pretreatment - XRD - TG-MS - GC - Kinetics through model fitting 	<ul style="list-style-type: none"> - Maximum levoglucosan yield of 27% % for low HR - Formation of oxygenated chemicals in presence of alkali metal. - Lower activation energy in for a chemically pretreated sample 	<ul style="list-style-type: none"> - Isoconversional method for kinetics parameters determination - Use of multiple HR for kinetic study (3-5) - Numerical prediction of byproducts - Effect of Temperature, HR, RT on byproducts - Lignocellulosic composition
3	[71]	Cassava Peels	<ul style="list-style-type: none"> - Effect of chemical pretreatment of cassava peels for activation carbon production Experimental investigation	<ul style="list-style-type: none"> - Chemical pretreatment - Slow pyrolysis, carbonization 	<ul style="list-style-type: none"> - Optimum carbonization temperature of 350°C - Optimum biomass RT of 45minutes - Better result for Zinc chloride-based pretreatment 	<ul style="list-style-type: none"> - Fast pyrolysis - Thermochemical characterization - Lignocellulosic composition
4	[72]	Cassava Rhizome	<ul style="list-style-type: none"> - Effect of temperature on bio-oil yield - Char analysis Experimental investigation	<ul style="list-style-type: none"> - Fluidized Bed pyrolysis reactor - GC-MS 	<ul style="list-style-type: none"> - Maximum bio-oil yield of 63.23% at 427°C - GCV of bio-oil of 26.9MJ/kg 	<ul style="list-style-type: none"> - Thermochemical characterization - Kinetic parameters - Effect of heating rate, HR, RT - Prediction through detailed kinetics - Lignocellulosic composition
5	[73]	<ul style="list-style-type: none"> - Cassava stalk and - Cassava Rhizome 	<ul style="list-style-type: none"> - Effect of temperature on bio-oil yield - Bio-oil and gas composition Experimental investigation	<ul style="list-style-type: none"> - Fluidized Bed pyrolysis reactor - GPC - TCD 	<ul style="list-style-type: none"> - Maximum bio-oil yield of 62% at 475°C for CS - Maximum bio-oil yield of 65% at 510°C for CR 	<ul style="list-style-type: none"> - Thermochemical characterization - Kinetic parameters - Effect of heating rate, HR, RT - Prediction through detailed kinetics - Lignocellulosic composition

6	[21]	<ul style="list-style-type: none"> - Cassava stalk and - Cassava Rhizome 	<ul style="list-style-type: none"> - Thermochemical Characterization 	<ul style="list-style-type: none"> - Proximate and Ultimate analysis - TGA - Structural analysis 	<ul style="list-style-type: none"> - 78-80% of volatile content - High H₂ content: 7% - Cell: 35.7% and 31.2% - HCell 41.7% and 44.5% - Lignin 22.5% and 24.3% - Extractives: 13.2 and 10.8% 	<ul style="list-style-type: none"> - TGA at different heating rate - Kinetic parameters - Thermodynamic study - Empirical determination of Lignocellulosic composition
7	[74]	<ul style="list-style-type: none"> - Cassava stalk and - Cassava Rhizome 	<ul style="list-style-type: none"> - Effect of hot vapor filtration unit on bio-oil yield Experimental investigation 	<ul style="list-style-type: none"> - Fluidized Bed pyrolysis reactor - Hot vapor filtration unit 	<ul style="list-style-type: none"> - The hot vapor filtration unit increase the yield of bio-oil and char while reducing gas yield 	<ul style="list-style-type: none"> - TGA at different heating rate - Kinetic parameters - Effect of heating rate, HR, RT - Prediction through detailed kinetics
8	[20]	<ul style="list-style-type: none"> - Cassava stalk and Cassava Rhizome - Sugarcane leaves - Sugarcane tops 	<ul style="list-style-type: none"> - Effect of temperature and condensation temperature on bio-oil yield Experimental investigation 	<ul style="list-style-type: none"> - Free-fall pyrolysis reactor 	<ul style="list-style-type: none"> - About 70% of bio-oil yield could be obtained at pyrolysis temperature of 450°C and condensation temperature of 10°C. 	<ul style="list-style-type: none"> - Thermochemical characterization - Kinetic parameters - Prediction through detailed kinetics - Lignocellulosic composition
9	[70]	<ul style="list-style-type: none"> - Cassava peels 	<ul style="list-style-type: none"> - Bio-oil production in a fixed bed reactor 	<ul style="list-style-type: none"> - Fixed Bed pyrolysis reactor 	<ul style="list-style-type: none"> - Bio-oil yield decreases with the drying temperature - A maximum bio-oil yield is obtained at a pyrolysis temperature of 500°C 	<ul style="list-style-type: none"> - TGA experiment - Thermochemical characterization - Kinetic parameters - Thermodynamic study - Effect of heating rate, HR, RT - Prediction through detailed kinetics - Lignocellulosic composition

2.5.1. Research gaps on cassava waste pyrolysis

Cassava waste valorization through thermochemical conversion, especially through pyrolysis has been the subject of many researches as presented in Table 2.2. However, not all types of cassava plant residue have yet been fully investigated. A lot of research were done for cassava rhizome and cassava stalk and very few on cassava peels. From the research gaps found, we can see that the determination of lignocellulosic composition comes up often, both through chemical methods and empirical methods. In addition, the kinetics of cassava residue has not yet been sufficiently studied.

This work aims to fill some of these gaps by studying the pyrolysis of cassava peels which has not been much studied so far. Recent methods known to be more accurate were used for the determination of kinetic parameters using TGA data at different heating rates (4 heating rates were used). Furthermore, a comparative assessment of different methods of fast determination of lignocellulosic composition was performed. And finally using a detailed kinetic model of biomass pyrolysis, the effect of pyrolysis conditions was investigated numerically by an originally developed Matlab code.

CHAPTER 3. RESEARCH METHODOLOGY

3.1. Materials

Cassava tubers were collected from a cassava farm of Jimma Agricultural Research Center. First, cassava tubers were cleaned with water to remove impurities such as mud, sand, etc., and then cassava peels (CP) were taken from the washed cassava tubers. The wet CPs were made to undergo sun-drying for 5 days before oven drying for 24 hours at 105°C, followed by grinding and sieving. For all experiments reported in this thesis, the size of the samples was equal to or inferior to 0.5mm.



Figure 3.1. a) cassava from the field; b) sun-drying of cassava peels; c) dried cassava peels before grinding; d) ground cassava peels

3.2. Material characterization

3.2.1. Ultimate and proximate analysis

ASTM standard for proximate analysis of Cassava peels (CP) powder (ASTM D3172-13 Standard Practice for Proximate Analysis of Coal and Coke, 2013), and TGA equipment for the proximate analysis of 10.0 mg were used. The ultimate analysis was done by a 'Vario MACRO

Cube CHNOS Elemental Analyzer'. About 50 mg of samples were completely burnt using oxygen. The definitions of moisture content, volatile, ash content, and fixed carbon are shown as follows:

Moisture content,

$$MC(\%) = \frac{W - B}{W} * 100\% \quad (3.1)$$

Volatile,

$$V(\%) = \frac{B - C}{W} * 100\% \quad (3.2)$$

Ash content,

$$A(\%) = \frac{F}{W} * 100\% \quad (3.3)$$

Fixed carbon,

$$FC(\%) = 100\% - [MC(\%) + V(\%) + A(\%)] \quad (3.4)$$

where W is the mass of the original test specimen, B is the test specimen after drying in the moisture test, C is the mass of test specimen after heating in volatile matter test, F is the mass of ash residue. Each test was conducted three times and the average value of the data from the three tests was reported.

3.2.2. Thermogravimetric analysis (TGA)

TGA experiment using a standard TGA equipment (model: ATAT2012, software: BJ HENVEN) was conducted. Ultra-pure Argon gas at a flow rate of 300ml/min was used to provide the inert condition for the CP. 10mg of CP was placed in the TGA chamber and heated at constant heating rate from room temperature to 800 °C. The operation was repeated for four different heating rates: 5K/min, 15K/min, 20K/min, and 30K/min.

3.3. Lignocelulosique composition

3.3.1. Analytical/chemical method

3.3.1.1. Apparatus and Chemicals

The following apparatus were employed: Soxhlet extractor, Muffle furnace, Beaker, Conical flask, Measuring balance, Aluminum foil, Oven, Grinder, pH meter, Filter paper, UV-spectroscopy, Water bath, and Vacuum filter. The necessary chemicals include: Sodium hydroxide (FINEM 99.5%), Ethanol (98%), Sulfuric acid (UNICHEM, India 98%), distilled water, glacial acetic acid (Neolab, 96%), Toluene (99%), Acetone (99.5%), Diethyl ether (98%).

3.3.1.2. Determination of extractives in cassava peel

Before using the standard methods such as ASTM, TAPPI, or NREL the sample biomass should be free of extractives. The extractive free sample was prepared by using a Soxhlet extractor. The extractives component of cassava peel was extracted by using the TAPPI (Technical Association of Pulp and Paper Industry) standard methods T-204 cm-17 described in [30]. The Soxhlet apparatus was used and a two-gram oven-dried sample was placed in an extraction thimble. The refluxing solvent ratio is a 1:2 solution of ethanol and toluene mixture. The extraction is to be conducted for 8 h. After completing the extraction, the residue was dried in an oven at 105°C and was weighed until a constant weight was obtained. Finally, the amount of extractive in the sample was determined from the difference in weight of the sample before and after extraction [75].

3.3.1.3. Determination of Lignin in cassava peel

The lignin content in cassava peel was determined following the TAPPI T 222-om (1998) standard method for both acid-insoluble and acid-soluble lignin.

For *acid-insoluble lignin (Klason lignin)*, one gram of the extract-free sample was placed in a 100 mL beaker, 15 ml of 72 % sulphuric acid was added gradually in small increments while stirring the sample with a glass rod. After the sample has dispersed, the beaker was kept in a water bath at 50 °C for 2 hours with constant string. At the end of the 2 h, the solution was diluted to 3% and boiled for 4 hours. Then the solution was left overnight and filtered by using a vacuum filter. The solid residue (acid-insoluble lignin) was used for acid-insoluble lignin determination and the filtrate is used for the determination of acid-soluble lignin. The acid-insoluble lignin obtained was washed free of acid with hot water and dried to a constant weight at 105 °C in the oven [76]. Finally, the acid-insoluble lignin is calculated as:

$$AIL(\%) = \frac{A}{B} * 100\% \quad (3.5)$$

Where *A* is the oven-dry weight of Klason lignin, and *B* is the weight of the initial sample (g).

Acid-soluble lignin is determined from the filtrate obtained from the determination of acid-insoluble lignin. The determination was done from ultraviolet absorbance (UV) measured at 240 nm using 3 % tetra-oxo-sulfate acid (VI) (H₂SO₄) as a reference. The lignin content in the filtrate is calculated as:

$$ASL = \frac{A * V_f * D}{\epsilon * m * p} \quad (3.6)$$

$$D = \frac{\text{Volume of the sample} + \text{Volume of diluting sample}}{\text{Volume of the sample}} \quad (3.7)$$

Where A is the UV-Vis absorbance of the sample at an appropriate wavelength, V_f is the volume of the filtrate, D is the dilution factor, ϵ is the absorption coefficient of the sample, m is the mass of the sample (mg), and p is the path length of the cuvette (cm). Finally, the amount of lignin was calculated from the summation of acid-soluble and insoluble lignin [77].

3.3.1.4. Determination of Hemicellulose content

The hemicellulose content is determined according to ASTM D5896-96 (2012) standard method described in [77]. To determine hemicellulose 1g sample from a dried extractive-free sample was taken and 10 ml of 0.5 mol of NaOH solution was added to it. Then the solution was kept in a boiling water bath for 3.5 h at 80°C. Then it was washed with distilled water until its pH was neutralized.

3.3.1.5. Determination Cellulose content

Cellulose content was determined using Kushner- Hoffer method [78]. Accurately 1 g of the oven-dried sample is placed in a 250 mL round bottom flask fitted with a reflux condenser. 15 mL of 80 % acetic acid and 1.5 mL of concentrated nitric acid (HNO₃) were added and the mixture was boiled for 20 min. Then, about 20 mL of 95 % cold ethanol was added and the resultant mixture was cooled and filtered. The residue was washed successively with hot benzene and diethyl ether. The residue was dried overnight to a constant weight and was kept in a muffle furnace at about 500°C for 5 h. The loss in weight upon ignition was taken as a measure of the cellulose content.

3.3.2. Empirical method based on elemental composition

When no direct information is available on the cellulose, hemicellulose, lignin, and extractives contents, the method proposed by Debiagi et al. [30] allows the characterization of biomass feedstock on the basis of its elemental H/C/O composition. This biomass characterization method estimates a biochemical composition in terms of seven reference components. The predicted biomass composition must satisfy only the three H, C, and O balances, therefore there are 5 degrees of freedom converted into 5 splitting parameters ($\alpha/\beta/\gamma/\delta$ and ϵ). These parameters define the three reference mixtures whose relative concentration is derived by the H/C/O balances.

The biomass was considered as a linear combination of 3 reference mixtures as reported in the H/C diagram in Figure 3.2, (RM-1, RM-2, and RM-3), defined by five splitting parameters

($\alpha/\beta/\gamma/\delta$ and ε). α defines the molar ratio of 60% cellulose and 40% hemicellulose contained in RM1. β and γ define the two mixtures RM-2 and RM-3 of the different lignins (80% LIG-O and 20% LIG-C, and 80% LIG-H and 20% LIG-C, respectively). (RM-2 and RM-3) are more flexible and they can move toward the reference species TGL or TANN, depending on the biomass composition. For biomass rich in hydrogen, the amount of TGL progressively increases in the RM-2 mixtures. Similarly, for biomass with low hydrogen content, the reference mixture RM-3 increases its content of the reference component of tannin species (TANN).

As an example, the hybrid poplar with an elemental composition of H/C/O = 0.0565/0.5092/0.4343, can be characterized using $\alpha/\beta/\gamma/\delta/\varepsilon = 0.6/0.8/0.8/1/0.8$. The value $\varepsilon = 0.8$ means that 80% of lignins (LIGO and LIGC) and 20% of TANN are combined to define RM-3. In this way, the biomass with low H content also enters into the characterization region. The amount of the reference mixture RM-2 is very low, because of the low hydrogen content. Thus, these biomass results are mostly split between RM-1 and RM-3. Similarly, the olive husks with H/C/O = 0.0696/0.5489/0.3815 are characterized by using the splitting parameters: $\alpha/\beta/\gamma/\delta/\varepsilon = 0.6/0.8/0.8/0.8/1$. The value $\delta = 0.8$ means that 80% of lignins (LIGH and LIGC) and 20% of TGL are combined to obtain RM-2, and this condition allows this biomass with high H content to enter the characterization region.

As discussed by Debiagi et al. [30] optimal splitting or characterization parameters can be obtained by minimizing the square deviations between the predicted and experimental values of cellulose, hemicellulose, lignin, and extractives using the feasible boundary conditions between 0 and 1 for the splitting parameters. TGL is expected to increase with the H content of the biomass sample, while TANN will increase when H content is decreasing. The default splitting parameters: $\alpha/\beta/\gamma/\delta/\varepsilon = 0.6/0.8/0.8/1/1$. While the default values of $\alpha/\beta/\gamma$ remain unchanged, the splitting parameters δ and ε are progressively reduced, increasing in this way the extractive content, in order to respect a feasible composition (i.e., non-negative values for all the seven reference components).

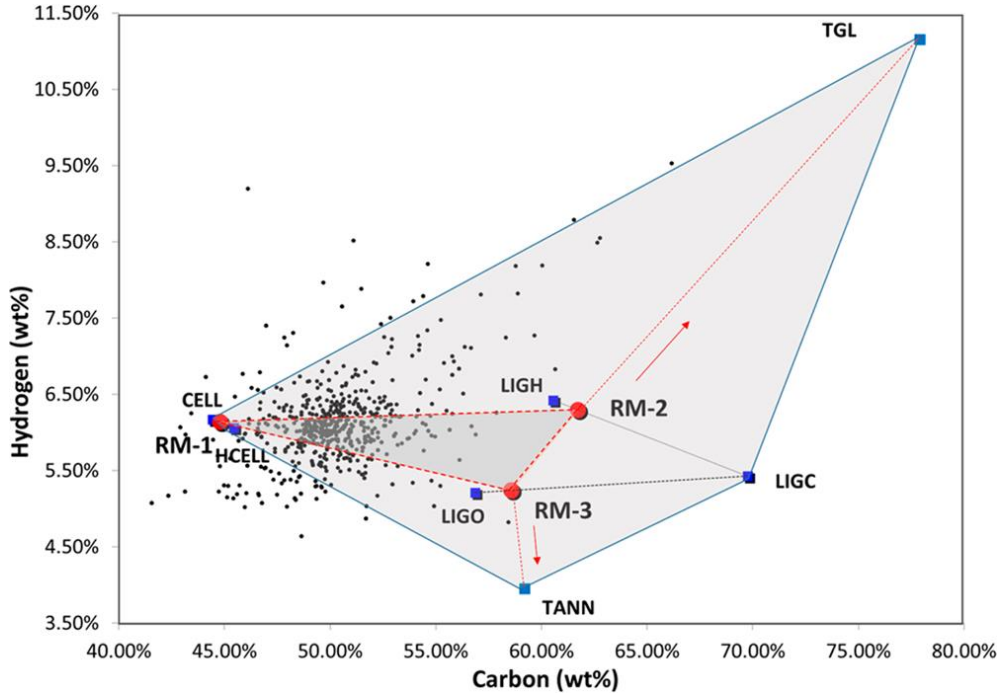


Figure 3.2. Extended biomass characterization. $H\%$ vs $C\%$ plot of biomass samples along with their reference species. [30]

3.3.3. Based on the TGA-PKM method [25]

This method is based on the TGA data. The first step is the normalization of the TG raw data in relation to the initial weight of the sample (m_0) and the final weight (m_f) of the sample. To do this, the weight fraction of the volatiles remaining in the sample has been calculated for each instant of discrete-time i , as indicated in Equation (3.8).

$$X_i = \frac{m_i - m_f}{m_0 - m_f} \quad (3.8)$$

In this case, m_f represents the mass of char obtained at the end of each TG analysis and includes the mass of ash and fixed carbon at the final temperature of the analysis.

For the determination of kinetics, it is more useful to use the derivative thermogravimetric (DTG) of weight loss as a function of time, because this signal is much more sensitive to small changes. The DTG curve was obtained from the weight over time derivative for each experimental point, i.e.

$$\frac{dX_i}{dt} = \frac{X_i - dX_{i-1}}{t_i - t_{i-1}} \quad (3.9)$$

3.3.3.1. Kinetic model

The thermochemical decomposition of the biomass can be represented by four main kinetics that corresponds to the degradation of hemicellulose, cellulose, lignin, and extractive. The most

commonly used model assumes that the process can be represented by the decomposition reactions of each of these compounds [79]. In addition, the decomposition of these compounds can be represented by a number of parallels and independent first-order Arrhenius-type reactions, named pseudo components. Thus, for the adjustment of the DTG curve of each biomass, it has been assumed that the process follows the model that consists of the decomposition of hemicellulose, cellulose, and lignin independently so that the overall kinetics can then be expressed as follows:

$$\frac{dX}{dt} = \frac{dX_H}{dt} + \frac{dX_C}{dt} + \frac{dX_L}{dt} + \frac{dX_E}{dt} \quad (3.10)$$

where H, C, L, and E represent the mass fraction of hemicellulose, cellulose, lignin, and extractives, respectively.

At the same time, the kinetics of each of these fractions can be represented by a set of parallel reactions, expressed in the form:

$$\frac{dX_H}{dt} = \sum_{j=1}^{m_H} \frac{dX_{H_j}}{dt} = \sum_{j=1}^{m_H} A_{H_j} \exp\left(-\frac{Ea_{H_j}}{RT}\right) X_{H_j} \quad (3.11)$$

$$\frac{dX_C}{dt} = \sum_{j=1}^{m_C} \frac{dX_{C_j}}{dt} = \sum_{j=1}^{m_C} A_{C_j} \exp\left(-\frac{Ea_{C_j}}{RT}\right) X_{C_j} \quad (3.12)$$

$$\frac{dX_L}{dt} = \sum_{j=1}^{m_L} \frac{dX_{L_j}}{dt} = \sum_{j=1}^{m_L} A_{L_j} \exp\left(-\frac{Ea_{L_j}}{RT}\right) X_{L_j} \quad (3.13)$$

$$\frac{dX_E}{dt} = \sum_{j=1}^{m_E} \frac{dX_{E_j}}{dt} = \sum_{j=1}^{m_E} A_{E_j} \exp\left(-\frac{Ea_{E_j}}{RT}\right) X_{E_j} \quad (3.14)$$

Where T : temperature, in K ; R : ideal gas constant, $8.314 \cdot 10^3 \text{ kJ } (K \text{ mol})^{-1}$; j : number of pseudocomponents of the fractions of hemicellulose, cellulose, lignin, and extractives, which take the values from 1 to the total number of pseudocomponents of each fraction of hemicellulose; cellulose, lignin and extractives (m_H , m_C , m_L and m_E); A_{H_j} , A_{C_j} , A_{L_j} and A_{E_j} : pre-exponential factors of the pseudocomponents of the hemicellulose; cellulose, lignin, and extractives fractions, expressed in s^{-1} and Ea_{H_j} , Ea_{C_j} , Ea_{L_j} and Ea_{E_j} : activation energies of the pseudocomponents of the hemicellulose; cellulose, lignin, and extractives fractions, expressed in kJ mol^{-1} .

In general, the kinetic equation of each pseudocomponent j , corresponding to fraction F ($F = H, C, L, E$), in a non-isothermal process at constant heating rate $\beta = dT/dt$, is given by:

$$\frac{dX_{Fj}}{X_{Ej}} = -\frac{A_{Fj}}{\beta} \exp\left(-\frac{Ea_{Fj}}{RT}\right) dT \quad (3.15)$$

The integral of the second term can be resolved by using the exponential integral, defined as follows:

$$\int_u^\infty \frac{e^{-u}}{u} du, \quad u = \frac{Ea}{R} \quad (3.16)$$

Thus, Equation (3.15), integrated between T_0 and T , can be expressed in the form

$$X_{Ej,i} = X_{Ej,0} \exp \left\{ -\frac{A_{Fj}}{\beta} \left[T_i \exp\left(-\frac{Ea_{Fj}}{RT_i}\right) - \int_{X_{Ej,0}/RT_i}^\infty \frac{\exp\left(-\frac{Ea_{Fj}}{RT_i}\right)}{T} dT \right] \right\} \quad (3.17)$$

Therefore, the kinetics of each pseudocomponent depends on three variables: the pre-exponential factor, the activation energy, and the initial concentration of the pseudocomponent in the biomass ($X_{Ej,0}$).

A restriction that the system must satisfy is that the sum of the mass fractions of all the pseudocomponents must be equal to the mass fraction of all volatiles generated for each instant of time $t = i$.

$$X_i = X_{H_i} + X_{C_i} + X_{L_i} + X_{E_i} = \sum_{j=1}^{m_H} X_{H_{j,i}} + \sum_{j=1}^{m_C} X_{C_{j,i}} + \sum_{j=1}^{m_L} X_{L_{j,i}} + \sum_{j=1}^{m_E} X_{E_{j,i}} \quad (3.18)$$

Combining Equations (3.17) and (3.18) for each instant of discrete-time i gives a system of equations with $3 * (m_H + m_C + m_L + m_E) - 1$ unknowns, which needs to be solved

3.3.3.2. Calculation Procedure

For the calculation of unknown variables, an optimization method based on the minimization by least squares has been used. As an objective function (OF), the square of the errors between the values of the experimental curve and the model was used for each instant of time i , in which the model was evaluated.

$$O.F. = \sum_{i=1}^n \left[\left(\frac{dX}{dt} \right)_{i,exp} - \left(\frac{dX}{dt} \right)_{i,model} \right]^2 \quad (3.19)$$

The solution was obtained through MATLAB using the *lsqcurvefit* command to find the constants that best fit the system of equations. The final solution was obtained when the percentage variation of the OF was less than 0.01% during five consecutive cycles of 200 iterations each ($\Delta OF_5 < 0.01\%$).

Additionally, the goodness of fit was evaluated by the adjusted R-squared, R^2_{Adj} , which represents the response that is explained by the model and was calculated as the ratio between the sum of the square of the residuals (SSE) and the total sum of squares (SST) as follows [80]:

$$R^2_{Adj} = 1 - \frac{(n-1) * SSE}{(n-(k+1)) * SST} = 1 - \frac{(n-1) * \sum_{i=1}^n \left[\left(\frac{dX}{dt} \right)_{i,exp} - \left(\frac{dX}{dt} \right)_{i,model} \right]^2}{(n-(k+1)) * \sum_{i=1}^n \left[\left(\frac{dX}{dt} \right)_{i,exp} - \overline{\left(\frac{dX}{dt} \right)_{i,exp}} \right]^2} \quad (3.20)$$

where k represents the number of variables.

The initial values of the constants were taken after an initial analysis of the kinetics, using as initial seed values the restrictions on the concentrations of the hemicellulose, cellulose, lignin, and extractives fractions obtained from the analytical method.

The decision tree of the calculation process is as presented in Figure 3.3.

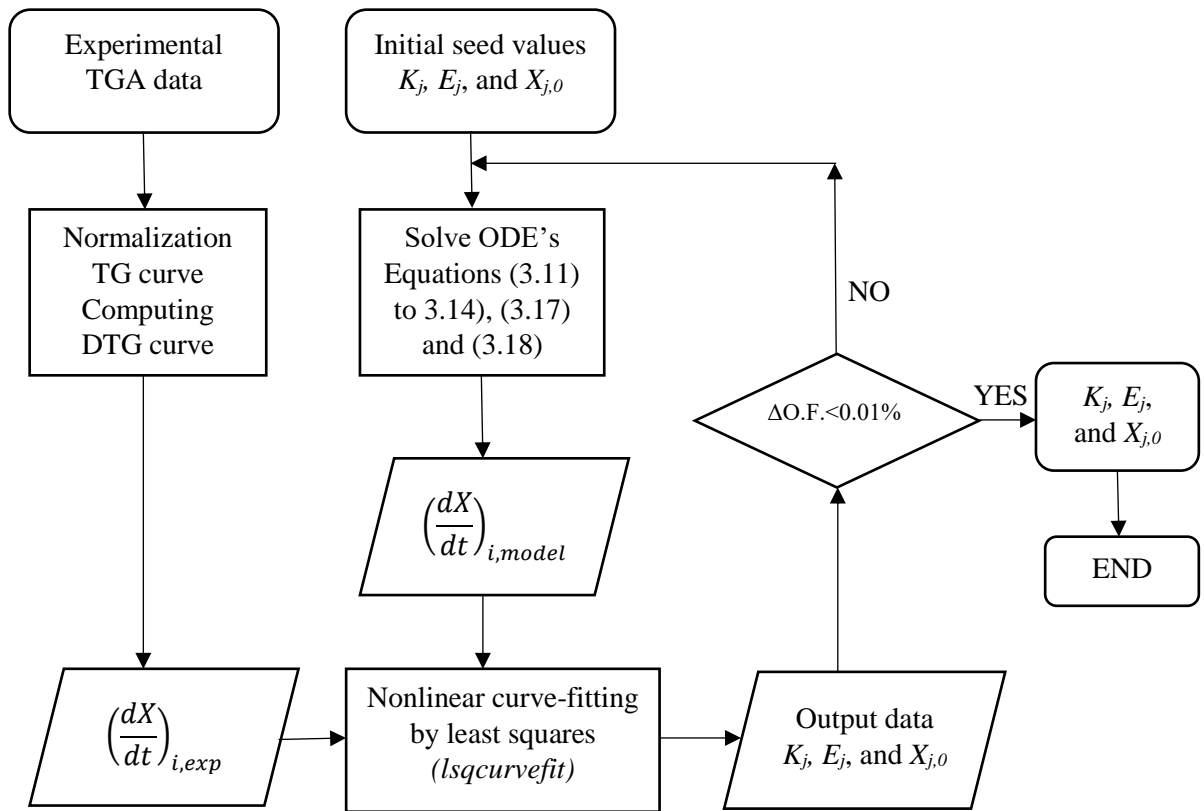


Figure 3.3. Decision tree of the calculation procedure

3.4. Kinetics of CP pyrolysis

The chemical reaction rate $d\alpha/dT$ is generally expressed as:

$$\frac{d\alpha}{dt} = K(T)f(\alpha) \quad (3.21)$$

where $f(\alpha)$ is a function related to conversion, T is the temperature (K), and α represents the degree of conversion that is described as:

$$\alpha = \frac{m_0 - m_t}{m_0 - m_f} \quad (3.22)$$

where m_0 , m_t , and m_f are the initial mass of the sample, the actual mass of the sample at time t , and the final mass of the sample in the reaction.

Arrhenius equation express $k(T)$ as:

$$K = A \exp\left(-\frac{Ea}{RT}\right) \quad (3.23)$$

where A (s^{-1}) is the Arrhenius pre-exponential factor, Ea (J/mol) is the activation energy of pyrolysis reaction, and R ($J\ mol^{-1}\ K^{-1}$) is the universal gas constant. The combination of Equations (3.21) and (3.23) gives:

$$\frac{d\alpha}{dt} = A \exp\left(-\frac{Ea}{RT}\right) f(\alpha) \quad (3.24)$$

Integrating the heating rate β (K/min) we get:

$$\frac{d\alpha}{dT} = \frac{A}{\beta} \exp\left(-\frac{Ea}{RT}\right) f(\alpha) \quad (3.25)$$

The integrated form of Equation (3.25) is:

$$G(\alpha) = \int_0^\alpha \frac{d}{f(\alpha)} = \frac{A}{\beta} \int_{T_0}^T \exp\left(-\frac{Ea}{RT}\right) dT \quad (3.26)$$

$$T = T_0 + \beta t \quad (3.27)$$

where $T_0(K)$ and $f(\alpha)$ are initial temperature and conversion function, respectively.

It is well known that the isoconversional method can easily give an estimation of E_a even without knowing the associated reaction mechanism. Thus, two isoconversional methods, FWO and KAS methods are used for activation energy calculation. The FWO method [57] can be described as:

$$\ln\beta = \text{constant} - 1.0516 \frac{Ea}{RT_\alpha} \quad (3.28)$$

where for a chosen value of α , the values of $\ln\beta$ and $1/T_\alpha$ can be correlated by a straight line and the activation energy can be calculated from the slope (Ozawa, 1970). Thus, a series of activation energy values can be obtained corresponding to different α . The KAS method [57] is also expressed seen as:

$$\ln\left(\frac{\beta}{T_\alpha^2}\right) = \text{constant} - \frac{Ea}{RT_\alpha} \quad (3.29)$$

The activation energy is determined from the slope ($-E\alpha/R$) of the straight line (Kissinger, 1957). The parameter estimation using model-free methods does not depend on the mechanism of reactions. FWO and KAS methods are widely used for calculating activation energy and Arrhenius pre-exponential factor during pyrolysis of carbonaceous material. The activation energy is directly related to the fuel reactivity.

As discussed by Vaibhav et al. [57], there is a more accurate approach called the Friedman method. Friedman's method is the simplest and one of the most widely used differential isoconversional methods for kinetic analysis. The method was first used by Friedman to study the kinetics of char-forming plastics by thermogravimetry. The Friedman equation is stated as follows:

$$\ln\left(\frac{d\alpha}{dt}\right)_{\alpha,i} = \ln[f(\alpha)A_{\alpha}] - \frac{E_{\alpha}}{RT_{\alpha,i}} \quad (3.30)$$

In the above equation, i denotes different temperature programs at which the no isothermal TGA runs are being conducted. In the case of isothermal runs, i will denote the individual temperature of the experiment. $\ln(d\alpha/dt)_{\alpha,i}$ denotes the set of $\ln(d\alpha/dt)$ values at a fixed value of conversion obtained at different heating rates. Similarly, $T_{\alpha,i}$ is the temperature at which “ α ” conversion has taken place at different heating rates. For a fixed value of conversion, the term $\ln[f(\alpha)A_{\alpha}]$ is constant. Thus, for each value of α , the plot of $\ln(d\alpha/dt)_{\alpha,i}$ versus $(1/T_{\alpha,i})$ should give a straight line with a slope equal to $(-E_{\alpha}/R)$.

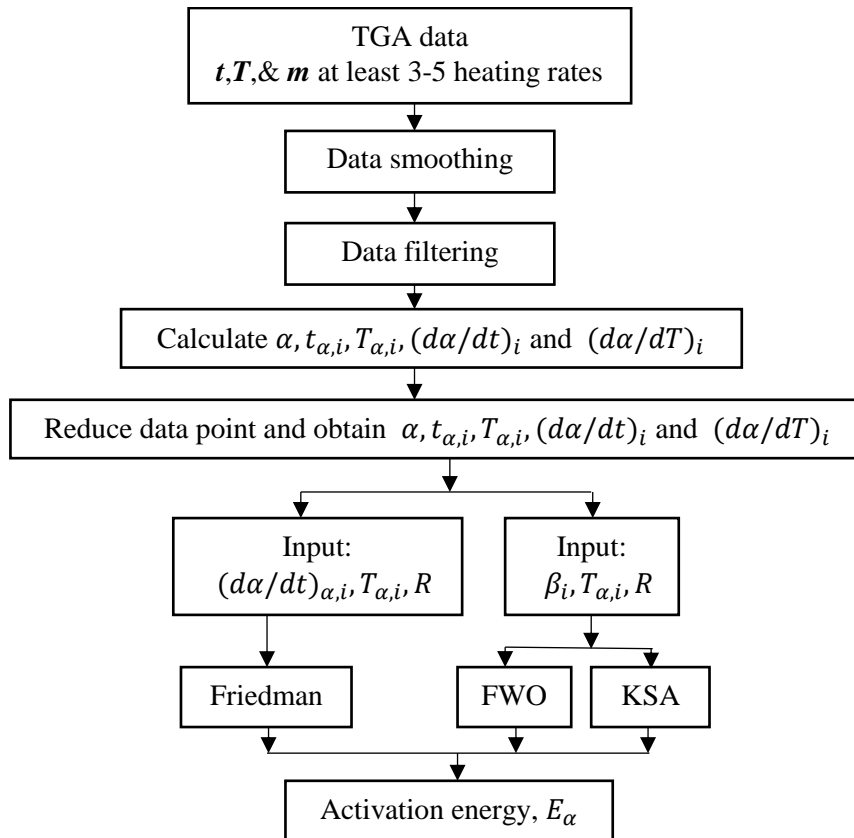


Figure 3.4. Steps involved in finding activation energy through isoconversional method

3.5. Detailed multistep kinetic scheme of biomass pyrolysis

Always referring to the previous seven reference components of Figure 2.2, a multicomponent and multi-step kinetic mechanism of primary biomass pyrolysis is reported in Table 3.1. [28]

Table 3.1. Multistep Kinetic Scheme of Biomass Pyrolysis

N°	Pyrolysis Reactions		Kinetic Parameters A(s ⁻¹), Ea (kcal/kmol)	ΔHr() (kcal/kmol)
Cellulose				
1	CELL	→ CELLA	$1.5 * 10^{14} * \exp(-47000/RT)$	-1300
2	CELLA	→ 0.45 HAA+0.2 GLYOX+0.1 MECO+0.25 HMFU+0.3 ALD3+0.15 CH ₃ OH+0.4 CH ₂ O+0.31 CO+0.41 CO ₂ +0.05 H ₂ +0.83 H ₂ O+0.02 HCOOH+0.2 G{CH ₄ }+0.05 G{H ₂ }+0.61 CHAR	$2 * 10^6 * \exp(-19100/RT)$	27100
3	CELLA	→ LVG	$4 * T * \exp(-10000/RT)$	23200
4	CELL	→ 5 H ₂ O+6 CHAR	$6.5 * 10^7 * \exp(-31000/RT)$	-62700
Hemicellulose				
5	HECELL	→ 0.58 HCE1+0.42 HCE2	$1 * 10^{10} * \exp(-31000/RT)$	-5000
6	HCE1	→ 0.025 H ₂ O+0.5 CO ₂ +0.025 HCOOH+0.5 CO+0.8 CH ₂ O+0.125 ETOH+0.1 CH ₃ OH+0.25 C ₂ H ₄ +0.125 G{H ₂ }+0.275 G{CO ₂ }+0.4 G{COH ₂ }+0.45 G{CH ₃ OH}+0.325 G{CH ₄ }+0.875 CHAR	$1.2 * 10^9 * \exp(-30000/RT)$	-500
7	HCE1	→ 0.25 H ₂ O+0.8 CO ₂ +0.05 HCOOH+0.1 CO+0.15 G{CO}+0.15 G{CO ₂ }+0.2 G{H ₂ }+0.3 CH ₂ O+1.2 G{COH ₂ }+0.625 G{CH ₄ }+0.375 G{C ₂ H ₄ }+0.875 CHAR	$1.5 * 10^{-1} * T * \exp(-8000/RT)$	-42400
8	HCE1	→ XYLAN	$3 * T * \exp(-11000/RT)$	17900
9	HCE2	→ 0.2 H ₂ O+0.175 CO+0.275 CO ₂ +0.5 CH ₂ O+0.1 ETOH+0.2 HAA+0.025 HCOOH+0.25 G{CH ₄ }+0.3 G{CH ₃ OH}+0.275 G{C ₂ H ₄ }+0.4 G{CO ₂ }+0.925 G{COH ₂ }+CHAR	$5 * 10^9 * \exp(-33000/RT)$	12000
Lignins				
10	LIGC	→ 0.35 LIGCC+0.1 COUMARYL+0.08 FENOL+0.41 C ₂ H ₄ +1.0 H ₂ O+0.7 G{COH ₂ }+0.3 CH ₂ O+0.32 CO+0.495 G{CH ₄ }+5.735 CHAR	$1.33 * 10^{15} * \exp(-48500/RT)$	-10300
11	LIGH	→ LIGOH+0.5 ALD3+0.5 C ₂ H ₄ +0.25 HAA	$6.7 * 10^{12} * \exp(-37500/RT)$	30700
12	LIGO	→ LIGOH+CO ₂	$3.3 * 10^8 * \exp(-25500/RT)$	26000
13	LIGCC	→ 0.3 COUMARYL+0.2 FENOL+0.35 HAA+0.7 H ₂ O+0.65 G{CH ₄ }+0.6 G{C ₂ H ₄ }+G{COH ₂ }+0.4 CO+0.4 G{CO}+6.75 CHAR	$1.67 * 10^6 * \exp(-31500/RT)$	-31100
14	LIGOH	→ LIG+0.9 H ₂ O+0.1 CH ₄ +0.6 CH ₃ OH+0.1 G{H ₂ }+0.3 G	$1 * 10^8 * \exp(-30000/RT)$	-26100

			{CH ₃ OH}+0.05 CO ₂ +0.55 CO+0.6 G{CO}+0.05 HCOOH +0.85 G{COH ₂ }+0.35 G{CH ₄ }+0.2 G{C ₂ H ₄ }+4.15 CHAR		
15	LIG	→	0.7 FE2MACR+0.3 ANISOLE+0.3 CO+0.3 G{CO}+0.3 MECHO	$4 * T * \exp(-12000/RT)$	46200
16	LIG	→	0.95 H ₂ O+0.2 CH ₂ O+0.4 CH ₃ OH+CO+0.2 CH ₄ +0.05 HCOOH+0.45 G{CO}+0.5 G{COH ₂ }+0.4 G{CH ₄ } +0.65 G{C ₂ H ₄ }+0.2 MECHO+0.2 ALD3+5.5 CHAR	$4 * 10^8 * \exp(-30000/RT)$	-21100
17	LIG	→	0.6 H ₂ O+0.4 CO+0.2 CH ₄ +0.4 CH ₂ O+0.2 G{CO}+0.4 G {CH ₄ }+0.5 G{C ₂ H ₄ }+0.4 G{CH ₃ OH}+2 G{COH ₂ } +6 CHAR	$8.3 * 10^{-2} * T * \exp(-8000/RT)$	-83600
Extractives					
18	TGL	→	ACRO+3 FFA	$7 * 10^{12} * \exp(-45700/RT)$	1300
19	CTANN	→	FENOL+ITANN	$5 * 10^1 * \exp(-11000/RT)$	1300
20	ITANN	→	6 CHAR+3 CO+3 H ₂ O	$1.5 * 10^{-2} * \exp(-6100/RT)$	10100
Metaplastic					
21	G{CO ₂ }	→	CO ₂	$1 * 10^6 * \exp(-24000/RT)$	-29100
22	G{CO}	→	CO	$5 * 10^{12} * \exp(-50000/RT)$	-13400
23	G{COH ₂ }	→	CO+H ₂	$5 * 10^{11} * \exp(-71000/RT)$	48600
24	G{H ₂ }	→	H ₂	$5 * 10^{11} * \exp(-75000/RT)$	0
25	G{CH ₄ }	→	CH ₄	$5 * 10^{12} * \exp(-71000/RT)$	0
26	G{CH ₃ OH}	→	CH ₃ OH	$2 * 10^{12} * \exp(-50000/RT)$	0
27	G{C ₂ H ₄ }	→	C ₂ H ₄	$5 * 10^{12} * \exp(-71000/RT)$	0

3.6. Heat transfer model

During the pyrolysis process, the pores of the solid are enlarged and the solid particle merely becomes more porous, the biomass converts into gases, volatiles, and char. Inside the pyrolysis particle, heat is transmitted by the following mechanisms:

- conduction inside the solid particle,
- convection inside the particle pores and
- convection and radiation from the surface of the particle/pellet.

For simplicity, it is assumed that heat is transmitted inside the solid by conduction only. The heat transfer coefficient represents the overall effect of the above mechanisms. The temperature distribution along the radius of the biomass particle was described by Fourier's law of heat conduction that has the mathematical form:

$$\frac{\partial T}{\partial t} = \frac{k}{\rho_{true} C_p} \left[\frac{\partial^2 T}{\partial r^2} + \frac{2}{r} \frac{\partial T}{\partial r} \right] \quad (3.31)$$

with the following boundary conditions:

$$r = 0, \quad \frac{\partial T}{\partial r} = 0 \quad (3.32)$$

$$r = R, \quad -k \frac{\partial T}{\partial r} = h * (T_s - T_{sys}) \quad (3.33)$$

The surface temperature, T_s (K), could be determined by solving Equation (3.33) numerically with Crank–Nicolson implicit scheme. In solving Equation (3.32), the temperature change in the system during the heating period and the particle shrinkage were included. The initial temperature of the particles was assumed to be uniform at room temperature (25°C) in any radius position. For simplification, several assumptions were applied in developing the model:

- the shape of the biomass particle is spherical.
- the mechanism of heat transfer inside the biomass particle is only conduction.
- the temperature gradient inside the biomass particle is a function of the radius position with surface temperatures less than or equal to the temperature in the system ($T_s \leq T_{sys}$).
- Some physical properties of the biomass such as density, specific heat capacity, and thermal conductivity are constant.

The set of parameter values used in the calculation is as follows: $h = 5.69 + 0.0098 T_{sys}$ (Ahuja et al., 1996), $C_p = 1449 \text{ J kg}^{-1} \text{ K}^{-1}$, $k = 0.156 \text{ Wm}^{-1} \text{ K}^{-1}$, $\rho_{bulk} = 289 \text{ kg m}^{-3}$ and $v = 0.226$ [69]. The simulation process was run by using computer programming on the MATLAB platform

(Version R2020a). The true density of the biomass particle was calculated by using the following equation:

$$\rho_{true} = \frac{\rho_{bulk}}{(1 - v)} \quad (3.34)$$

Where v is the voidage.

3.7. Solution Strategy

Since the computational domain consists only of one cell, the only mechanism influencing the evolution of the species concentration and of the temperature are the chemical reactions. The evolution of species was determined by the following equation:

$$\frac{\partial \rho Y_i}{\partial t} = \omega_i(Y_i, T) \quad (3.35)$$

Y_i , ω_i , T , ρ , t are the species mass fraction, the reaction rate, the temperature, the density, and the time, respectively.

Briefly summarized the solution can be obtained as follows:

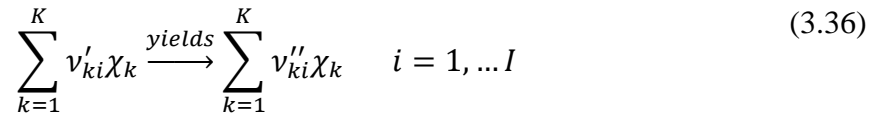
- Solve the chemistry: The purpose is to get the reaction rates for each species involved and the heat realized by the chemical reaction.
- Solve the species equation: The purpose is to get the species concentration at the new time step.
- Solve the energy equation (heat transfer equation): Here we get the temperature at the new time step.

The source code can be found in appendix C.

3.7.1. Chemical reactions

3.7.1.1 Chemical equations

An elementary chemical reaction involving K species in I reactions are summarized in Table 3.1 and can be expressed in the following form:



v'_{ki} , v''_{ki} and χ_k are the forward, the backward stoichiometric coefficient, and the chemical symbol of the specie k , respectively.

3.7.1.2 Chemical reaction rate

Having established the chemical reactions which are desired to be solved, the next step is to describe the velocity at which the chemical reaction occurs, i.e. the change of the concentration of the single species with time. The reaction rate of the reaction i can be written as:

$$\omega_i = k_{fi} \prod_k [X]_k^{v'_{ki}} - k_{ri} \prod_k [X]_k^{v''_{ki}} \quad (3.37)$$

k_{fi} and k_{ri} are the forward and reverse rate constant reaction i . Note that pyrolysis is an irreversible reaction, therefore, $k_{ri} = 0$. k_{fi} are calculated by the equation (3.23).

In order to get the reaction rate of the species k , the reaction rates of each reaction containing the species k have to be multiplied with the stoichiometric coefficient and summed with a positive sign if the species is a product in with, a negative sign if the species is a reactant. It can be written as:

$$\omega_k = \sum_i \omega_i (v'_{ki} - v''_{ki}) \quad (3.38)$$

CHAPTER 4. RESULT AND DISCUSSION

4.1 Proximate and elemental composition

The proximate and ultimate analysis results are presented in Table 4.1. The result from proximate analysis show CP contains a high volatile matter content (78.82%), this indicates that CP has tremendous potential as a source of biofuel because liquid chemicals mainly originate from it. From the ultimate analysis results, the CP contains 59.31% C, 9.78% H, 2.08% N, 28.74% O, and 0.11% S on a weight dry-ash free weight basis. It is important to note that the hydrogen content is relatively high compared to the average of woody biomass. Ash content of CP is also lower than woody biomass, note that the ash content and composition may have a significant impact on overall biomass pyrolysis performance according to literature, the elements contained in it can act as a catalyst.

During the pyrolysis process, CaO can enhance the hydrogen gas content while also increasing the char content as well; Fe₂O₃-Al₂O₃ catalyst is known to have a positive impact on hydrogen production; Fe₂O₃ (hematite) can facilitate the breakdown of tar and oxidation of phenols produced [12]. Ash composition determination was beyond the scope of the present study but we highly recommend further studies to take this into account. The higher heating value (HHV) and lower heating value (LHV) of CP can be calculated by using the equations (4.1) and (4.2).

$$HHV(\text{MJ}/\text{kg}) = 0.338C + 1.428(H - O/8) + 0.095S \quad (4.1)$$

$$LHV(\text{MJ}/\text{kg}) = HHV(\text{MJ}/\text{kg}) - 8.396 * H * 2.442 \quad (4.2)$$

where C, H, O, and S are the presence of carbon, hydrogen, oxygen, and sulfur content in CP respectively on a weight dry-ash free basis [36].

Table 4.1. Main characteristic of cassava peels sample

Proximate analysis (wt%, as-received basis)	
Moisture	8.28
Volatile matter	78.82
Fixed Carbon	7.49
Ash	5.41
Ultimate analysis (wt%, dry ash-free basis [81])	
C	59.31
H	9.78
N	2.08
S	0.11
O	28.74
Molecular formula	CH _{1.98} N _{0.03} S _{0.0007} O _{0.36}
Heating value (MJ/kg, dry basis)	
HHV	28.29
LHV	26.88

4.2 Thermal degradation process

The Thermogravimetric analysis was conducted under argon conditions to create an inert atmosphere during the experiment. The performance of the TG and DTG curves shows similar behavior at different heating rates (Figure 4.1). The degradation of lignocellulosic compounds begins at temperature exceeding 150°C [25]. A large peak is observed in the range of temperature between 250 and 380 °C and corresponds to the degradation of cellulose. Two other peaks, which are more or less perceptible depending on the type of biomass, can be seen overlapping the cellulose peak. Thus, at temperatures between 200 and 300 °C, the degradation of hemicellulose occurs, which proves a deformation of the cellulose peak in that temperature range. Finally, lignin is the component with the most complex structure, and its decomposition range is the widest, occurring from temperatures lesser than 200 °C to the final temperature of the analysis. The degradation of lignin is more significant near the 450 °C zone, where a small peak can be observed that overlaps with the end of the cellulose degradation.

The positions and especially the value of the peaks are dependent on the heating rate of the pyrolysis process. The higher the heating rate, the higher are the peaks temperatures as observed in Figure 4.1. At a higher heating rate, the heat transfer efficiency is generally low because the core temperature would be relatively lower than the outer surface temperature. The heating rate also greatly affects the conversion process leading to different product distribution as well. The heating rate greatly affects the conversion process leading to different product distribution.

Ideally, the Thermogravimetric analysis must be done at a constant heating rate for each run, the increase of temperature with respect to the time must remain constant. However, as shown in Figure 4.1, d, the temperature change over time does not follow a straight line, for temperatures below 450 °C, a constant heating rate is observed and, results in constant slopes for the 4 runs (5K / min, 15K / min 20K / min, and 30K / min). Above 450 °C, the apparatus used for the thermogravimetric experiment had difficulty in maintaining constant the heating rate, that is why we can observe irregularities. This is due to the low thermal power of the device which cannot exceed 30K/min. However, as more than 60% of the degradation takes place at less than 400°C, it is still possible to exploit usefully the data of the experiment, but with special attention to the high temperatures and heating rate.

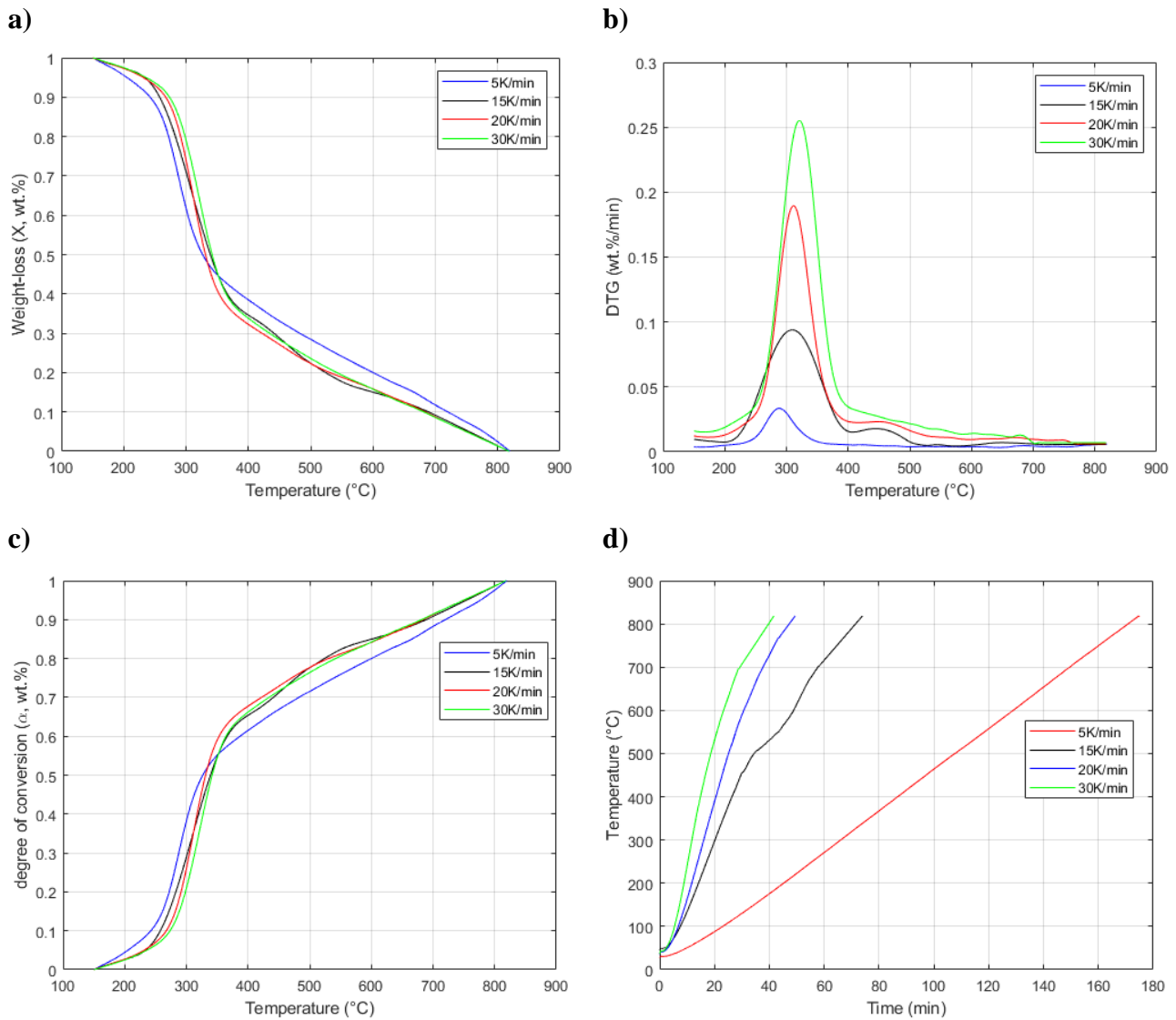


Figure 4.1. TG and DTG curves of CP pyrolysis. a) X curves; b) DTG curves; c) α curves; d) Temperature vs time curves.

4.3 Lignocellulosic composition

4.3.1. Analytical/chemical Method

The lignocellulosic biomass wt.% composition was determined by chemical methods within the laboratories of the School of Chemical engineering at Jimma Institute Technology. The results are summarized in Table 4.2. The results obtained are in-line with the general composition of biomass: Cellulose (30–55 wt %), hemicellulose (13–35 wt %), lignin (14–36 wt %), and extractives lower than 15–20% [24]. Note that CP contains a large amount of extractives: around 15%, this is due to the high starch content of cassava products [82], [83].

Table 4.2. Lignocellulosic composition of Cassava peels, experimental result on DAF basis

Component	Result			Average value
	Run 1	Run 2	Run 3	
Extractives	14.96	15.67	16.06	15.56±0.40
Hemicellulose	29.79	29.40	29.63	29.59±0.13
Cellulose	33.90	34.50	33.70	34.03±0.31
Lignin	20.59	21.02	20.79	20.8±0.14

NB: the average result is reported as a mean value with average deviation values of three replicates.

4.3.2 Prediction based on elemental composition

From the result obtained by elemental analysis, it is clear that CP is a type of biomass rich in hydrogen compared to the average of the majority of biomass. The method proposed by Debiagi et al. [30], which extends the characterization of biomass from the elemental composition by taking into account the extractive compounds, is only valid if the H / C ratios are in a certain area as shown in Figure 3.2. The same study conducted on more than 600 types of biomass concluded that the TGL content in RM2 species increases with the hydrogen content while for biomass low in hydrogen, the TGL content tends towards zero in favor of TANN. Thus, biomass rich in hydrogen can be subdivided only into RM1 and RM2 species and those very low in hydrogen into RM1 and RM3. Recall that RM1 species contains cellulose and hemicellulose (60% cellulose contains 40% hemicellulose by default if the experimental data are not available), RM2 includes hydrogen-rich lignin (LIG-H) and a portion of LIG-C in a ratio of 80% LIG-H against 20% of LIG-C. As for the RM3 group, this contains the oxygen-rich lignin (LIG-O) and a small amount of LIG-C in a ratio of 80% LIG-H against 20% LIG-C.

The reference species RM-1 remains a proper average of cellulose and hemicellulose, the reference lignin mixtures (RM-2 and RM-3) are more flexible and they can move toward the reference species TGL or TANN, depending on the biomass composition, including, in this way, most of the biomass samples. As mentioned earlier, for biomass rich in hydrogen, the amount of TGL progressively increases in the RM-2 mixtures. Similarly, for biomass with low hydrogen content, the reference mixture RM-3 increases its content of the reference component of tannin species (TANN).

As an example, the hybrid poplar with an elemental composition (on a daf basis) of H/C/O = 0.0565/0.5092/0.4343, outside the applicability range of the previous model, is now characterized including 20% TANN in RM-3. Thus, the splitting parameters become $\alpha/\beta/\gamma/\delta/\varepsilon = 0.6/0.8/0.8/1/0.8$, where the value $\varepsilon = 0.8$ means that 80% of lignins (LIGO and LIGC) and 20% of TANN are combined to define RM-3. In this way, the biomass with low H content also

enters into the characterization region. The solution of the linear system of H/C/O balance equations gives the following mass composition of the reference mixtures:

$$\text{RM-1} = 0.5597 \quad \text{RM-2} = 0.0020 \quad \text{RM-3} = 0.4384$$

The amount of the reference mixture RM-2 is very low, because of the low hydrogen content and can be neglected compared to the other references. Thus, these biomass results are mostly split between RM-1 and RM-3. Similarly, biomass with high hydrogen content is mostly split between RM-1 and RM-2.

Cassava peels with H / C / O = 0.0978 / 0.5931 / 0.2874 are outside of the scope of applicability of this method (Figure 4.2). However, the findings of this study can be valued here and allow us mainly to characterize the type of Extractives obtained by the chemical (experimental) method on the one hand and on the other hand allow us to logically define the percentage of each type of lignin. Thus, using the splitting parameters: $\alpha / \beta / \gamma / \delta / \varepsilon = 0.86/0.8/0.8/0.8/1$, it is possible to characterize our sample. The value $\alpha = 0.86$ is taken from the experimental result, the value $\delta = 0.8$ means that 80% of lignins (LIGH and LIGC) and 20% of TGL are combined to obtain RM-2.

The mass composition for the seven reference species of Cassava Peels are presented in Table 4.3.

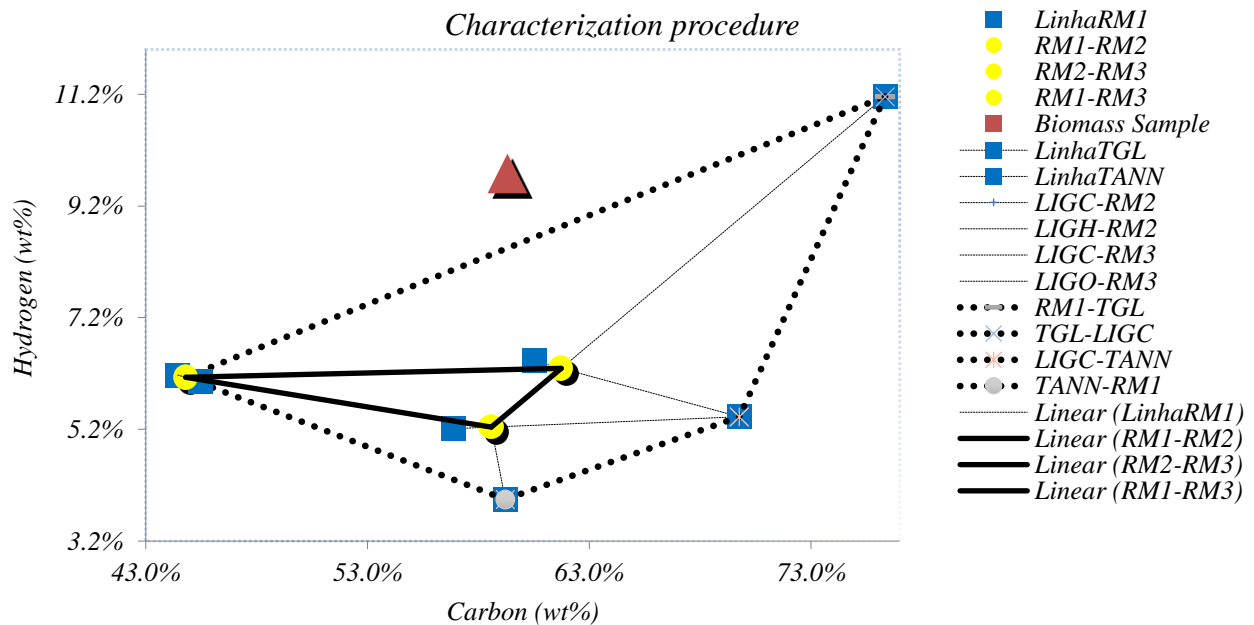


Figure 4.2. Biomass characterization. Reference species and Cassava Peel sample in the H% vs C% plot

Table 4.3. Mass composition for the seven reference species of Cassava Peels

			LIGNIN			EXTRACTIVES			
	CELL	HCELL	LIGC	LIGH	LIGO	TGL	TANN	H2O	ASH
DAF	34.0300	29.5900	2.5761	18.2239	0.0000	15.5600	0.0000	-	-
wet AF	31.2327	27.1577	2.3644	16.7259	0.0000	14.2810	0.0000	8.2200	-
wet+ash	29.3917	25.5569	2.2250	15.7399	0.0000	13.4392	0.0000	8.2200	5.4100

4.2.3 TGA-PKM method

The TGA-PKM method was proposed by D. Díez, et al. [25] for fast determination of the lignocellulosic composition of biomass in weight % on a dry and ash and extractives-free basis. From that study D. Díez, et al. [25], it was difficult to isolate the extractives from the other components during the thermogravimetric analysis (TGA) since the extractives thermally degrade in the temperature range of 200–400 °C, which falls within the range in which hemicellulose, cellulose, and lignin are degraded. This approach has been proven to be very effective for the fast determination of the main component of the majority of biomass namely: cellulose, hemicellulose, and lignin. However, for biomass rich in extractives such as cassava peels, for example, this method has limits since during thermal degradation, the extractive compounds also degrade.

In this study, it is proposed to extend the method by taking into account extractives compounds, this increases the number of pseudocomponents and therefore the number of parameters to be estimated. Therefore the convergence of the method becomes very problematic and invites the researchers to be more astute in the choice of the initial conditions.

First, it was necessary to determine the minimum number of pseudocomponents needed to adequately represent the evolution of each of the four fractions (cellulose, hemicellulose, lignin, and extractive) and all volatiles generated during the thermal degradation process. For this, in the present study, the degradation behavior of each one of these four components was assumed to be as presented by Debiagi et al. [30] (see Figure 3.3). From the DTG curves of these components, it can be clearly seen that cellulose presents only one peak, hemicellulose two main peaks, three peaks for lignin, one peak for TGL, and two for TANN. Therefore, for our study, the minimum number of pseudocomponents necessary for the quantification of each fraction is shown in Table 4.4. The use of a larger number of pseudocomponents could induce overfitting.

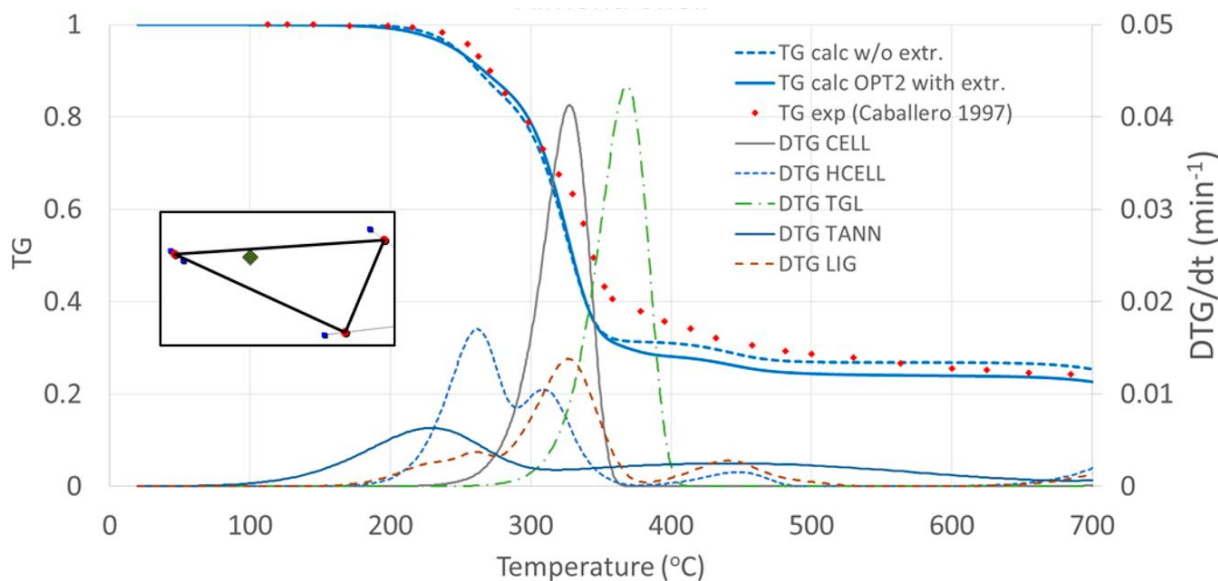


Figure 4.3. TGA and DTG curves of biomass components [30]

Table 4.4. Minimum number of components for each biomass fraction.

Component	Temperature Range, °C	Number of Pseudocomponents
Hemicellulose	200–350	2
Cellulose	250–350	1
Lignin	150–1000	3
TGL	280-400	1
TANN	150-1000	2

As discussed previously, this method is very sensitive to the initial conditions of the kinetic parameters. These initial values must be chosen carefully (Table 4.6). Moreover, to improve the accuracy of estimation of the kinetic parameters, it was found that the use of upper and lower limits of the kinetic parameters (Tables 4.7 and 4.8) was necessary, not only to ensure adequate values of the pre-exponential and activation energy but, also, to provide adequate seed values for the determination of the hemicellulose, cellulose, lignin and extractives fractions. . A single heating rate of 20K/min was employed in the determination of the main lignocellulosic fractions. A low heating rate achieves a better separation of the degraded compounds and is less time-consuming. However, it is possible to use three or more heating rates for the quantification of the four main fractions but this is more time-consuming and it does not change much to the final results [25].

It is important to note that the greater the number of variables to be estimated, the more difficult the algorithm has to converge towards a realistic solution, so it is important to reduce the number of variables as much as possible. In this study, as discussed in the previous section, the probability of having TANN type extractives is very low and these can therefore be assumed

to be non-existent in the sample used in this study, the related pseudocomponents are thus reduced to zero in the solution.

Table 4.6. Initial kinetic parameters of the pseudocomponents (PC).

Kinetic Parameters	PC 1	PC 2	PC 3	PC 4	PC 5	PC 6	PC 7	PC 8	PC 9
K (s ⁻¹)	8.20*10 ⁶	1.40*10 ⁵	9.44*10 ¹³	5.03*10 ⁰¹	6	1	1.55*10 ⁵	2.00	2.00
E (kJ mol ⁻¹)	95.00	125.00	175.00	45.00	35.00	50.00	90.00	45.00	45.00
X _{j,0} (wt.%)	0.25	0.09	0.32	0.03	0.18	0.03	0.15	0.00	0.00

Table 4.7. Lower bounds of the pseudocomponents (PC).

Kinetic Parameters	PC 1	PC 2	PC 3	PC 4	PC 5	PC 6	PC 7	PC 8	PC 9
K (s ⁻¹)	5.74*10 ⁶	9.82*10 ⁴	6.61*10 ¹³	35.2	3.91	72.3	1.08*10 ⁵	1.40	1.40
E (kJ mol ⁻¹)	66.50	87.50	122.50	31.50	24.50	35.00	63.00	31.50	31.50
X _{j,0} (wt.%)	0.05	0.05	0.32	0.01	0.13	0.00	0.13	0.00	0.00

Table 4.8. Upper bounds of the pseudocomponents (PC).

Kinetic Parameters	PC 1	PC 2	PC 3	PC 4	PC 5	PC 6	PC 7	PC 8	PC 9
K (s ⁻¹)	9.84*10 ⁶	1.68*10 ⁵	1.130*10 ¹⁴	60.4	6.71	1.24	1.86*10 ⁵	2.4	2.4
E (kJ mol ⁻¹)	114.00	150.00	210.00	54.00	42.00	60.00	108.00	54.00	54.00
X _{j,0} (wt.%)	0.25	0.25	0.40	0.05	0.20	0.03	0.20	0.00	0.00

Finally, considering the above, the values of the kinetic parameters of each pseudocomponents were calculated by the TGA-PKM method and are reported in Table 4.9. Note that since we considered that all the extractives in our biomass are TGL type, during the calculation TANN pseudocomponents were not taken into consideration. Overall, the results obtained in this study are in reasonable ranges when compared to the results corresponding to the kinetics of other biomasses published, as can be seen in Table 4.10.

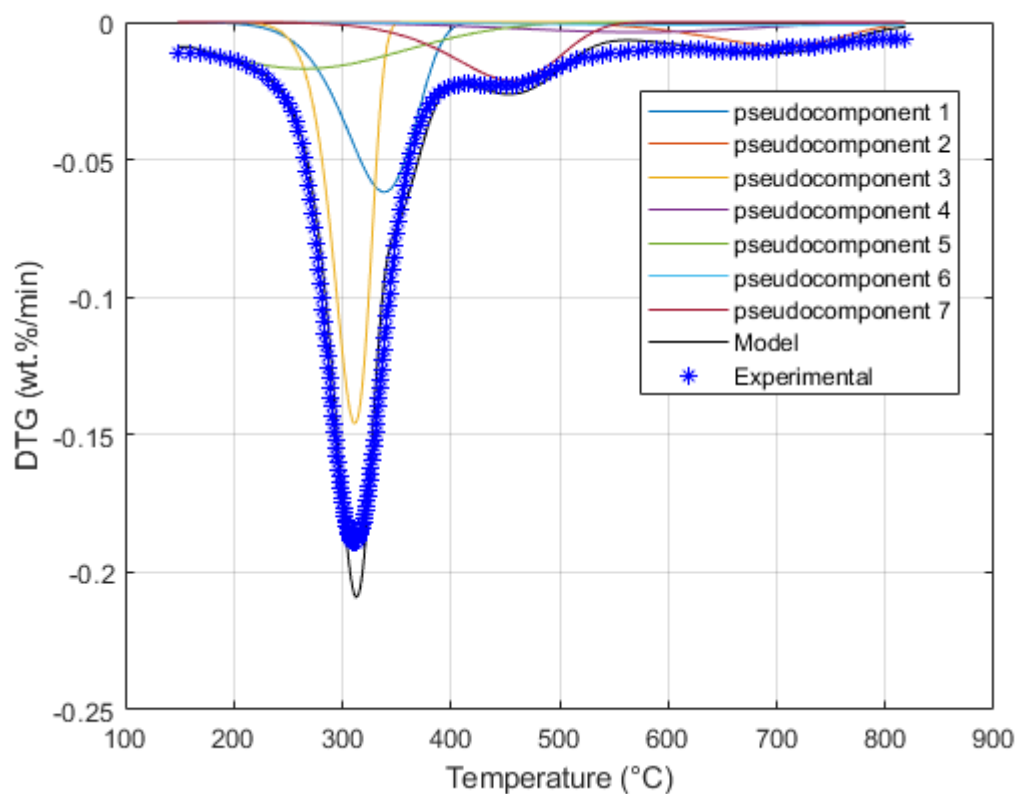
Table 4.9. Kinetic parameters of the pseudocomponents.

Kinetic Parameters	Hemicellulose		Cellulose	Lignin			Extractives
	PC 1	PC 2	PC 3	PC 4	PC 5	PC 6	PC 7
K (s ⁻¹)	9.52*10 ⁶	1.45*10 ⁵	6.70*10 ¹³	60.8	5.08	1.44	1.08*10 ⁵
E (kJ mol ⁻¹)	99.52	130.89	171.29	47.84	33.30	40.85	92.51
X _{j,0} (wt.%)	0.25	0.06	0.32	0.06	0.18	0.03	0.13

Table 4.10. Kinetic parameters from other studies.

Component	Temperature, °C	E, kJ mol ⁻¹	K, min ⁻¹	Reference
Hemicellulose	200–350	127.00	9.5×10^{10}	[84]
		83.20–96.40	4.55×10^6 – 1.57×10^8	[85]
Cellulose	300–340	227.02	3.36×10^{18}	[86]
		239.70–325.00	16.30×10^{19} – 3.62×10^{26}	[85]
Lignin	220–380	7.80	2.96×10^{-3}	[86]
	25–900	47.90–54.50	6.80×10^2 – 6.60×10^4	[87]
	160–680	25.20	4.70×10^2	[88]
		20.00–29.10	5.35×10 –3.18	[85]

Figure 4.4 shows the fit of the model to the DTG experimental data, as well as the contribution of the different pseudocomponents to the model. It can be seen that a good fit is achieved between the global model, obtained as the envelope resulting from the sum of all pseudocomponents, and the experimental curve.

**Figure 4.4.** Model fitted to the experimental DTG curve.

By comparison, between the kinetic constants in Table 4.9 and Figure 4.4, it can be seen that low activation energy leads to a reaction in the low-temperature zone and vice versa. With

respect to the pre-exponential factor, low values cause the reaction rate to be slower and to take place over a wider temperature range, which is characteristic of the lignin pseudocomponents. On the contrary, high values of the pre-exponential factor increase the reaction rate, leading to a narrower temperature range, which is characteristic of cellulose, for example. On the other hand, at the same activation energy, a higher pre-exponential factor causes the reaction to take place in the high-temperature zone. For example, there are lignin pseudocomponents with similar activation energy as hemicellulose pseudocomponents (Table 4.9) but with much lower pre-exponential factors, which cause the reaction to take place at higher temperatures. The quality of the fit is expressed as $R^2 = 0.9765$, and it is a very good convergence.

Let us indicate here the difficulty of convergence of the algorithm to differentiate between cellulose and extractives of the TGL type, indeed these compounds degrade in the same temperature range and at almost the same speed (see Figures 4.4). To force the algorithm, it was important, based on the experimental data to set the cellulose limits in a certain range, so the algorithm is forced to take into account TGL. It is for this reason that the percentage of cellulose in Table 5.9 has fallen to the minimum set in Table 4.7. This difficulty was also reported by D. Diez et al. [25], who did not take into account all extractives in their simulation to get around this problem. This approach gives acceptable results for biomass less rich in extractives, but in our case, this approach would lead to major errors.

TGA-PKM method, therefore, addresses this major problem for the characterization of biomass rich in extractives. TGL behaves almost the same as cellulose, and TANN like lignin (see Figure 4.3). However, the method remains very interesting for the fast determination of lignocellulosic components on a dry, ash, and extractive-free basis. Therefore we recommend this method for the characterization of low extractives biomass. For biomass rich in extractives, this method can still be used, but if and only if, before proceeding with the thermogravimetry experiment, care has been taken to extract the extractive compounds in the biomass. Note that extractives can be easily removed from biomass using organic solvents, such as benzene, alcohol, or water [25].

For validation and comparison purposes, Table 4.11 shows the comparison between the experimentally determined composition and the data obtained with the TGA-PKM method. As it can be seen, despite the difficulties and limitations of this method, there is a good agreement between the data obtained through the experiment and the TGA-PKM model.

Table 4.11. Comparison between the experiment and thermogravimetric analysis pseudocomponent kinetic model (TGA-PKM) results.

Component	Analytical Method wt.%, Dry, Ash and Extractives-Free Basis	TGA-PKM Method wt.%, Dry, Ash and Extractives-Free Basis	Error, wt.%	%Error
Hemicellulose	29.59	30.83	-1.24.	-4.19%
Cellulose	34.03	32.00	2.03	5.96%
Lignin	20.08	26.81	-6.73	-33.66%
Extractives	15.56	13.00	2.56	16.45%

The following error ranges are obtained between the values measured experimentally and those inferred by the TGA-PKM method for each of the main fractions: hemicellulose (−1.24%), cellulose (−2.03%), lignin (−6.73%), and extractive (2.56). The level of accuracy achieved is considered acceptable, taking into account that it is within the error range of the chemical methods. For example, Korpinen et al. [85] found that the determination of lignin by different chemical methods can be as high as 10 wt.%; Ioelovich et al. [89] also determined a difference of 4 wt.% between the TAPPI and NERL methods in the determination of the cellulose content. In this way, the TGA-PKM method allows obtaining a fast estimation of the contents of the main lignocellulosic fractions within the ranges that would be obtained by chemical analysis. Therefore, for biomass with the elemental composition that falls dawn outside, the TGA-PKM method is another option for fast determination of lignocellulosic fractions content.

4.4 Isoconversional kinetic model of CP

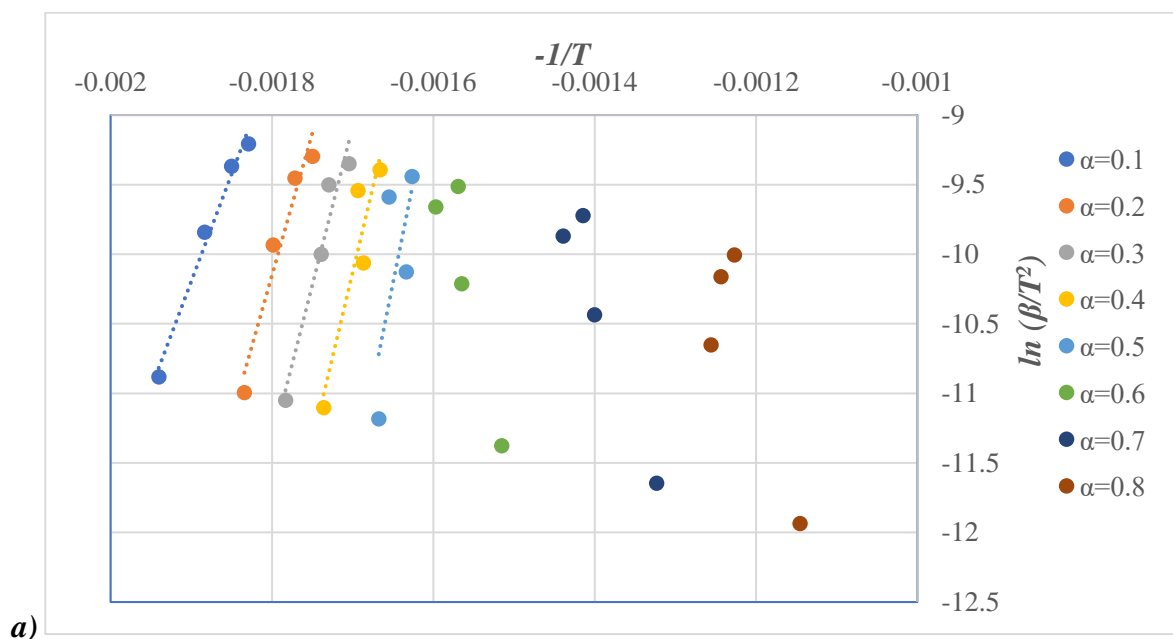
Figures 4.3a, 4.3b and 4.3c show the FWO and KAS and Friedman plots for CP-based pyrolysis processes. The first two are integral methods and are the most popular for the analysis of the kinetics of biomass material during the pyrolysis [36], [57]; the last, Friedman method, is a differential method and is considered to be more precise one as discussed in [57] despite its complexity. As mentioned in section 4.2; During the thermogravimetric analysis, the device used had difficulty in maintaining the heating rate constant due to its low thermal power, so above 400 ° C, the heating rate was fluctuating. This explains the lack of collinearity for conversion rate values greater than 50% (see Figure 4.3). For this reason, the energy activation values were calculated only for the conversion rate below 50%. A simple linear interpolation was applied to estimate the energy activation value above 50% conversion rate.

On the basis of the results found, it can be noted that the three methods give different values. The activation energy varies from 115.52kJ / mol to 341.01kJ / mol for the KSA method, 123.9kJ / mol to 351.4kJ/mol for the FWO method, and 160.05kJ/mol to 602.92kJ/mol for the

Friedman method. The mean activation energy (E_a) of CP calculated using KAS, FWO, and Friedman method was 224.87kJ/mol, 234.3kJ/mol, and 347.87kJ/mol respectively in this study. These values, especially those obtained by FWO and KSA methods are similar to literature values for the traditional biomass pyrolysis process [12].

Table 4.12. Kinetics parameters of cassava peels at different degrees of conversion

Alpha	Friedman			FWO			KSA		
	Ea (kJ/mol)	A (1/sec)	R2	Ea (kJ/mol)	A (1/sec)	R2	Ea (kJ/mol)	A (1/sec)	R2
0.10	160.05	5.16E+09	0.91	123.90	2.17E+07	0.99	115.52	6.03E+06	0.98
0.20	198.75	1.70E+12	0.98	162.93	7.95E+09	0.95	154.11	2.11E+09	0.94
0.30	219.94	4.00E+13	0.95	183.67	1.79E+11	0.95	174.61	4.60E+10	0.95
0.40	255.10	7.40E+15	0.85	200.78	2.30E+12	0.86	191.50	5.76E+11	0.85
0.50	379.05	6.41E+23	0.54	253.11	5.52E+15	0.51	243.51	1.33E+15	0.49
0.60	443.81	8.56E+27		281.96	3.94E+17		272.11	9.19E+16	
0.70	523.37	9.73E+32		316.68	6.63E+19		306.56	1.49E+19	
0.80	602.92	1.08E+38		351.40	1.10E+22		341.01	2.39E+21	
Mean	347.87	1.25E+37	0.85	234.30	1.29E+21	0.85	224.87	2.79E+20	0.84



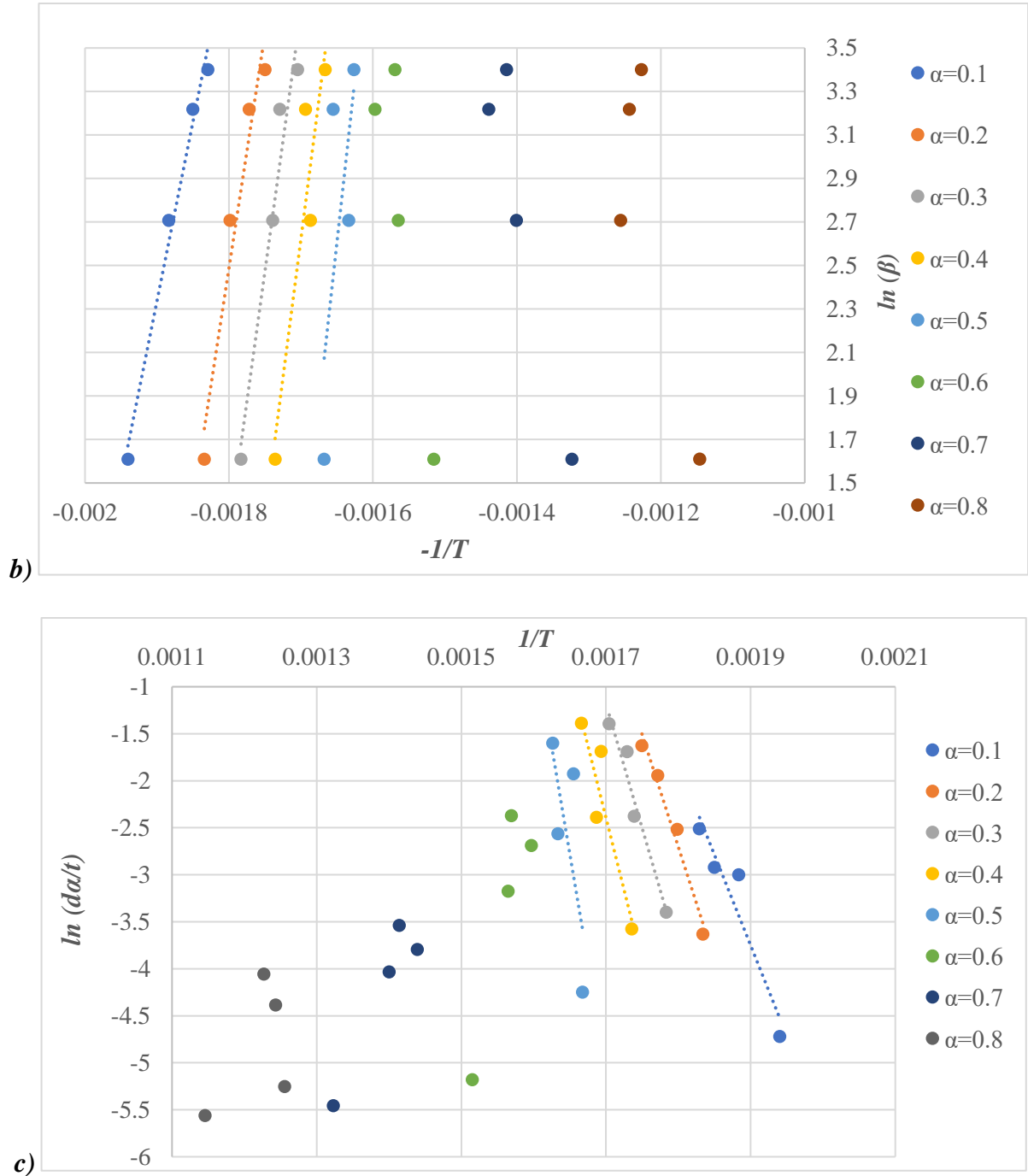


Figure 4.5. Model-free kinetics. a) KAS model. b) FWO model. c) Friedman model

4.5 Thermodynamics of CP

Arrhenius pre-exponential factor (A), enthalpy (ΔH), Gibbs free energy (ΔG), and entropy (ΔS) are the important thermodynamic parameters. As described in [57], these parameters can be calculated based on the activation energy by the following equations.

$$A_{\alpha} = \frac{\beta E_{\alpha} \exp\left(\frac{E_{\alpha}}{RT_m}\right)}{RT_m^2} \quad (4.3)$$

$$\Delta H_{\alpha} = E_{\alpha} - RT_{\alpha} \quad (4.4)$$

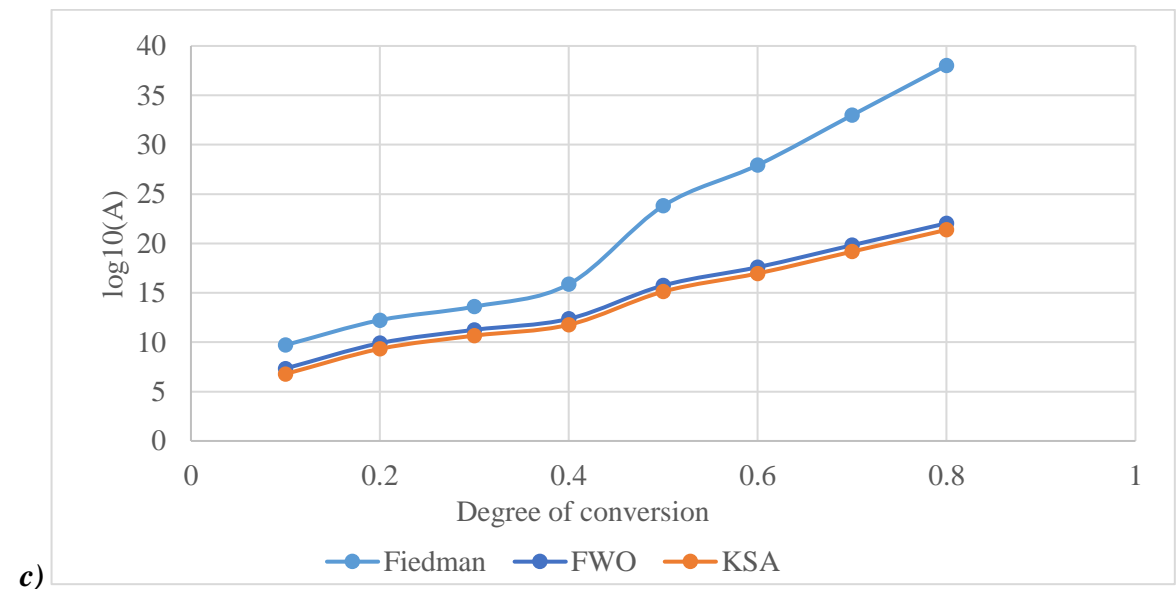
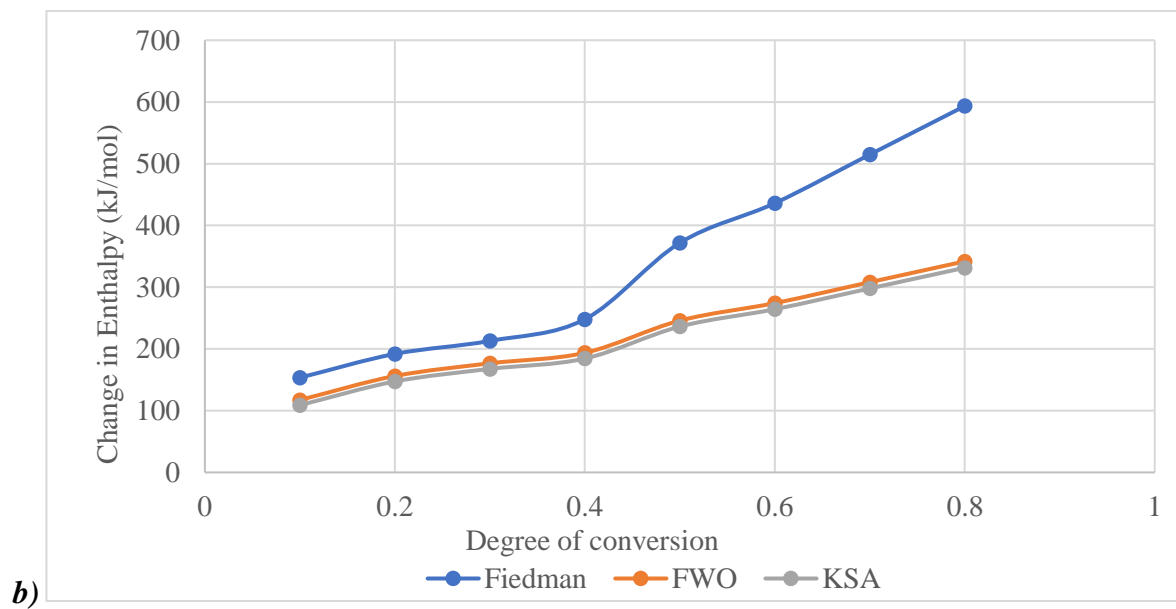
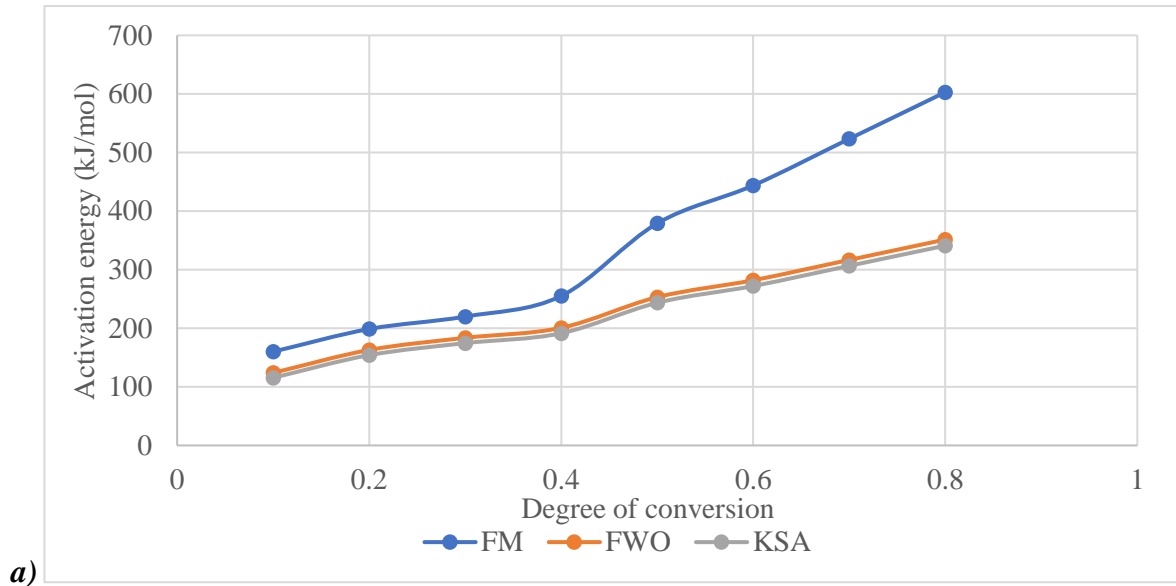
$$\Delta G_{\alpha} = E_{\alpha} - RT_m \ln \left(K_B \frac{T_m}{hA_{\alpha}} \right) \quad (4.5)$$

$$\Delta S_{\alpha} = \frac{\Delta H_{\alpha} - \Delta G_{\alpha}}{T_m} \quad (4.6)$$

where K_B is the Boltzmann constant ($1.38064852 \cdot 10^{-23} \text{m}^2 \text{kg s}^{-2} \text{K}^{-1}$), h is Plank's constant ($6.62607004 \cdot 10^{-34} \text{m}^2 \text{kg s}^{-1}$), β is the heating rate, and T_m is the peak temperature.

Figure 4.6 demonstrates the thermodynamic parameters of CP using the Friedman method. The Arrhenius exponential factor implies the empirical relation between reaction rate coefficient and temperature, varies from 238.16 s^{-1} to $1.71 \cdot 10^{21} \text{ s}^{-1}$ with a mean value of $1.02 \cdot 10^{21} \text{ s}^{-1}$. The enthalpy, total heat content of the system, ranges from 33.48 to 241.26 kJ/mol with a mean value of 111.68 kJ/mol. The Gibbs free energy may be inferred as the energy for the formation of the activated complex. It is also the available energy from biomass associated with the pyrolysis process. The Gibbs free energy (142.64–155.32 kJ/mol) does not change much for either method for different conversion. It has a mean value of 148.61 kJ/mol. The likelihood of the pyrolysis reaction can be determined from the difference between activation energy and enthalpy values. At thermodynamic equilibrium, the change in Gibbs free energy is 0. Since the products are withdrawn from the system continuously, the system never reaches true thermodynamic equilibria as evidenced from the results. The Entropy, the measure of disorder, changes from -217.26 J/K to 162.91 J/K with a mean value of -65.84 J/K .

As biomass pyrolysis is a complex process, a negative entropy value can occur. It is possible to have a lower degree of disorder of the products compared to the reactants due to the bond dissociation. A lower value of ΔS may relate to only physical change and little chemical reactivity. However, higher reactivity and rapid activated complex formation are marked by a higher value of ΔS Kaur et al. [90].



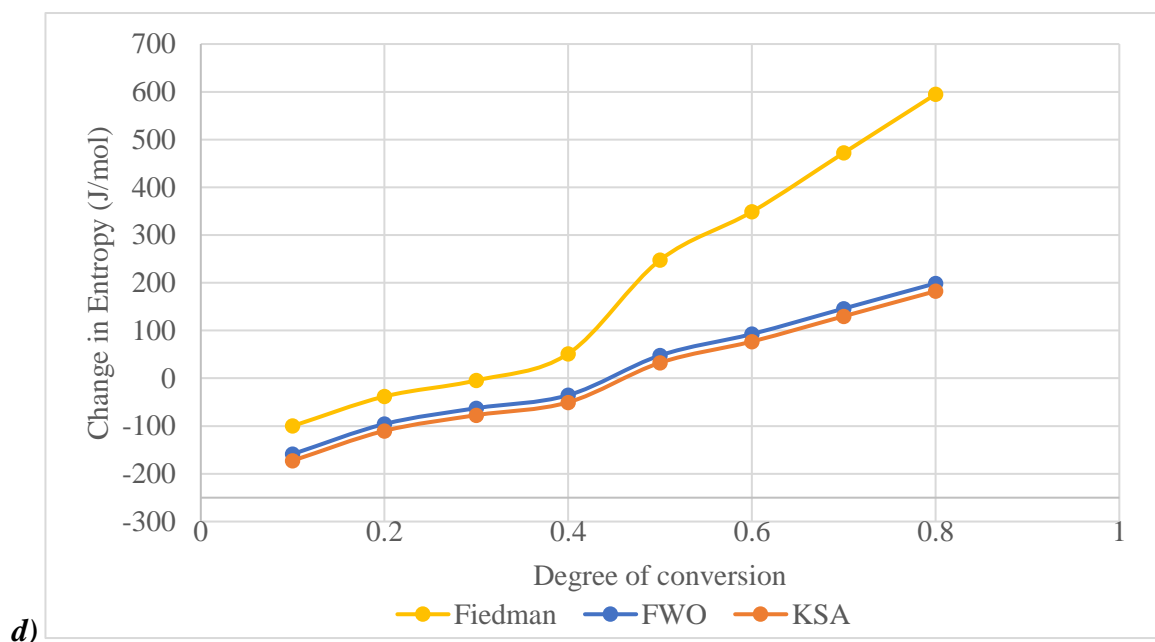


Figure 4.6. Thermodynamic parameters of CP from Friedman, FWO, and KSA method. a) Activation energy. b) Change in Enthalpy. c) \log_{10} (Arrhenius exponential factor). d) Change in Entropy.

4.6 Effect of pyrolysis parameters on released products

This section presents and discusses the findings of the main objective of this thesis work which was to investigate the influence of pyrolysis operating parameters on the bio-oil yield from CP. For a given reactor, the main parameters that influence the pyrolysis process are mainly the heating rate, pyrolysis temperature, vapor residence time, biomass residence time, and particle size of the biomass. For the particle size less than 0.5mm, the effect of the size of the particle can be neglected (see Figure 4.7 and 4.8), this assumption allows considering that the particle heats up instantaneously and therefore we can neglect the temperature difference in the particle as well as heat transfer by convection and radiation within the porous media of the particle. Thus, only the heat transfer by conduction in the particle is dominant.

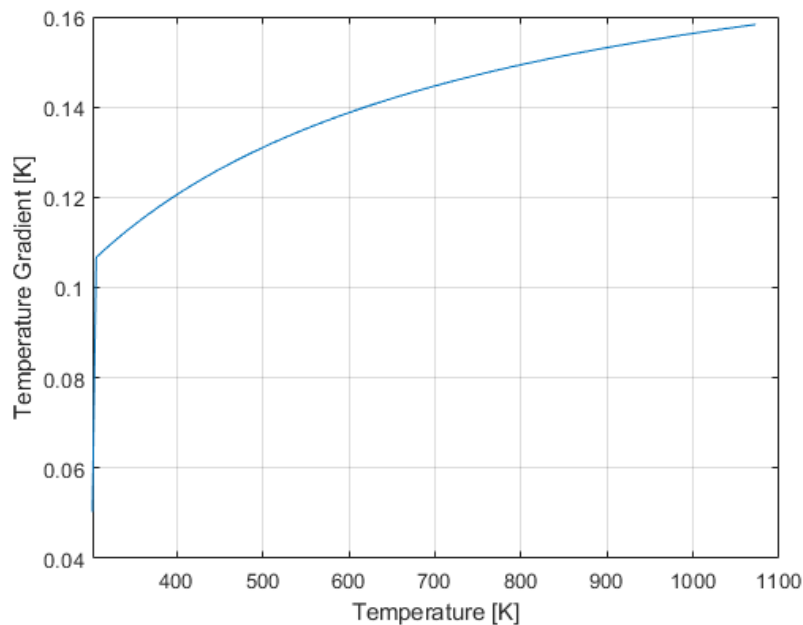


Figure 4.7. Temperature gradient between the surface and the center of the particle
($HR=100K/min$)

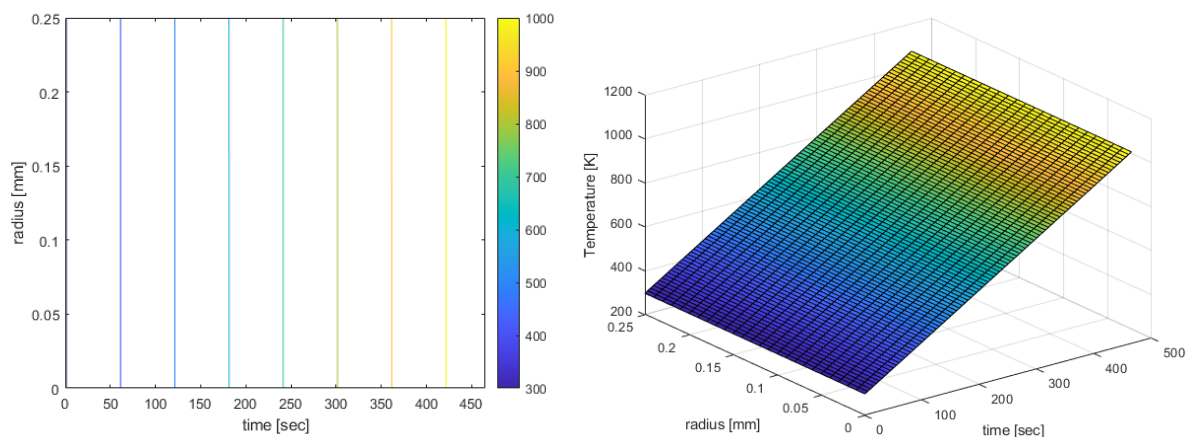


Figure 4.8. Temperature profile as function of reaction time, position at $100K/min$

The longer the biomass traps in the reactor, the more all the biomass has the chance to be broken down into byproducts. Since the objective of this study is to convert all biomass into byproducts (char, gas, and bio-oil), it is important to keep the biomass in the reactor until it is completely converted. So in this section, the objective is to study the effect of the heating rate, vapor residence time, and pyrolysis temperature on the byproduct yields using the multistep detailed kinetics.

An original *Matlab* code had been developed to solve the detailed multistep kinetics of biomass pyrolysis with 27 reactions and 48 species. The developed code gives a similar result to the commercial code developed by Politecnico di Milano inside the CRECK project. Table 4.13

compared the result obtained by the code used in this study with the ones obtained by CRECK software for the same type of biomass. The difference is between -4.35 to -3.89% for solid yield, 0.75 to 1.04 % for gas yield, and 2.36 to 3.4 % for liquid yield, suggesting a very good agreement.

Table 4.13. Comparison between code developed in this study and CRECK software results

	Pine Sawdust		Wheat Straw			
Temperature	700°C		700°C			
Heating rate	80K/min		80K/min			
	Ranzi et al. [23]	Present work	Ranzi et al. [23]	Present work	Error	% Error
Gas yield, %	13.9	13.15	13.3	12.26	0.75-1.04	5.39-7.81%
Liquid yield, %	65.6	62.2	64.5	62.14	2.36-3.4	3.79-6.7%
Solid yield, %	20.3	24.65	21.7	25.59	-4.35 to -3.89	-20.14 to -19.16%

4.6.1 Effect of the heating rate

The heating rate is a very important parameter in the design of pyrolysis reactors. For the same maximum temperature, the higher the heating rate, the faster the biomass is devolatilized and the more likely we are to produce a large quantity of bio-oil. Remember that the main objective of slow pyrolysis is the production of biochar, while fast and flash pyrolysis mainly aims to produce bio-oil. However, during pyrolysis, the bio-oil trend undergoes a secondary reaction commonly known as "tar cracking". the tar cracking depends mainly on the temperature of the reactor and vapor residence time inside the reactor, it does not depend on the heating rate so that this process takes place at the temperature of the reactor.

Studying the effect of all these parameters simultaneously would require more complex algorithms and consume a lot of time. Therefore, in this study, at first, the effect of the heating rate only is investigated by neglecting the effect of tar cracking and for a single pyrolysis temperature. For this, a temperature of 1000K was chosen to ensure that all the biomass was converted. Table 4.14 presents the findings of the present investigation, the bio-oil yield increase with the heating rate.

From the result reported in Table 4.14, It can be seen that the bio-oil yield increase with the heating rate up to a maximum between 80K/min and 100K/min. This is logical because when we move from slow pyrolysis to fast pyrolysis, the bio-oil yield increases. Beyond 100K/min the bio-oil yield starts decreasing when the heating rate increases.

From the above mentioned predicted results, it was inferred that for a given temperature, the bio-oil yield is maximal when the heating rate is between 80K/min and 100K/min, it is therefore advantageous to have a heating rate in that range, but this must match with the technical feasibility of the pyrolysis reactor.

4.6.2 Effect of vapor residence time and pyrolysis temperature.

If one were to neglect tar cracking, the reactor temperature may not have an effect on the yield of bio-oil since the latter does not undergo any secondary conversion in the reactor. On the other hand, it is not realistic to neglect the tar cracking during pyrolysis because the vapors stay some time inside the reactor before it is evacuated, and during this time, they are undergoing a secondary transformation. As it can be logically understood, the greater the residence time, the more the bio-oil is expected to get cracked into gas. To maximize the bio-oil, for a given pyrolysis temperature, it is, therefore, preferable to minimize the vapor residence time in the reactor. The residence time depends mainly on the nitrogen (or other inert gas used) flow rate per volume of the reactor, the larger the reactor, the more inert gas is needed to reduce.

A cost analysis must be carried out in the optimization of vapor residence time for a given reactor since using a high flow rate of nitrogen to create the inert conducive condition for the pyrolysis may be costly in the long term. For some applications, the gas produced by the pyrolysis is used as fuel to heat the reactor, so it is possible to use the CO₂ from the combustion as pyrolysis inert gas to reduce the cost that the use of nitrogen would incur for example. Figure 4.9. gives an illustration of the effect of vapor residence time on bio-oil yield at 800K and heating rate of 80K/min. It is assumed that the reactor temperature remains constant and equal to 800K.

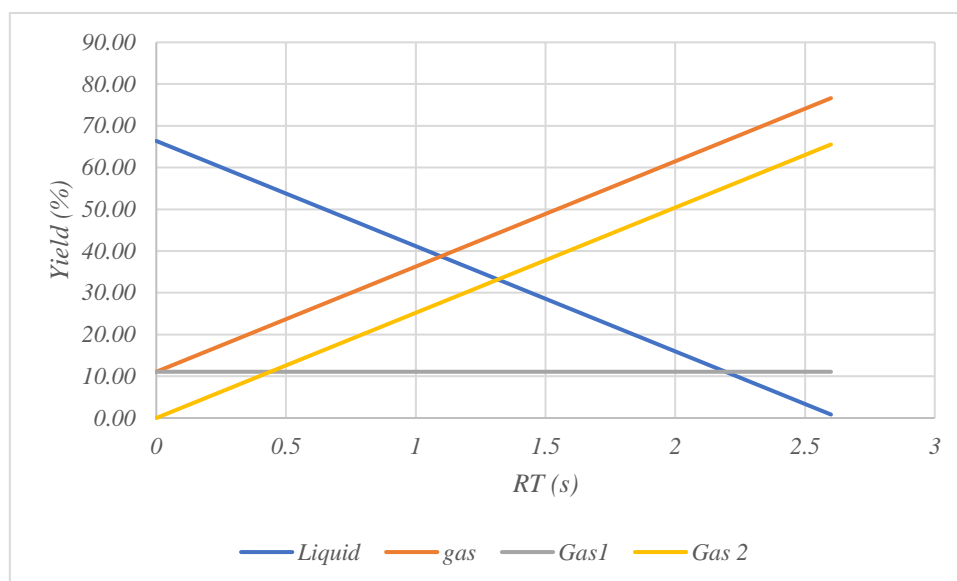


Figure 4.9. Effect of vapor residence time on bio-oil yield at 800K, $\beta=100\text{K/min}$

So far, the effects of the heating rate and the vapor residence time on the bio-oil yield from CP pyrolysis were discussed. However, one of the key parameters remains the pyrolysis temperature which at the same time influences the byproduct yields, the pyrolysis time, and the tar cracking. Although it is recommended to have the heating rate between 80K/min and 100K/min and the residence time as lower as possible, for practical reasons and taking into account the technical feasibility, the impact of the pyrolysis temperature was analyzed by setting $\beta = 100\text{K/min}$ and $RT = 0.25, 0.5, 0.75$ and 1s .

From the results reported in Figure 4.10, one can see that the bio-oil yield increases with the temperature until around 475°C and starts decreasing. For temperatures below 475°C , the tar cracking effect is not very significant but all the biomass did not undergo complete conversion, which justifies a large amount of solids at the end of the process. Above 475°C , the biomass conversion is high but a part of bio-oil is transformed into gas, which justifies the increase in gas in this area. Hence, It can be concluded that the optimum temperature is around 475°C but it is important to note that each type of reactor configuration requires a specific study to optimize the residence time taking into account the geometry and the cost analysis and then move on to the optimization of the temperature.

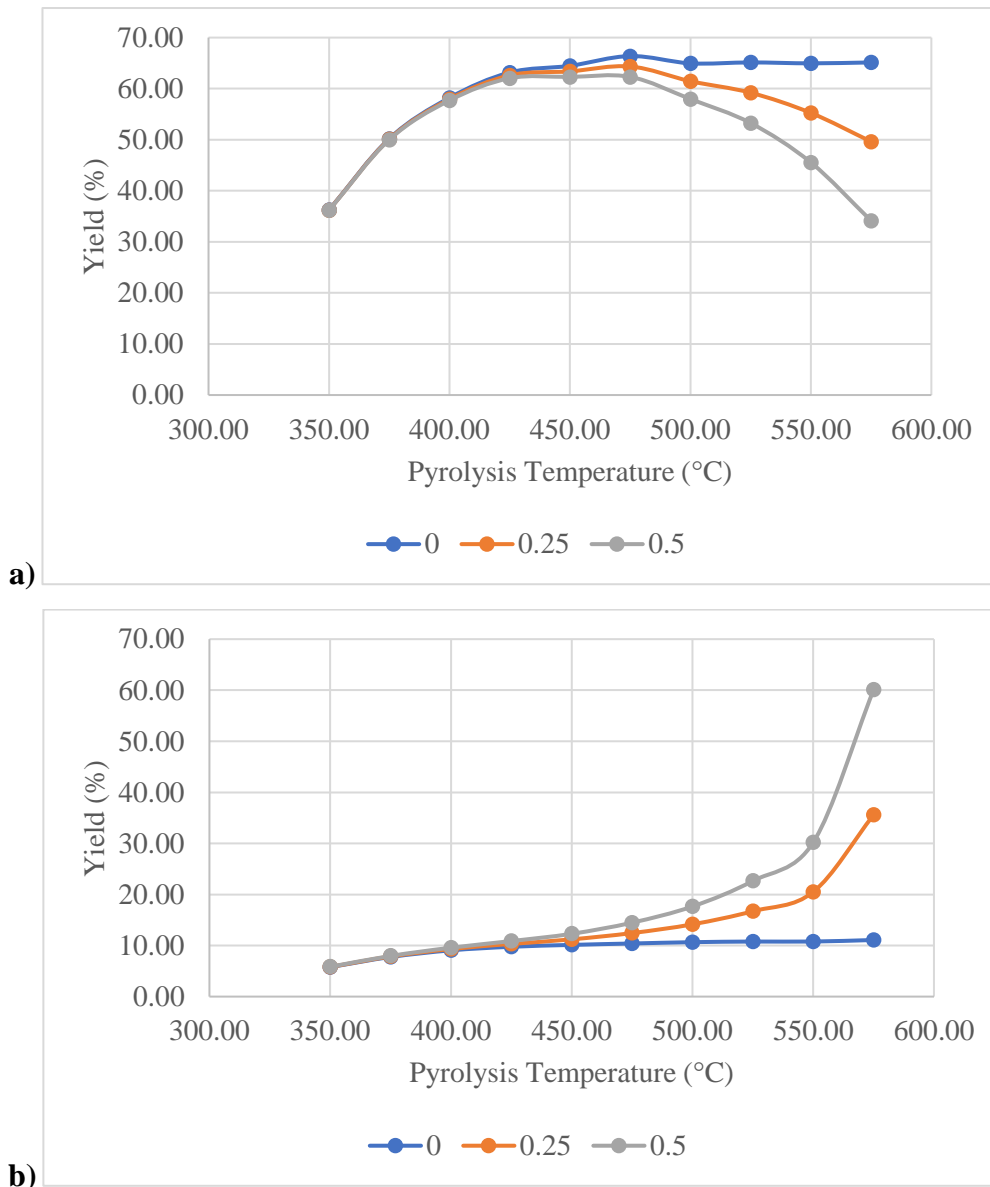


Figure 4.10. Effect of pyrolysis temperature on a) bio-oil yield; b) gas yield

For the sake of comparison, the result from the present model prediction was compared to the experimental result for cassava stalk (CS) and rhizome (CR) published by Pattiya et al.[20]. Their pyrolysis was conducted in a free-fall reactor made up of 304 stainless steel tubes of 1m height and 7.7mm internal diameter, the nitrogen flow rate was equal to 3l/min. From Figure 4.11, one can see that results from this study follow a similar trend with the results from Cassava Stalk (CR) experiment with a maximum bio-oil yield at approximately 475°C.

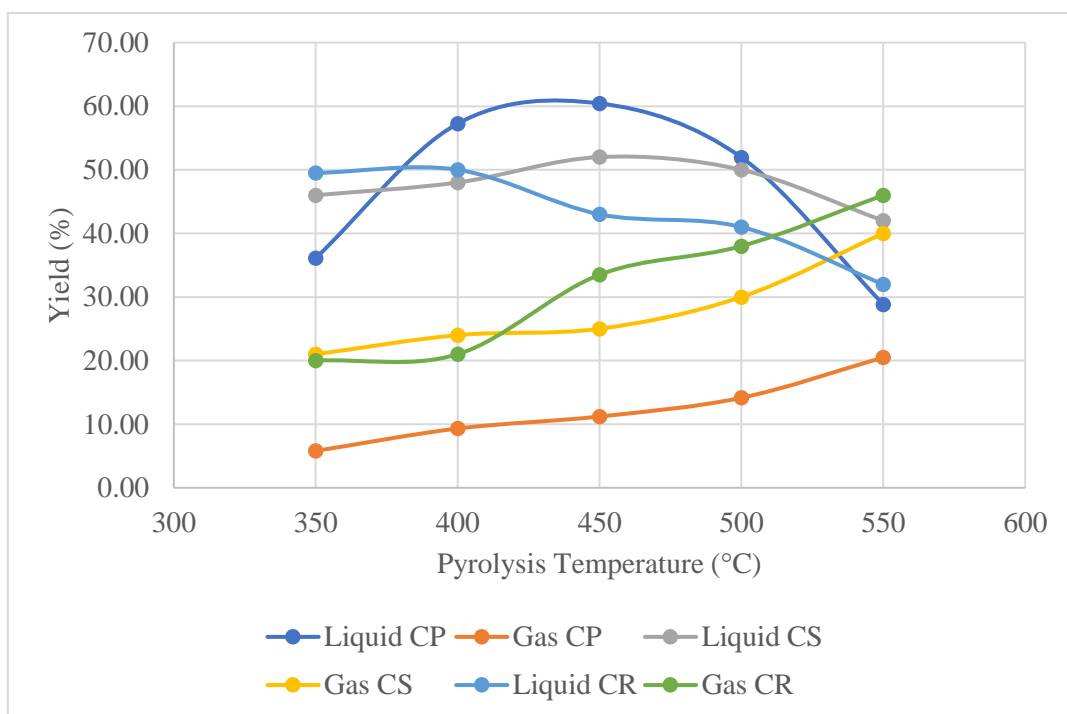


Figure 4.11. Comparison with experimental data, $RT=0.25s$

The similarity between the pyrolysis behavior of cassava peels and cassava stalk can be explained by their high hydrogen content. Indeed, the H_2 content of CR is lower compared to CS [73] and CS. Since the elemental composition of cassava stalk is close to the one of cassava peels, the lignocellulosic composition also may be close.

CHAPTER 5. GENERAL CONCLUSION AND RECOMMENDATIONS

The objectives of this work were to study the influence of pyrolysis operating parameters on the bio-oil yield from cassava peels. Cassava peels were collected from fresh cassava tubers, dried, and ground to get particle size less than 0.5mm. The thermogravimetric analysis carried out allowed to experimentally study the behavior of the thermal devolatilization of CP under four different heating rates. From the integral (FWO and KSA methods) and differential (Friedman method), it was possible to determine the simple one-step kinetic parameters of CP pyrolysis and deduce the thermodynamic parameters such as a change in enthalpy, Gibbs energy, and entropy. Proximate and Ultimate analysis performed, helped to characterize the CP sample and the lignocellulosic composition was determined experimentally using chemical methods. Furthermore, the feasibility of using the TGA-PKM method to determine the lignocellulosic composition was carried out, and finally, using the detailed multistep kinetics models developed by Ranzi et al. [23], a parametric sensitivity analysis was conducted to study the influence of pyrolysis parameters on the released product yield.

Calculation program codes were developed in *Matlab* for the numerical simulation of mathematical models. From the results obtained, the following conclusions can be drawn:

- From proximate analysis alone, it was noticed that CP contains a great potential for producing bio-oil via thermochemical conversion due to its high content in volatile matters (78.82%). Their high hydrogen content (9.5%) was also found to be higher than the average for woody biomass.
- Due to the performance problem of the TGA equipment, it was difficult to maintain the heating rate as constant above 400°C, thus the TGA data above that temperature was not obtained based on a constant heating rate. However, to work around this problem when determining kinetics parameters, computations were made for the conversion rate less than 50% and linear interpolation was used for the conversion rate greater than 50%. The results obtained by KSA and FWO methods were more close to those listed in the literature compared to those obtained by Friedman methods. Friedman's method gave relatively higher values.
- The TGA-PKM method for the fast determination of the lignocellulosic composition of biomass is a very good method for biomass with fewer extractives content. But for the

biomass rich in extractives, this method presents a limitation since the extractive values are devolatilized in the same temperature range as the cellulose and the lignin, and it thus becomes difficult to distinguish between the compounds. Thus it was recommended for these types of biomass rich in extractives, to proceed with the removal of extraction content before going to the TGA experiment so that the analysis is done on dry ash and extractive-free basis.

- The analysis of the influences of pyrolysis operating parameters on the byproduct yield helped to notice that the study of the optimization of these parameters cannot rest only on the technical basis but should involve the cost analysis. The heating rate has a proportional influence on the bio-oil yield but the technical feasibility limits it to increase it indefinitely. The RT should be reduced to a minimum to limit the effect of tar cracking, however for a real reactor it is impossible to override this parameter, however, it can be reduced by increasing the flow rate of the gas used to create the inert condition inside the reactor. Since using a large amount of inert gas can be expensive, the cost analysis must be included when optimizing this parameter.
- Bio-oil production from CP pyrolysis is a very attractive option not only from an environmental point of view by valorizing the cassava residues and thus reducing the pollution due to this waste but also and above all, for its energy contribution, its great potential to produce biofuel from waste. Thus bio-oil from CP pyrolysis can significantly contribute to the UN SDGs in terms of energy, environment, reduction of poverty, and creation of employment.

However, it would be pretentious and illusory to think that the study on the effect of pyrolysis operating parameters on the byproduct yields can be considered as complete from the present study. Any other contribution aimed at improving and/or supplementing this present work was of paramount importance. For example:

- In this study, following the problems from TGA data, it was not possible to determine accurately the pyrolysis kinetics parameter for the conversion rate greater than 50%. It is recommended to carry out a new experiment with more precise and reliable equipment in order to complete the results obtained by interpolation in this study. Even a second attempt using another TGA apparatus also failed due to miscellaneous problems.
- The TGA-PKM method for the determination of the lignocellulosic composition of the biomass was shown to have limits for extractive-rich biomass and it had been

recommended to remove all extractive compounds before conducting the TGA experiment for more precision in the estimation of cellulose, hemicellulose, and lignin on dry ash and extractive free basis.

- The vapor residence time greatly affects the bio-oil yield from pyrolysis, and this RT depends mainly on the pyrolysis reactor and inert gas flow rate. In order to optimize this parameter, it was found that cost considerations must be taken into account since to reduce RT one must increase the inert gas flow rate and this involves additional operating cost. A detailed study in this direction is therefore strongly encouraged.
- For the sake of simplicity, the algorithm used in this study does not take into account heat transfer by convection and radiation in the porous media of the biomass particle, however, this assumption can only be applied if the particle size is less than 0.5mm. it is therefore difficult to assess the effect of the particle size on the pyrolysis process. This complexity can be overcome by using more robust algorithms contained in software such as OpenFOAM or ANSYS. This implies inserting the detailed biomass kinetics into the Multi-Phase Particle In Cell (MPPIC) solver designed for the Computational Particle Fluid Dynamics (CPFD).

In short, all the recommendations made can be taken as scope for further work toward accomplishing and improving the study presented in this dissertation. To this end, we encourage a complementary experimental study is highly encouraged.

REFERENCES

- [1] L. Fülöp and J. Ecker, “An overview of biomass conversion: exploring new opportunities,” *PeerJ*, vol. 8, p. e9586, Jul. 2020, doi: 10.7717/peerj.9586.
- [2] M. M. Parascanu, P. Sánchez, G. Soreanu, J. L. Valverde, and L. Sanchez-Silva, “Mexican biomasses valorization through pyrolysis process: Environmental and costs analysis,” *Waste Manag.*, vol. 95, pp. 171–181, Jul. 2019, doi: 10.1016/j.wasman.2019.06.007.
- [3] J. Lehto, A. Oasmaa, Y. Solantausta, M. Kytö, and D. Chiaramonti, “Review of fuel oil quality and combustion of fast pyrolysis bio-oils from lignocellulosic biomass,” *Appl. Energy*, vol. 116, pp. 178–190, Mar. 2014, doi: 10.1016/j.apenergy.2013.11.040.
- [4] T. Green, O. I. Miria, R. Crook, and A. Ross, “Energy Calculator for Solar Processing of Biomass with Application to Uganda,” *Energies*, vol. 13, no. 6, p. 1485, Mar. 2020, doi: 10.3390/en13061485.
- [5] Y. Zhang, Q. Jiang, W. Xie, Y. Wang, and J. Kang, “Effects of temperature, time and acidity of hydrothermal carbonization on the hydrochar properties and nitrogen recovery from corn stover,” *Biomass Bioenergy*, vol. 122, pp. 175–182, Mar. 2019, doi: 10.1016/j.biombioe.2019.01.035.
- [6] R. Slezak, L. Krzystek, and S. Ledakowicz, “Steam gasification of pyrolysis char from spent mushroom substrate,” *Biomass Bioenergy*, vol. 122, pp. 336–342, Mar. 2019, doi: 10.1016/j.biombioe.2019.02.007.
- [7] X. Hu and M. Gholizadeh, “Biomass pyrolysis: A review of the process development and challenges from initial researches up to the commercialisation stage,” *J. Energy Chem.*, vol. 39, pp. 109–143, Dec. 2019, doi: 10.1016/j.jechem.2019.01.024.
- [8] J. Akhtar and N. Saidina Amin, “A review on operating parameters for optimum liquid oil yield in biomass pyrolysis,” *Renew. Sustain. Energy Rev.*, vol. 16, no. 7, pp. 5101–5109, Sep. 2012, doi: 10.1016/j.rser.2012.05.033.
- [9] C. A. Mullen, A. A. Boateng, N. M. Goldberg, I. M. Lima, D. A. Laird, and K. B. Hicks, “Bio-oil and bio-char production from corn cobs and stover by fast pyrolysis,” *Biomass Bioenergy*, vol. 34, no. 1, pp. 67–74, Jan. 2010, doi: 10.1016/j.biombioe.2009.09.012.
- [10] S. Ismadji, Y.-H. Ju, C. X. Lin, A. Kurniawan, and O. L. Ki, “Bio-oil from Cassava Peel: Potential Renewable Energy Source,” p. 7, 2012.
- [11] J. L. F. Alves, J. C. G. da Silva, V. F. da Silva Filho, R. F. Alves, W. V. de Araujo Galdino, and R. F. De Sena, “Kinetics and thermodynamics parameters evaluation of pyrolysis of invasive aquatic macrophytes to determine their bioenergy potentials,” *Biomass Bioenergy*, vol. 121, pp. 28–40, Feb. 2019, doi: 10.1016/j.biombioe.2018.12.015.
- [12] A. H. Rony *et al.*, “Kinetics, thermodynamics, and physical characterization of corn stover (*Zea mays*) for solar biomass pyrolysis potential analysis,” *Bioresour. Technol.*, vol. 284, pp. 466–473, Jul. 2019, doi: 10.1016/j.biortech.2019.03.049.
- [13] L. P. R. Alyson, C. Glauber, E. P. S. Maria, and C. G. Wolia, “Application of cassava harvest residues (*Manihot esculenta* Crantz) in biochemical and thermochemical conversion process for bioenergy purposes: A literature review,” *Afr. J. Biotechnol.*, vol. 17, no. 3, pp. 37–50, Jan. 2018, doi: 10.5897/AJB2017.16322.
- [14] D. O. Olukanni and T. O. Olatunji, “Cassava Waste Management and Biogas Generation Potential in Selected Local Governments Areas in Ogun State Nigeria,” *ENGINEERING*, preprint, Sep. 2018. doi: 10.20944/preprints201809.0087.v1.
- [15] “21252030 Agenda for Sustainable Development web.pdf.” Accessed: Sep. 26, 2021. [Online]. Available: <https://sustainabledevelopment.un.org/content/documents/21252030%20Agenda%20for%20Sustainable%20Development%20web.pdf>
- [16] D. Mohan, C. U. Pittman, and P. H. Steele, “Pyrolysis of Wood/Biomass for Bio-oil: A Critical Review,” *Energy Fuels*, vol. 20, no. 3, pp. 848–889, May 2006, doi: 10.1021/ef0502397.
- [17] L. Zhang, R. Liu, R. Yin, and Y. Mei, “Upgrading of bio-oil from biomass fast pyrolysis in China: A review,” *Renew. Sustain. Energy Rev.*, vol. 24, pp. 66–72, Aug. 2013, doi: 10.1016/j.rser.2013.03.027.

- [18] S. Hameed, "A review on biomass pyrolysis models_ Kinetic, network and mechanistic models," *Biomass Bioenergy*, p. 19, 2019.
- [19] Nishu *et al.*, "A review on the catalytic pyrolysis of biomass for the bio-oil production with ZSM-5: Focus on structure," *Fuel Process. Technol.*, vol. 199, p. 106301, Mar. 2020, doi: 10.1016/j.fuproc.2019.106301.
- [20] A. Pattiya, S. Sukkasi, and V. Goodwin, "Fast pyrolysis of sugarcane and cassava residues in a free-fall reactor," *Energy*, vol. 44, no. 1, pp. 1067–1077, Aug. 2012, doi: 10.1016/j.energy.2012.04.035.
- [21] A. Pattiya, "Thermochemical Characterization of Agricultural Wastes from Thai Cassava Plantations," *Energy Sources Part Recovery Util. Environ. Eff.*, vol. 33, no. 8, pp. 691–701, Feb. 2011, doi: 10.1080/15567030903228922.
- [22] J. Zhang, "Thermal behaviors and kinetics for fast pyrolysis of chemical pretreated waste cassava residues," p. 11, 2020.
- [23] E. Ranzi, P. E. A. Debiagi, and A. Frassoldati, "Mathematical Modeling of Fast Biomass Pyrolysis and Bio-Oil Formation. Note I: Kinetic Mechanism of Biomass Pyrolysis," *ACS Sustain. Chem. Eng.*, vol. 5, no. 4, pp. 2867–2881, Apr. 2017, doi: 10.1021/acssuschemeng.6b03096.
- [24] E. Ranzi, P. E. A. Debiagi, and A. Frassoldati, "Mathematical Modeling of Fast Biomass Pyrolysis and Bio-Oil Formation. Note II: Secondary Gas-Phase Reactions and Bio-Oil Formation," *ACS Sustain. Chem. Eng.*, vol. 5, no. 4, pp. 2882–2896, Apr. 2017, doi: 10.1021/acssuschemeng.6b03098.
- [25] D. Díez, A. Urueña, R. Piñero, A. Barrio, and T. Tamminen, "Determination of Hemicellulose, Cellulose, and Lignin Content in Different Types of Biomasses by Thermogravimetric Analysis and Pseudocomponent Kinetic Model (TGA-PKM Method)," *Processes*, vol. 8, no. 9, p. 1048, Aug. 2020, doi: 10.3390/pr8091048.
- [26] L. J. R. Nunes, J. C. De Oliveira Matias, and J. P. Da Silva Catalão, "Physical Pretreatment of Biomass," in *Torrefaction of Biomass for Energy Applications*, Elsevier, 2018, pp. 45–88. doi: 10.1016/B978-0-12-809462-4.00002-X.
- [27] A. Chenu and G. D. Scholes, "Coherence in Energy Transfer and Photosynthesis," *Annu. Rev. Phys. Chem.*, vol. 66, no. 1, pp. 69–96, 2015, doi: 10.1146/annurev-physchem-040214-121713.
- [28] E. Ranzi, T. Faravelli, and F. Manenti, "Pyrolysis, Gasification, and Combustion of Solid Fuels," in *Advances in Chemical Engineering*, vol. 49, Elsevier, 2016, pp. 1–94. doi: 10.1016/bs.ache.2016.09.001.
- [29] L. J. R. Nunes, J. C. De Oliveira Matias, and J. P. Da Silva Catalão, "Introduction," in *Torrefaction of Biomass for Energy Applications*, Elsevier, 2018, pp. 1–43. doi: 10.1016/B978-0-12-809462-4.00001-8.
- [30] P. E. A. Debiagi *et al.*, "Extractives Extend the Applicability of Multistep Kinetic Scheme of Biomass Pyrolysis," *Energy Fuels*, vol. 29, no. 10, pp. 6544–6555, Oct. 2015, doi: 10.1021/acs.energyfuels.5b01753.
- [31] "Stabilization of biomass-derived pyrolysis oils - Venderbosch - 2010 - Journal of Chemical Technology & Biotechnology - Wiley Online Library." <https://onlinelibrary.wiley.com/doi/full/10.1002/jctb.2354> (accessed Nov. 07, 2021).
- [32] H. C. Ong, W.-H. Chen, Y. Singh, Y. Y. Gan, C.-Y. Chen, and P. L. Show, "A state-of-the-art review on thermochemical conversion of biomass for biofuel production: A TG-FTIR approach," *Energy Convers. Manag.*, vol. 209, p. 112634, Apr. 2020, doi: 10.1016/j.enconman.2020.112634.
- [33] M. Y. Guida and A. Hannioui, "A review on thermochemical treatment of biomass: Pyrolysis of olive mill wastes in comparison with other types of biomass," *Prog. Agric. Eng. Sci.*, vol. 12, no. 1, pp. 1–23, Dec. 2016, doi: 10.1556/446.12.2016.1.
- [34] "Synthesis of Transportation Fuels from Biomass: Chemistry, Catalysts, and Engineering | Chemical Reviews." <https://pubs.acs.org/doi/abs/10.1021/cr068360d> (accessed Nov. 07, 2021).
- [35] O. Marchenko, S. Solomin, A. Kozlov, V. Shamanskiy, and I. Donskoy, "Economic Efficiency Assessment of Using Wood Waste in Cogeneration Plants with Multi-Stage Gasification," *Appl. Sci.*, vol. 10, no. 21, p. 7600, Oct. 2020, doi: 10.3390/app10217600.
- [36] V. Dhyani and T. Bhaskar, "A comprehensive review on the pyrolysis of lignocellulosic biomass," *Renew. Energy*, vol. 129, pp. 695–716, 2018.

- [37] T. J. Morgan, S. Q. Turn, and A. George, "Fast Pyrolysis Behavior of Banagrass as a Function of Temperature and Volatiles Residence Time in a Fluidized Bed Reactor," *PLOS ONE*, vol. 10, no. 8, p. e0136511, Aug. 2015, doi: 10.1371/journal.pone.0136511.
- [38] M. A. Moneim, A. M. A. El Naggar, H. A. El Sayed, M. S. Mostafa, N. M. Khalil, and M. E. D. Hassan, "Direct conversion of an agricultural solid waste to hydrocarbon gases via the pyrolysis technique," *Egypt. J. Pet.*, vol. 27, no. 4, pp. 991–995, Dec. 2018, doi: 10.1016/j.ejpe.2018.03.008.
- [39] "Pyrolysis and biochar potential using crop residues and agricultural wastes in China - ScienceDirect." <https://www.sciencedirect.com/science/article/abs/pii/S1470160X14003070?via%3Dihub> (accessed Nov. 07, 2021).
- [40] C.-C. Kung, F. Kong, and Y. Choi, "Pyrolysis and biochar potential using crop residues and agricultural wastes in China," *Ecol. Indic.*, vol. 51, pp. 139–145, Apr. 2015, doi: 10.1016/j.ecolind.2014.06.043.
- [41] D. Nhuchhen, P. Basu, and B. Acharya, "A Comprehensive Review on Biomass Torrefaction," *Int. J. Renew. Energy Biofuels*, pp. 1–56, May 2014, doi: 10.5171/2014.506376.
- [42] D. Nhuchhen, P. Basu, and B. Acharya, "A Comprehensive Review on Biomass Torrefaction," *Int. J. Renew. Energy Biofuels*, pp. 1–56, May 2014, doi: 10.5171/2014.506376.
- [43] W.-H. Chen *et al.*, "Progress in biomass torrefaction: Principles, applications and challenges," *Prog. Energy Combust. Sci.*, vol. 82, p. 100887, Jan. 2021, doi: 10.1016/j.pecs.2020.100887.
- [44] J. A. Okolie, R. Rana, S. Nanda, A. K. Dalai, and J. A. Kozinski, "Supercritical water gasification of biomass: a state-of-the-art review of process parameters, reaction mechanisms and catalysis," *Sustain. Energy Fuels*, vol. 3, no. 3, pp. 578–598, 2019, doi: 10.1039/C8SE00565F.
- [45] J. E. White, W. J. Catallo, and B. L. Legendre, "Biomass pyrolysis kinetics: A comparative critical review with relevant agricultural residue case studies," *J. Anal. Appl. Pyrolysis*, vol. 91, no. 1, pp. 1–33, May 2011, doi: 10.1016/j.jaap.2011.01.004.
- [46] T. Kan, V. Strezov, and T. J. Evans, "Lignocellulosic biomass pyrolysis: A review of product properties and effects of pyrolysis parameters," *Renew. Sustain. Energy Rev.*, vol. 57, pp. 1126–1140, 2016.
- [47] A. V. Bridgwater, "Review of fast pyrolysis of biomass and product upgrading," *Biomass Bioenergy*, vol. 38, pp. 68–94, Mar. 2012, doi: 10.1016/j.biombioe.2011.01.048.
- [48] M. M. Wright, D. E. Daugaard, J. A. Satrio, and R. C. Brown, "Techno-economic analysis of biomass fast pyrolysis to transportation fuels," *Fuel*, vol. 89, pp. S2–S10, Nov. 2010, doi: 10.1016/j.fuel.2010.07.029.
- [49] S. Mutsengerere, C. H. Chihobo, D. Musademba, and I. Nhapi, "A review of operating parameters affecting bio-oil yield in microwave pyrolysis of lignocellulosic biomass," *Renew. Sustain. Energy Rev.*, vol. 104, pp. 328–336, Apr. 2019, doi: 10.1016/j.rser.2019.01.030.
- [50] A. M. Parvez, M. T. Afzal, P. Jiang, and T. Wu, "Microwave-assisted biomass pyrolysis polygeneration process using a scaled-up reactor: Product characterization, thermodynamic assessment and bio-hydrogen production," *Biomass Bioenergy*, vol. 139, p. 105651, Aug. 2020, doi: 10.1016/j.biombioe.2020.105651.
- [51] "Shakya: Pyrolysis of waste plastics to generate useful... - Google Scholar." https://scholar.google.com/scholar_lookup?title=Pyrolysis%20of%20waste%20plastics%20to%20generate%20useful%20fuel%20containing%20hydrogen%20using%20a%20solar%20thermochemical%20process&author=BD%20Shakya&publication_year=2007 (accessed Nov. 08, 2021).
- [52] M. C. Ndukwu, I. T. Horsfall, E. A. Ubouh, F. N. Orji, I. E. Ekop, and N. R. Ezejiofor, "Review of solar-biomass pyrolysis systems: Focus on the configuration of thermal-solar systems and reactor orientation," *J. King Saud Univ. - Eng. Sci.*, vol. 33, no. 6, pp. 413–423, Sep. 2021, doi: 10.1016/j.jksues.2020.05.004.
- [53] S. Papari and K. Hawboldt, "A review on the pyrolysis of woody biomass to bio-oil: Focus on kinetic models," *Renew. Sustain. Energy Rev.*, vol. 52, pp. 1580–1595, Dec. 2015, doi: 10.1016/j.rser.2015.07.191.
- [54] S. M. Gouws, M. Carrier, J. R. Bunt, and H. W. J. P. Neomagus, "Co-pyrolysis of coal and raw/torrefied biomass: A review on chemistry, kinetics and implementation," *Renew. Sustain. Energy Rev.*, vol. 135, p. 110189, Jan. 2021, doi: 10.1016/j.rser.2020.110189.

- [55] A. I. Osman, A. Abdelkader, C. Farrell, D. Rooney, and K. Morgan, "Reusing, recycling and up-cycling of biomass: A review of practical and kinetic modelling approaches," *Fuel Process. Technol.*, vol. 192, pp. 179–202, Sep. 2019, doi: 10.1016/j.fuproc.2019.04.026.
- [56] G. Wang *et al.*, "A review of recent advances in biomass pyrolysis," *Energy Fuels*, vol. 34, no. 12, pp. 15557–15578, 2020.
- [57] V. Dhyani and T. Bhaskar, "Kinetic Analysis of Biomass Pyrolysis," in *Waste Biorefinery*, Elsevier, 2018, pp. 39–83. doi: 10.1016/B978-0-444-63992-9.00002-1.
- [58] F. Thurner and U. Mann, "Kinetic investigation of wood pyrolysis," *Ind. Eng. Chem. Process Des. Dev.*, vol. 20, no. 3, pp. 482–488, Jul. 1981, doi: 10.1021/i200014a015.
- [59] D. S. Scott, J. Piskorz, and D. Radlein, "Liquid products from the continuous flash pyrolysis of biomass," *Ind. Eng. Chem. Process Des. Dev.*, vol. 24, no. 3, pp. 581–588, Jul. 1985, doi: 10.1021/i200030a011.
- [60] A. G. W. Bradbury, Y. Sakai, and F. Shafizadeh, "A kinetic model for pyrolysis of cellulose," *J. Appl. Polym. Sci.*, vol. 23, no. 11, pp. 3271–3280, 1979, doi: 10.1002/app.1979.070231112.
- [61] C. Di Blasi, "Modeling chemical and physical processes of wood and biomass pyrolysis," *Prog. Energy Combust. Sci.*, vol. 34, no. 1, pp. 47–90, Feb. 2008, doi: 10.1016/j.pecs.2006.12.001.
- [62] C. A. Koufopoulos, N. Papayannakos, G. Maschio, and A. Lucchesi, "Modelling of the pyrolysis of biomass particles. Studies on kinetics, thermal and heat transfer effects," *Can. J. Chem. Eng.*, vol. 69, no. 4, pp. 907–915, 1991, doi: 10.1002/cjce.5450690413.
- [63] E. Ranzi *et al.*, "Chemical Kinetics of Biomass Pyrolysis," *Energy Fuels*, vol. 22, no. 6, pp. 4292–4300, Nov. 2008, doi: 10.1021/ef800551t.
- [64] A. Cuoci *et al.*, "A General Mathematical Model of Biomass Devolatilization Note 2. Detailed kinetics of volatile species," p. 7.
- [65] R. Kumar and V. Strezov, "Thermochemical production of bio-oil: A review of downstream processing technologies for bio-oil upgrading, production of hydrogen and high value-added products," *Renew. Sustain. Energy Rev.*, vol. 135, p. 110152, Jan. 2021, doi: 10.1016/j.rser.2020.110152.
- [66] C. R. Ellison, R. Hoff, C. Mărculescu, and D. Boldor, "Investigation of microwave-assisted pyrolysis of biomass with char in a rectangular waveguide applicator with built-in phase-shifting," *Appl. Energy*, vol. 259, p. 114217, Feb. 2020, doi: 10.1016/j.apenergy.2019.114217.
- [67] A. R. Albis A., E. O. Munoz, I. P. Ariza, A. F. Suarez Escobar, and C. S. Ariza Barraza, "TG characterization of pyrolysis of cassava starch residues catalyzed by ferric sulfate," *Contemp. Eng. Sci.*, vol. 11, no. 72, pp. 3587–3597, 2018, doi: 10.12988/ces.2018.87365.
- [68] M. Rehan *et al.*, "Effect of zeolite catalysts on pyrolysis liquid oil," *Int. Biodeterior. Biodegrad.*, vol. 119, pp. 162–175, Apr. 2017, doi: 10.1016/j.ibiod.2016.11.015.
- [69] O. L. Ki, A. Kurniawan, C. X. Lin, Y.-H. Ju, and S. Ismadji, "Bio-oil from cassava peel: A potential renewable energy source," *Bioresour. Technol.*, vol. 145, pp. 157–161, Oct. 2013, doi: 10.1016/j.biortech.2013.01.122.
- [70] P. O. Okekunle, O. E. Itabiyi, S. O. Adetola, I. O. Alayande, H. O. Ogundiran, and K. G. Odeh, "BIOFUEL PRODUCTION BY PYROLYSIS OF CASSAVA PEEL IN A FIXED BED REACTOR," *Int. J. Energy Clean Environ.*, vol. 17, no. 1, pp. 57–65, 2016, doi: 10.1615/InterJenerCleanEnv.2017018176.
- [71] "Utilization of Cassava Peel Waste as A Raw Material for Activated Carbon Production : Approach to Environmental Protection in Nigeria," *Int. J. Eng. Res.*, vol. 3, no. 1, p. 8, 2014.
- [72] S. Suttibak, K. Sriprateep, and A. Pattiya, "Production of Bio-oil via Fast Pyrolysis of Cassava Rhizome in a Fluidised-Bed Reactor," *Energy Procedia*, vol. 14, pp. 668–673, 2012, doi: 10.1016/j.egypro.2011.12.993.
- [73] A. Pattiya, "Bio-oil production via fast pyrolysis of biomass residues from cassava plants in a fluidised-bed reactor," *Bioresour. Technol.*, vol. 102, no. 2, pp. 1959–1967, Jan. 2011, doi: 10.1016/j.biortech.2010.08.117.
- [74] A. Pattiya and S. Suttibak, "Production of bio-oil via fast pyrolysis of agricultural residues from cassava plantations in a fluidised-bed reactor with a hot vapour filtration unit," *J. Anal. Appl. Pyrolysis*, vol. 95, pp. 227–235, May 2012, doi: 10.1016/j.jaap.2012.02.010.
- [75] A. O. Ayeni, O. A. Adeeyo, O. M. Oresgun, and E. Oladimeji, "Compositional analysis of lignocellulosic materials : Evaluation of an economically viable method suitable for woody and

- non-woody biomass American Journal of Engineering Research (AJER),” *Am. J. Eng. Res.*, vol. 4, no. 4, pp. 14–19, 2015.
- [76] E. Galiwango, N. S. A. Rahman, A. H. Al-Marzouqi, M. M. Abu-Omar, and A. A. Khaleel, “Klason Method: An Effective Method for Isolation of Lignin Fractions from Date Palm Biomass Waste,” *Chem. Process Eng. Res.*, vol. 57, no. 0, pp. 46–58, 2018.
- [77] C. Vijayanand, S. Kamaraj, S. Karthikeyan, and S. Sriramajayam, “Characterization of Indigenous Biomass,” *Int. J. Agric. Sci.*, vol. 8, no. 50, pp. 2124–2127, 2016.
- [78] T. Oluwasola, A. Labunmi, L. Bodunde, and J. Owolabi, “PHYSICO-CHEMICAL COMPOSITION OF LIGNOCELLULOSE BIOMASS FROM *Gliricidia Sepium* AND *Cola Gigantea*,” *Am. J. Innov. Res. Appl. Sci.*, no. Mcc, pp. 131–140, 2018.
- [79] L. Burhenne, J. Messmer, T. Aicher, and M.-P. Laborie, “The effect of the biomass components lignin, cellulose and hemicellulose on TGA and fixed bed pyrolysis,” *J. Anal. Appl. Pyrolysis*, vol. 101, pp. 177–184, May 2013, doi: 10.1016/j.jaap.2013.01.012.
- [80] C. M. O’Brien, “Statistical Applications for Environmental Analysis and Risk Assessment by Joseph Ofungwu,” *Int. Stat. Rev.*, vol. 82, no. 3, pp. 487–488, 2014, doi: 10.1111/insr.12085_11.
- [81] J. Eliasson and V. Carlsson, *Agricultural waste and wood waste for pyrolysis and biochar: An assessment for Rwanda*. 2020. Accessed: Nov. 08, 2021. [Online]. Available: <http://urn.kb.se/resolve?urn=urn:nbn:se:kth:diva-283611>
- [82] T. Mulualem, N. Semman, G. Etana, and S. Alo, “Evaluation of Cassava (<i>Manihot esculenta</i> Crantz) Genotypes for Total Cyanide Content, Storage Tuber and Starch Yield in South Western Ethiopia,” *Int. J. Biomed. Mater. Res.*, vol. 8, no. 2, p. 14, 2020, doi: 10.11648/j.ijbmr.20200802.11.
- [83] S. Sivamani, A. P. Chandrasekaran, M. Balajii, M. Shanmugaparakash, A. Hosseini-Bandegharai, and R. Baskar, “Evaluation of the potential of cassava-based residues for biofuels production,” *Rev. Environ. Sci. Biotechnol.*, vol. 17, no. 3, pp. 553–570, Sep. 2018, doi: 10.1007/s11157-018-9475-0.
- [84] W.-H. Chen, C.-W. Wang, H. C. Ong, P. L. Show, and T.-H. Hsieh, “Torrefaction, pyrolysis and two-stage thermodegradation of hemicellulose, cellulose and lignin,” *Fuel*, vol. 258, p. 116168, Dec. 2019, doi: 10.1016/j.fuel.2019.116168.
- [85] J. Y. Yeo, B. L. F. Chin, J. K. Tan, and Y. S. Loh, “Comparative studies on the pyrolysis of cellulose, hemicellulose, and lignin based on combined kinetics,” *J. Energy Inst.*, vol. 92, no. 1, pp. 27–37, Feb. 2019, doi: 10.1016/j.joei.2017.12.003.
- [86] H. Yang, R. Yan, H. Chen, D. H. Lee, and C. Zheng, “Characteristics of hemicellulose, cellulose and lignin pyrolysis,” *Fuel*, vol. 86, no. 12–13, pp. 1781–1788, Aug. 2007, doi: 10.1016/j.fuel.2006.12.013.
- [87] H. Zhou, Y. Long, A. Meng, Q. Li, and Y. Zhang, “The pyrolysis simulation of five biomass species by hemicellulose, cellulose and lignin based on thermogravimetric curves,” *Thermochim. Acta*, vol. 566, pp. 36–43, Aug. 2013, doi: 10.1016/j.tca.2013.04.040.
- [88] A. Skreiberg, Ø. Skreiberg, J. Sandquist, and L. Sørum, “TGA and macro-TGA characterisation of biomass fuels and fuel mixtures,” *Fuel*, vol. 90, no. 6, pp. 2182–2197, Jun. 2011, doi: 10.1016/j.fuel.2011.02.012.
- [89] R. Korpinen, M. Kallioinen, J. Hemming, A. Pranovich, M. Mänttari, and S. Willför, “Comparative evaluation of various lignin determination methods on hemicellulose-rich fractions of spruce and birch obtained by pressurized hot-water extraction (PHWE) and subsequent ultrafiltration (UF),” *Holzforschung*, vol. 68, no. 8, pp. 971–979, Dec. 2014, doi: 10.1515/hf-2013-0233.
- [90] R. Kaur, P. Gera, M. K. Jha, and T. Bhaskar, “Pyrolysis kinetics and thermodynamic parameters of castor (*Ricinus communis*) residue using thermogravimetric analysis,” *Bioresour. Technol.*, vol. 250, pp. 422–428, Feb. 2018, doi: 10.1016/j.biortech.2017.11.077.

APPENDIX

Appendix A: TGA data (after smoothing and reduction)

Alpha	5K/min		15K/min		20K/min		30K/min	
	T	dadt	T	dadt	T	dadt	T	dadt
0.00	150.10	0.00376	149.27	0.00864	149.89	0.01201	150.61	0.01624
0.02	174.48	0.00406	190.00	0.00974	188.06	0.01245	190.67	0.01699
0.04	195.86	0.00468	220.63	0.01570	218.67	0.01665	222.79	0.02327
0.06	214.22	0.00564	241.41	0.02718	241.75	0.02467	246.91	0.03489
0.08	229.77	0.00680	250.64	0.03991	256.99	0.03635	263.14	0.05395
0.10	242.35	0.00891	257.87	0.04985	267.50	0.05395	273.65	0.08122
0.12	251.71	0.01207	264.00	0.05817	274.63	0.07492	280.74	0.10999
0.14	258.61	0.01589	269.38	0.06522	279.95	0.09511	286.24	0.13610
0.16	263.97	0.01987	274.26	0.07122	284.31	0.11326	290.85	0.15910
0.18	268.37	0.02347	278.78	0.07633	288.07	0.12923	294.88	0.17915
0.20	272.19	0.02651	283.02	0.08064	291.43	0.14307	298.52	0.19647
0.22	275.64	0.02895	287.06	0.08426	294.49	0.15490	301.87	0.21125
0.24	278.86	0.03084	290.95	0.08724	297.36	0.16486	305.02	0.22370
0.26	281.91	0.03221	294.71	0.08962	300.07	0.17303	308.01	0.23393
0.28	284.87	0.03307	298.39	0.09146	302.68	0.17950	310.89	0.24207
0.30	287.77	0.03344	302.00	0.09277	305.20	0.18432	313.68	0.24819
0.32	290.66	0.03330	305.58	0.09357	307.68	0.18755	316.41	0.25238
0.34	293.58	0.03267	309.12	0.09388	310.12	0.18922	319.10	0.25465
0.36	296.58	0.03155	312.67	0.09369	312.56	0.18932	321.78	0.25501
0.38	299.72	0.02997	316.23	0.09300	315.00	0.18788	324.46	0.25347
0.40	303.07	0.02796	319.82	0.09180	317.47	0.18489	327.16	0.25002
0.42	306.69	0.02557	323.47	0.09006	320.00	0.18033	329.90	0.24460
0.44	310.70	0.02289	327.19	0.08775	322.60	0.17420	332.71	0.23715
0.46	315.23	0.02006	331.01	0.08485	325.31	0.16645	335.61	0.22759
0.48	320.46	0.01717	334.97	0.08131	328.16	0.15705	338.64	0.21582
0.50	326.64	0.01430	339.12	0.07707	331.20	0.14599	341.85	0.20174
0.52	334.15	0.01154	343.50	0.07207	334.50	0.13324	345.29	0.18521
0.54	343.65	0.00901	348.20	0.06620	338.15	0.11882	349.06	0.16610
0.56	355.80	0.00711	353.35	0.05932	342.29	0.10285	353.30	0.14433
0.58	370.45	0.00610	359.16	0.05126	347.15	0.08567	358.23	0.11991
0.60	386.86	0.00563	366.03	0.04181	353.11	0.06803	364.27	0.09337
0.62	404.34	0.00543	374.95	0.03091	360.79	0.05130	372.32	0.06715
0.64	422.35	0.00530	388.21	0.02082	371.16	0.03725	383.60	0.04658
0.66	441.20	0.00500	405.97	0.01584	385.14	0.02764	398.40	0.03537
0.68	461.20	0.00461	424.65	0.01621	402.53	0.02317	415.61	0.03121
0.70	482.67	0.00427	441.07	0.01771	421.85	0.02249	434.01	0.02905
0.72	504.97	0.00410	455.80	0.01743	441.45	0.02306	453.56	0.02654
0.74	527.95	0.00407	470.24	0.01543	460.88	0.02260	474.26	0.02417
0.76	551.34	0.00406	485.86	0.01149	481.05	0.01995	495.59	0.02197

0.78	575.53	0.00392	503.70	0.00725	503.61	0.01574	517.80	0.01982
0.80	599.88	0.00385	523.37	0.00523	531.22	0.01245	541.95	0.01734
0.82	625.73	0.00363	546.84	0.00485	563.83	0.01060	568.93	0.01523
0.84	652.27	0.00382	580.18	0.00507	596.82	0.00982	596.50	0.01397
0.86	676.46	0.00438	620.60	0.00595	627.70	0.00988	623.82	0.01310
0.88	697.93	0.00452	658.36	0.00684	656.70	0.01059	652.06	0.01295
0.90	719.80	0.00412	688.76	0.00638	683.68	0.01042	680.90	0.01116
0.92	743.25	0.00396	715.53	0.00575	709.15	0.00973	708.54	0.00836
0.94	766.02	0.00436	741.10	0.00562	735.85	0.00854	735.68	0.00652
0.96	786.10	0.00496	766.84	0.00564	763.31	0.00729	763.19	0.00651
0.98	803.90	0.00552	792.57	0.00567	790.79	0.00650	790.72	0.00666
1.00	819.42	0.00606	818.26	0.00572	818.36	0.00608	818.30	0.00716

Appendix B: Detailed pyrolysis kinetics data

B.1. Species properties

	NAME	Formula	C	H	O	Molar Weight		NAME	Formula	C	H	O	Molar Weight
s	CELL	C6H10O5	6	10	5	162	1	ALD3	C3H6O	3	6	1	58
s	CELLA	C6H10O5	6	10	5	162	1	ANISOL	C6H5OCH3	7	8	1	108
s	HCE	C5H8O4	5	8	4	132	1	C2H5OH	C2H5OH	2	6	1	46
s	HCEA1	C5H8O4	5	8	4	132	1	C3H4O2	C3H4O2	3	4	2	72
s	HCA2	C5H8O4	4	8	4	120	1	CH2O	CH2O	1	2	1	30
s	LIG	C11H12O4	11	12	4	208	1	CH3OH	CH3OH	1	4	1	32
s	LIG-C	C15H14O4	15	14	4	258	1	COUMARYL	C9H10O2	9	10	2	150
s	LIG-H	C22H28O9	22	28	9	436	1	ETOH	C2H5OH	2	6	1	46
s	LIG-O	C20H22O10	20	22	10	422	1	FE2MACR	C11H12O4	11	12	4	208
s	LIG-CC	C15H14O4	15	14	4	258	1	FFA	C18H32O2	18	32	2	280
s	LIG-OH	C19H22O8	19	22	8	378	1	GLYOX	C2H2O2	2	2	2	58
s	TGL	C57H100O7	57	100	7	896	1	H2O	H2O	0	2	1	18
s	TANN	C15H12O7	15	12	7	304	1	HAA	C2H4O2	2	4	2	60
s	ITANN	C9H6O6	9	6	6	210	1	HCOOH	HCOOH	1	2	2	46
s	GCO2	CO2	1	0	2	44	1	HMFU	C6H6O3	6	6	3	126
s	GCO	CO1	1	0	1	28	1	LVG	C6H10O5	6	10	5	162
s	GCOH2	COH2	1	2	1	30	1	MECHO	CH3CHO	2	4	1	44
s	GH2	H2	0	2	0	2	1	PHENOL	C6H6O1	6	6	1	94
s	GCH4	CH4	1	4	0	16	1	XYL	C5H8O4	5	8	4	132
s	GCH3OH	CH3OH	1	4	1	32	g	H2	H3	0	2	0	2
s	GC2H4	C2H4	2	4	0	28	g	CO	CO	1	0	1	28
s	GCH2	CH3	1	3	0	15	g	CO2	CO2	1	0	2	44
s	CHAR	C	1	0	0	12	g	CH4	CH4	1	4	0	16
1	ACRO	C2H3CHO	3	4	1	56	g	C2H4	C2H4	2	4	0	28

Appendix C: Matlab Codes

C.1. TGA data smoothing and reduction

```

%% Initialization
R=8.314/1000;
t05=xlsread('TGA','800K','B5:B6639
');
t15=xlsread('TGA','800K','I5:I2976
');
t20=xlsread('TGA','800K','P5:P2010
');
t30=xlsread('TGA','800K','W5:W1692
');

T05=xlsread('TGA','800K','C5:C6639
');
T15=xlsread('TGA','800K','J5:J2976
');
T20=xlsread('TGA','800K','Q5:Q2010
');
T30=xlsread('TGA','800K','X5:X1692
');

m05=xlsread('TGA','800K','E5:E6639
');
m15=xlsread('TGA','800K','L5:L2976
');
m20=xlsread('TGA','800K','S5:S2010
');
m30=xlsread('TGA','800K','Z5:Z1692
');

Beta=[5 15 20 30];

plot(T05,m05,'r',T15,m15,'k',T20,m
20,'b',T30,m30,'g')
xlabel('Temperature (°C)')
ylabel('Weight loss (mg)')
legend('5K/min','15K/min','20K/min
','30K/min')
grid on

figure
plot(t05,T05,'r',t15,T15,'k',t20,T
20,'b',t30,T30,'g')
legend('5K/min','15K/min','20K/min
','30K/min')
xlabel('Time (min)')
ylabel('Temperature (°C)')
grid on
%% Smoothing

t1=smooth(t05,0.1,'loess');
t2=smooth(t15,0.2,'loess');
t3=smooth(t20,0.1,'loess');
t4=smooth(t30,0.1,'loess');

T1=smooth(T05,0.1,'loess');
T2=smooth(T15,0.2,'loess');

```

```

T3=smooth(T20,0.1,'loess');
T4=smooth(T30,0.1,'loess');

m1=smooth(m05,0.1,'loess');
m2=smooth(m15,0.2,'loess');
m3=smooth(m20,0.1,'loess');
m4=smooth(m30,0.1,'loess');

figure
plot(T1,m1,'r',T2,m2,'k',T3,m3,'b'
,T4,m4,'g')
legend('5K/min','15K/min','20K/min
','30K/min')
xlabel('Temperature (°C)')
ylabel('Weight loss (mg)')
grid on
figure
plot(t05,T05,'r',t15,T15,'k',t20,T
20,'b',t30,T30,'g')
legend('5K/min','15K/min','20K/min
','30K/min')
xlabel('Time (min)')
ylabel('Temperature (°C)')
grid on
%% Data filtering

n11=numel(T1);
n21=numel(T2);
n31=numel(T3);
n41=numel(T4);

T1(T1<150)=[];
T2(T2<150)=[];
T3(T3<150)=[];
T4(T4<150)=[];

n12=numel(T1);
n22=numel(T2);
n32=numel(T3);
n42=numel(T4);

n1=n11-n12+1;
n2=n21-n22+1;
n3=n31-n32+1;
n4=n41-n42+1;

t1=t1(n1:n11);
t2=t2(n2:n21);
t3=t3(n3:n31);
t4=t4(n4:n41);

m1=m1(n1:n11);
m2=m2(n2:n21);
m3=m3(n3:n31);
m4=m4(n4:n41);

figure
plot(T1,m1,'r',T2,m2,'k',T3,m3,'b'
,T4,m4,'g')

```

```

legend('5K/min','15K/min','20K/min',
', '30K/min')
xlabel('Temperature (°C)')
ylabel('Weight loss (mg)')
grid on

figure
plot(t05,T05,'r',t15,T15,'k',t20,T
20,'b',t30,T30,'g')
legend('5K/min','15K/min','20K/min',
', '30K/min')
xlabel('Time (min)')
ylabel('Temperature (°C)')
grid on
%% calculatation of alpha, and dadT

a1=(max(m1)-m1)/(max(m1)-min(m1));
a2=(max(m2)-m2)/(max(m2)-min(m2));
a3=(max(m3)-m3)/(max(m3)-min(m3));
a4=(max(m4)-m4)/(max(m4)-min(m4));

for i=1:length(T1)
    if i==1
        dadT1(i,1)=(a1(i)-
a1(i+1))/(T1(i)-T1(i+1));
    else
        dadT1(i,1)=(a1(i)-a1(i-
1))/(T1(i)-T1(i-1));
    end
end
for i=1:length(T2)
    if i==1
        dadT2(i,1)=(a2(i)-
a2(i+1))/(T2(i)-T2(i+1));
    else
        dadT2(i,1)=(a2(i)-a2(i-
1))/(T2(i)-T2(i-1));
    end
end
for i=1:length(T3)
    if i==1
        dadT3(i,1)=(a3(i)-
a3(i+1))/(T3(i)-T3(i+1));
    else
        dadT3(i,1)=(a3(i)-a3(i-
1))/(T3(i)-T3(i-1));
    end
end
for i=1:length(T4)
    if i==1
        dadT4(i,1)=(a4(i)-
a4(i+1))/(T4(i)-T4(i+1));
    else
        dadT4(i,1)=(a4(i)-a4(i-
1))/(T4(i)-T4(i-1));
    end
end
end
figure

```

```

plot(T1,a1,'b',T2,a2,'k',T3,a3,'r',
,T4,a4,'g')
legend('5K/min','15K/min','20K/min',
', '30K/min')
xlabel('Temperature (°C)')
ylabel('degree of conversion
(\alpha, wt.%)')
grid on
figure
plot(T1,dadT1,'b',T2,dadT2,'k',T3,
dadT3,'r',T4,dadT4,'g')
legend('5K/min','15K/min','20K/min',
', '30K/min')
xlabel('Temperature (°C)')
ylabel('DTG (wt.%/K)')
grid on

%% dadt
for i=1:length(T1)
    if i==1
        dadt1(i,1)=(a1(i)-
a1(i+1))/(t1(i)-t1(i+1));
    else
        dadt1(i,1)=(a1(i)-a1(i-
1))/(t1(i)-t1(i-1));
    end
end
for i=1:length(T2)
    if i==1
        dadt2(i,1)=(a2(i)-
a2(i+1))/(t2(i)-t2(i+1));
    else
        dadt2(i,1)=(a2(i)-a2(i-
1))/(t2(i)-t2(i-1));
    end
end
for i=1:length(T3)
    if i==1
        dadt3(i,1)=(a3(i)-
a3(i+1))/(t3(i)-t3(i+1));
    else
        dadt3(i,1)=(a3(i)-a3(i-
1))/(t3(i)-t3(i-1));
    end
end
for i=1:length(T4)
    if i==1
        dadt4(i,1)=(a4(i)-
a4(i+1))/(t4(i)-t4(i+1));
    else
        dadt4(i,1)=(a4(i)-a4(i-
1))/(t4(i)-t4(i-1));
    end
end
end
figure
plot(T1,dadt1,'b',T2,dadt2,'k',T3,
dadT3,'r',T4,dadt4,'g')
legend('5K/min','15K/min','20K/min',
', '30K/min')
xlabel('Temperature (°C)')

```

```

ylabel('DTG (wt.%/min)')
grid on
%% Weight loss X and dXdt
X1=1-((max(m1)-m1)/(max(m1)-min(m1)));
X2=1-((max(m2)-m2)/(max(m2)-min(m2)));
X3=1-((max(m3)-m3)/(max(m3)-min(m3)));
X4=1-((max(m4)-m4)/(max(m4)-min(m4)));

for i=1:length(T1)
    if i==1
        dadt1(i,1)=(X1(i)-X1(i+1))/(t1(i)-t1(i+1));
    else
        dadt1(i,1)=(X1(i)-X1(i-1))/(t1(i)-t1(i-1));
    end
end
for i=1:length(T2)
    if i==1
        dadt2(i,1)=(X2(i)-X2(i+1))/(t2(i)-t2(i+1));
    else
        dadt2(i,1)=(X2(i)-X2(i-1))/(t2(i)-t2(i-1));
    end
end
for i=1:length(T3)
    if i==1
        dadt3(i,1)=(X3(i)-X3(i+1))/(t3(i)-t3(i+1));
    else
        dadt3(i,1)=(X3(i)-X3(i-1))/(t3(i)-t3(i-1));
    end
end
for i=1:length(T4)
    if i==1
        dadt4(i,1)=(X4(i)-X4(i+1))/(t4(i)-t4(i+1));
    else
        dadt4(i,1)=(X4(i)-X4(i-1))/(t4(i)-t4(i-1));
    end
end

figure
plot(T1,X1,'b',T2,X2,'k',T3,X3,'r',T4,X4,'g')
legend('5K/min','15K/min','20K/min','30K/min')
xlabel('Temperature (°C)')
ylabel('Weight-loss (X, wt.%)')
grid on
figure
plot(T1,dadt1,'b',T2,dadt2,'k',T3,dadt3,'r',T4,dadt4,'g')

```

```

legend('5K/min','15K/min','20K/min','30K/min')
xlabel('Temperature (°C)')
ylabel('DTG (wt.%/min)')
grid on

%% Reduction of data

j=0;
for ai=0:0.02:1
    j=j+1;
    Ai(j,1)=ai;
    t01(j,1)=interp1(a1,t1,ai);
    t02(j,1)=interp1(a2,t2,ai);
    t03(j,1)=interp1(a3,t3,ai);
    t04(j,1)=interp1(a4,t4,ai);

    T01(j,1)=interp1(a1,T1,ai);
    T02(j,1)=interp1(a2,T2,ai);
    T03(j,1)=interp1(a3,T3,ai);
    T04(j,1)=interp1(a4,T4,ai);

    dadt01(j,1)=interp1(a1,dadt1,ai);
    dadt02(j,1)=interp1(a2,dadt2,ai);
    dadt03(j,1)=interp1(a3,dadt3,ai);
    dadt04(j,1)=interp1(a4,dadt4,ai);
end

figure
plot(T01,Ai,'b',T02,Ai,'k',T03,Ai,'r',T04,Ai,'g')
legend('5K/min','15K/min','20K/min','30K/min')
grid on
figure
plot(T01,dadt01,'b',T02,dadt02,'k',T03,dadt03,'r',T04,dadt04,'g')
legend('5K/min','15K/min','20K/min','30K/min')
grid on

%% Smoothing 2

t01=smooth(t01,0.1,'loess');
t02=smooth(t02,0.1,'loess');
t03=smooth(t03,0.1,'loess');
t04=smooth(t04,0.1,'loess');

T01=smooth(T01,0.1,'loess');
T02=smooth(T02,0.1,'loess');
T03=smooth(T03,0.1,'loess');
T04=smooth(T04,0.1,'loess');

dadt01=smooth(dadt01,0.1,'loess');
dadt02=smooth(dadt02,0.1,'loess');
dadt03=smooth(dadt03,0.1,'loess');

```

```

dadt04=smooth(dadt04,0.1,'loess');

figure
plot(T01,Ai,'b',T02,Ai,'k',T03,Ai,
'r',T04,Ai,'g')
legend('5K/min','15K/min','20K/min',
',','30K/min')
grid on
figure
plot(T01,dadt01,'b',T02,dadt02,'k',
T03,dadt03,'r',T04,dadt04,'g')
legend('5K/min','15K/min','20K/min',
',','30K/min')
grid on

```

C.2.TGA-PKM method code

```

%% Initialization
R=8.314/1000;
t05=xlsread('TGA','800K','B5:B6639');
t15=xlsread('TGA','800K','I5:I2976');
t20=xlsread('TGA','800K','P5:P2010');
t30=xlsread('TGA','800K','W5:W1692');

T05=xlsread('TGA','800K','C5:C6639');
T15=xlsread('TGA','800K','J5:J2976');
T20=xlsread('TGA','800K','Q5:Q2010');
T30=xlsread('TGA','800K','X5:X1692');

m05=xlsread('TGA','800K','E5:E6639');
m15=xlsread('TGA','800K','L5:L2976');
m20=xlsread('TGA','800K','S5:S2010');
m30=xlsread('TGA','800K','Z5:Z1692');

Beta=[5 15 20 30];

%
plot(T05,m05,'r',T15,m15,'k',T20,m
20,'b',T30,m30,'g')
% xlabel('Temperature (°C)')
% ylabel('Weight loss (mg)')
%
legend('5K/min','15K/min','20K/min',
',','30K/min')
% grid on
%
% figure

```

```

%
plot(t05,T05,'r',t15,T15,'k',t20,T
20,'b',t30,T30,'g')
%
legend('5K/min','15K/min','20K/min',
',','30K/min')
% xlabel('Time (min)')
% ylabel('Temperature (°C)')
% grid on
%% Smoothing

```

```

t1=smooth(t05,0.1,'loess');
t2=smooth(t15,0.2,'loess');
t3=smooth(t20,0.1,'loess');
t4=smooth(t30,0.1,'loess');

```

```

T1=smooth(T05,0.1,'loess');
T2=smooth(T15,0.2,'loess');
T3=smooth(T20,0.1,'loess');
T4=smooth(T30,0.1,'loess');

```

```

m1=smooth(m05,0.1,'loess');
m2=smooth(m15,0.2,'loess');
m3=smooth(m20,0.1,'loess');
m4=smooth(m30,0.1,'loess');

```

```

n11=numel(T1);
n21=numel(T2);
n31=numel(T3);
n41=numel(T4);

```

```

T1(T1<150)=[];
T2(T2<150)=[];
T3(T3<150)=[];
T4(T4<150)=[];

```

```

n12=numel(T1);
n22=numel(T2);
n32=numel(T3);
n42=numel(T4);

```

```

n1=n11-n12+1;
n2=n21-n22+1;
n3=n31-n32+1;
n4=n41-n42+1;

```

```

t1=t1(n1:n11);
t2=t2(n2:n21);
t3=t3(n3:n31);
t4=t4(n4:n41);

```

```

m1=m1(n1:n11);
m2=m2(n2:n21);
m3=m3(n3:n31);
m4=m4(n4:n41);

```

```

%% calculation of X, and dXdT
and dXdt

```



```

X1=1-((max(m1)-m1)/(max(m1)-min(m1)));
X2=1-((max(m2)-m2)/(max(m2)-min(m2)));
X3=1-((max(m3)-m3)/(max(m3)-min(m3)));
X4=1-((max(m4)-m4)/(max(m4)-min(m4)));

for i=1:length(T1)
    if i==1
        dadT1(i,1)=(X1(i)-X1(i+1))/(T1(i)-T1(i+1));
    else
        dadT1(i,1)=(X1(i)-X1(i-1))/(T1(i)-T1(i-1));
    end
end
for i=1:length(T2)
    if i==1
        dadT2(i,1)=(X2(i)-X2(i+1))/(T2(i)-T2(i+1));
    else
        dadT2(i,1)=(X2(i)-X2(i-1))/(T2(i)-T2(i-1));
    end
end
for i=1:length(T3)
    if i==1
        dadT3(i,1)=(X3(i)-X3(i+1))/(T3(i)-T3(i+1));
    else
        dadT3(i,1)=(X3(i)-X3(i-1))/(T3(i)-T3(i-1));
    end
end
for i=1:length(T4)
    if i==1
        dadT4(i,1)=(X4(i)-X4(i+1))/(T4(i)-T4(i+1));
    else
        dadT4(i,1)=(X4(i)-X4(i-1))/(T4(i)-T4(i-1));
    end
end

for i=1:length(T1)
    if i==1
        dadt1(i,1)=(X1(i)-X1(i+1))/(t1(i)-t1(i+1));
    else
        dadt1(i,1)=(X1(i)-X1(i-1))/(t1(i)-t1(i-1));
    end
end
for i=1:length(T2)
    if i==1
        dadt2(i,1)=(X2(i)-X2(i+1))/(t2(i)-t2(i+1));
    else
        dadt2(i,1)=(X2(i)-X2(i-1))/(t2(i)-t2(i-1));
    end
end
for i=1:length(T3)
    if i==1
        dadt3(i,1)=(X3(i)-X3(i+1))/(t3(i)-t3(i+1));
    else
        dadt3(i,1)=(X3(i)-X3(i-1))/(t3(i)-t3(i-1));
    end
end
for i=1:length(T4)
    if i==1
        dadt4(i,1)=(X4(i)-X4(i+1))/(t4(i)-t4(i+1));
    else
        dadt4(i,1)=(X4(i)-X4(i-1))/(t4(i)-t4(i-1));
    end
end

%% Reduction of data
j=0;
for ai=0:0.005:1
    j=j+1;
    X(j,1)=ai;
    T01(j,1)=interp1(X1,T1,ai);
    T02(j,1)=interp1(X2,T2,ai);
    T03(j,1)=interp1(X3,T3,ai);
    T04(j,1)=interp1(X4,T4,ai);

    dXdT01(j,1)=interp1(X1,dadT1,ai);
    dXdT02(j,1)=interp1(X2,dadT2,ai);
    dXdT03(j,1)=interp1(X3,dadT3,ai);
    dXdT04(j,1)=interp1(X4,dadT4,ai);

    t01(j,1)=interp1(X1,t1,ai);
    t02(j,1)=interp1(X2,t2,ai);
    t03(j,1)=interp1(X3,t3,ai);
    t04(j,1)=interp1(X4,t4,ai);

    dXdt01(j,1)=interp1(X1,dadt1,ai);
    dXdt02(j,1)=interp1(X2,dadt2,ai);
    dXdt03(j,1)=interp1(X3,dadt3,ai);
    dXdt04(j,1)=interp1(X4,dadt4,ai);
end

%% Smoothing 2
T01=smooth(T01,0.1,'loess');

```

```

T02=smooth(T02,0.1,'loess');
T03=smooth(T03,0.1,'loess');
T04=smooth(T04,0.1,'loess');

dXdT01=smooth(dXdT01,0.1,'loess');
dXdT02=smooth(dXdT02,0.1,'loess');
dXdT03=smooth(dXdT03,0.1,'loess');
dXdT04=smooth(dXdT04,0.1,'loess');

t01=smooth(t01,0.1,'loess');
t02=smooth(t02,0.1,'loess');
t03=smooth(t03,0.1,'loess');
t04=smooth(t04,0.1,'loess');

dXdt01=smooth(dXdt01,0.1,'loess');
dXdt02=smooth(dXdt02,0.1,'loess');
dXdt03=smooth(dXdt03,0.1,'loess');
dXdt04=smooth(dXdt04,0.1,'loess');

figure
plot(T1,X1,'b',T2,X2,'k',T3,X3,'r',
,T4,X4,'g')
legend('5K/min','15K/min','20K/min',
,'30K/min')
xlabel('Temperature (°C)')
ylabel('Weight-loss (X, wt.%)')
grid on

figure
plot(T1,dadT1,'b',T2,dadT2,'k',T3,
dadT3,'r',T4,dadT4,'g')
legend('5K/min','15K/min','20K/min',
,'30K/min')
xlabel('Temperature (°C)')
ylabel('DTG (wt.%/K)')
grid on

figure
plot(T1,dadt1,'b',T2,dadt2,'k',T3,
dadT3,'r',T4,dadt4,'g')
legend('5K/min','15K/min','20K/min',
,'30K/min')
xlabel('Temperature (°C)')
ylabel('DTG (wt.%/min)')
grid on
%% Algorithme
%% Initialisation of K E X
R=8.314e-3;
K=xlsread('TGA','KEX','C5:I5');
E=xlsread('TGA','KEX','C6:I6');
XFo=xlsread('TGA','KEX','C7:I7');
TK=273.+T03;
T=T03;
t=t03;
beta=Beta(3);
dXdT=dXdT03;
dXdte=dXdT03;

%% Solve ODE

```

```

for j=1:length(K)
    e=-E(j)/R;
    i=0;
    for i=1:length(TK)
        A(i,j)=TK(i).*exp(e./TK(i));
        S=0;
        n=0;
        tol=1;
        h=0.1;
        x0=-e/TK(i);
        x=x0;
        nmax=1e+10;
        while tol>1e-8 && n<nmax
            y=x+h;
            B=exp(e./y)./y;
            b=exp(e./x)./x;
            I=(B+b)*(h/2);
            So=S+I;
            tol=abs(So-S);
            S=So;
            x=x+h;
            n=n+1;
            if n<1000
                tol=1;
            end
        end
        C(i,j)=I;
    end
end
D=A-C;
XX=zeros(length(TK),length(K));
XF=zeros(length(TK),length(K));
i=0;
j=0;
for j=1:length(K)
    i=0;
    Ko=-K(j)/beta;
    XX(:,j)=Ko.*D(:,j);
    TT(:,j)=T;
    for i=1:length(TK)
        XF(i,j)=XFo(j).*exp(XX(i,j));
    end
end
S=0;
i=0;
j=0;
for i=1:length(TK)
    S=0;
    j=0;
    for j=1:length(K)
        S=S+XF(i,j);
    end
    Xm(i)=S;
end
%TT=[T T T T T T T]; %!!!!!!!!!!!!!!
figure
plot(T,Xm,'*')
grid on
hold on

```

```

plot (T,X)

%% dxdtmodel
i=0;
j=0;
for j=1:length(K)
    i=0;
    for i=1:length(TK)
        Z(i,j)=i;
        if i==length(TK)
            dXdTm(i,j)=(XF(i,j)-
XF(i-1,j))/(TK(i)-TK(i-1));
        else
            dXdTm(i,j)=(XF(i,j)-
XF(i+1,j))/(TK(i)-TK(i+1));
        end
    end
end
i=0;
j=0;
for j=1:length(K)
    i=0;
    for i=1:length(TK)
        Z(i,j)=i;
        if i==length(TK)
            dXdTm(i,j)=(XF(i,j)-
XF(i-1,j))/(t(i)-t(i-1));
        else
            dXdTm(i,j)=(XF(i,j)-
XF(i+1,j))/(t(i)-t(i+1));
        end
    end
end
end
% dXdTm=beta.*dXdTm;
figure
plot(TT,dXdTm)
grid on
hold on
S=0;
i=0;
j=0;
for i=1:length(TK)
    S=0;
    j=0;
    for j=1:length(K)
        S=S+dXdTm(i,j);
    end
    dXdTmt(i,1)=S;
end
plot (T,dXdTmt,'k')
plot (T,dXdte,'b*')
%% Non linear curve-fitting by
least squares (lsqcurvefit)
lb=xlsread('TGA','KEX','C9:I11');
ub=xlsread('TGA','KEX','C13:I15');
Cff0=[K; E; XF0];
xdata=TK;
ydata=dXdte;
nn=1;
toll=1;
%%

```

```

while toll>1e-4 && nn<3

[Cff,resnorm,residual,exitflag,out
put] =lsqcurvefit(@fun,
Cff0,xdata,ydata,lb,ub);
    toll=resnorm;
    %CC(nn)=Cff;
    Cff0=Cff;
    nn=nn+1;
end
v=fun(Cff,xdata);
vv=fun1(Cff,xdata);
figure
plot (T,vv)
grid on
hold on
plot(T,v,'k',T,dXdte,'b*')
xlabel('Temperature (°C)')
ylabel('DTG (wt.%/min)')
legend('pseudocomponent
1','pseudocomponent
2','pseudocomponent
3','pseudocomponent
4','pseudocomponent
5','pseudocomponent
6','pseudocomponent
7','Model','Experimental')

%% OF, QOF anf R^2
OF=0;
QOF=0;
SST=0;
for i=1:length(v)
    s1=((dXdte(i))-(v(i)))^2;
    s2=((((dXdte(i))-
(v(i)))^2)/(length(v)))^0.5)/(abs(
min(dXdte)));
    sst=((dXdte(i))-
(mean(dXdte)))^2;
    OF=OF+s1;
    QOF=QOF+(100*s2);
    SST=SST+sst;
    SSE=OF;
end
n=length(dXdte);
R2=1-(((n-1)*SSE)/((n-
(21+1))*SST));

C.3. Kinetic parameters by  
Isoconversional method

Note here that the output from this code is
transferred in excel for final processing

%% Initialization
R=8.314/1000;

```

```

t05=xlsread('TGA','800K','B5:B6639
');
t15=xlsread('TGA','800K','I5:I2976
');
t20=xlsread('TGA','800K','P5:P2010
');
t30=xlsread('TGA','800K','W5:W1692
');

T05=xlsread('TGA','800K','C5:C6639
');
T15=xlsread('TGA','800K','J5:J2976
');
T20=xlsread('TGA','800K','Q5:Q2010
');
T30=xlsread('TGA','800K','X5:X1692
');

m05=xlsread('TGA','800K','E5:E6639
');
m15=xlsread('TGA','800K','L5:L2976
');
m20=xlsread('TGA','800K','S5:S2010
');
m30=xlsread('TGA','800K','Z5:Z1692
');

Beta=[5 15 20 30];

plot(T05,m05,'r',T15,m15,'k',T20,m
20,'b',T30,m30,'g')
xlabel('Temperature (°C)')
ylabel('Weight loss (mg)')
legend('5K/min','15K/min','20K/min
','30K/min')
grid on

figure
plot(t05,T05,'r',t15,T15,'k',t20,T
20,'b',t30,T30,'g')
legend('5K/min','15K/min','20K/min
','30K/min')
xlabel('Time (min)')
ylabel('Temperature (°C)')
grid on
%% Smoothing

t1=smooth(t05,0.1,'loess');
t2=smooth(t15,0.2,'loess');
t3=smooth(t20,0.1,'loess');
t4=smooth(t30,0.1,'loess');

T1=smooth(T05,0.1,'loess');
T2=smooth(T15,0.2,'loess');
T3=smooth(T20,0.1,'loess');
T4=smooth(T30,0.1,'loess');

m1=smooth(m05,0.1,'loess');
m2=smooth(m15,0.2,'loess');
m3=smooth(m20,0.1,'loess');

m4=smooth(m30,0.1,'loess');

figure
plot(T1,m1,'r',T2,m2,'k',T3,m3,'b'
,T4,m4,'g')
legend('5K/min','15K/min','20K/min
','30K/min')
xlabel('Temperature (°C)')
ylabel('Weight loss (mg)')
grid on

figure
n11=numel(T1);
n21=numel(T2);
n31=numel(T3);
n41=numel(T4);

T1(T1<150)=[];
T2(T2<150)=[];
T3(T3<150)=[];
T4(T4<150)=[];

n12=numel(T1);
n22=numel(T2);
n32=numel(T3);
n42=numel(T4);

n1=n11-n12+1;
n2=n21-n22+1;
n3=n31-n32+1;
n4=n41-n42+1;

t1=t1(n1:n11);
t2=t2(n2:n21);
t3=t3(n3:n31);
t4=t4(n4:n41);

m1=m1(n1:n11);
m2=m2(n2:n21);
m3=m3(n3:n31);
m4=m4(n4:n41);

figure
plot(T1,m1,'r',T2,m2,'k',T3,m3,'b'
,T4,m4,'g')
legend('5K/min','15K/min','20K/min
','30K/min')
xlabel('Temperature (°C)')
ylabel('Weight loss (mg)')
grid on

figure

```

```

plot(t05,T05,'r',t15,T15,'k',t20,T
20,'b',t30,T30,'g')
legend('5K/min','15K/min','20K/min
','30K/min')
xlabel('Time (min)')
ylabel('Temperature (°C)')
grid on
%% calculatlon of alpha, and dadT

a1=(max(m1)-m1)/(max(m1)-min(m1));
a2=(max(m2)-m2)/(max(m2)-min(m2));
a3=(max(m3)-m3)/(max(m3)-min(m3));
a4=(max(m4)-m4)/(max(m4)-min(m4));

for i=1:length(T1)
    if i==1
        dadT1(i,1)=(a1(i)-
a1(i+1))/(T1(i)-T1(i+1));
    else
        dadT1(i,1)=(a1(i)-a1(i-
1))/(T1(i)-T1(i-1));
    end
end
for i=1:length(T2)
    if i==1
        dadT2(i,1)=(a2(i)-
a2(i+1))/(T2(i)-T2(i+1));
    else
        dadT2(i,1)=(a2(i)-a2(i-
1))/(T2(i)-T2(i-1));
    end
end
for i=1:length(T3)
    if i==1
        dadT3(i,1)=(a3(i)-
a3(i+1))/(T3(i)-T3(i+1));
    else
        dadT3(i,1)=(a3(i)-a3(i-
1))/(T3(i)-T3(i-1));
    end
end
for i=1:length(T4)
    if i==1
        dadT4(i,1)=(a4(i)-
a4(i+1))/(T4(i)-T4(i+1));
    else
        dadT4(i,1)=(a4(i)-a4(i-
1))/(T4(i)-T4(i-1));
    end
end

figure
plot(T1,a1,'b',T2,a2,'k',T3,a3,'r'
,T4,a4,'g')
legend('5K/min','15K/min','20K/min
','30K/min')
xlabel('Temperature (°C)')
ylabel('Degree of conversion(%)')
grid on
figure

```

```

plot(T1,dadT1,'b',T2,dadT2,'k',T3,
dadT3,'r',T4,dadT4,'g')
legend('5K/min','15K/min','20K/min
','30K/min')
xlabel('Temperature (°C)')
ylabel('DTG (wt.%/K)')
grid on

%% dadt
for i=1:length(T1)
    if i==1
        dadt1(i,1)=(a1(i)-
a1(i+1))/(t1(i)-t1(i+1));
    else
        dadt1(i,1)=(a1(i)-a1(i-
1))/(t1(i)-t1(i-1));
    end
end
for i=1:length(T2)
    if i==1
        dadt2(i,1)=(a2(i)-
a2(i+1))/(t2(i)-t2(i+1));
    else
        dadt2(i,1)=(a2(i)-a2(i-
1))/(t2(i)-t2(i-1));
    end
end
for i=1:length(T3)
    if i==1
        dadt3(i,1)=(a3(i)-
a3(i+1))/(t3(i)-t3(i+1));
    else
        dadt3(i,1)=(a3(i)-a3(i-
1))/(t3(i)-t3(i-1));
    end
end
for i=1:length(T4)
    if i==1
        dadt4(i,1)=(a4(i)-
a4(i+1))/(t4(i)-t4(i+1));
    else
        dadt4(i,1)=(a4(i)-a4(i-
1))/(t4(i)-t4(i-1));
    end
end

figure
plot(T1,dadt1,'b',T2,dadt2,'k',T3,
dadt3,'r',T4,dadt4,'g')
legend('5K/min','15K/min','20K/min
','30K/min')
xlabel('Temperature (°C)')
ylabel('DTG (wt.%/min)')
grid on
%% Weight loss X and dXdT
X1=1-((max(m1)-m1)/(max(m1)-
min(m1)));
X2=1-((max(m2)-m2)/(max(m2)-
min(m2)));
X3=1-((max(m3)-m3)/(max(m3)-
min(m3)));

```

```

X4=1-((max(m4)-m4)/(max(m4)-
min(m4)));

for i=1:length(T1)
    if i==1
        dXdt1(i,1)=(X1(i)-
X1(i+1))/(t1(i)-t1(i+1));
    else
        dXdt1(i,1)=(X1(i)-X1(i-
1))/(t1(i)-t1(i-1));
    end
end
for i=1:length(T2)
    if i==1
        dXdt2(i,1)=(X2(i)-
X2(i+1))/(t2(i)-t2(i+1));
    else
        dXdt2(i,1)=(X2(i)-X2(i-
1))/(t2(i)-t2(i-1));
    end
end
for i=1:length(T3)
    if i==1
        dXdt3(i,1)=(X3(i)-
X3(i+1))/(t3(i)-t3(i+1));
    else
        dXdt3(i,1)=(X3(i)-X3(i-
1))/(t3(i)-t3(i-1));
    end
end
for i=1:length(T4)
    if i==1
        dXdt4(i,1)=(X4(i)-
X4(i+1))/(t4(i)-t4(i+1));
    else
        dXdt4(i,1)=(X4(i)-X4(i-
1))/(t4(i)-t4(i-1));
    end
end

figure
plot(T1,X1,'b',T2,X2,'k',T3,X3,'r',
T4,X4,'g')
legend('5K/min','15K/min','20K/min',
'30K/min')
xlabel('Temperature (°C)')
ylabel('Weight-loss (%kg/kg)')
grid on
figure
plot(T1,dXdt1,'b',T2,dXdt2,'k',T3,
dXdt3,'r',T4,dXdt4,'g')
legend('5K/min','15K/min','20K/min',
'30K/min')
xlabel('Temperature (°C)')
ylabel('DTG (wt.%/min)')
grid on

%% Reduction of data

j=0;
for ai=0:0.02:1
    j=j+1;
    xi=1-ai;
    Xi(j,1)=xi;
    Ai(j,1)=ai;
    t01(j,1)=interp1(a1,t1,ai);
    t02(j,1)=interp1(a2,t2,ai);
    t03(j,1)=interp1(a3,t3,ai);
    t04(j,1)=interp1(a4,t4,ai);

    T01(j,1)=interp1(a1,T1,ai);
    T02(j,1)=interp1(a2,T2,ai);
    T03(j,1)=interp1(a3,T3,ai);
    T04(j,1)=interp1(a4,T4,ai);

    dadt01(j,1)=interp1(a1,dadt1,ai);
    dadt02(j,1)=interp1(a2,dadt2,ai);
    dadt03(j,1)=interp1(a3,dadt3,ai);
    dadt04(j,1)=interp1(a4,dadt4,ai);

    dXdt01(j,1)=interp1(X1,dXdt1,xi);
    dXdt02(j,1)=interp1(X2,dXdt2,xi);
    dXdt03(j,1)=interp1(X3,dXdt3,xi);
    dXdt04(j,1)=interp1(X4,dXdt4,xi);
end

figure
plot(T01,Ai,'b',T02,Ai,'k',T03,Ai,
'r',T04,Ai,'g')
legend('5K/min','15K/min','20K/min',
'30K/min')
xlabel('Temperature (°C)')
ylabel('Degree of conversion(%)')
grid on
figure
plot(T01,dadt01,'b',T02,dadt02,'k',
T03,dadt03,'r',T04,dadt04,'g')
legend('5K/min','15K/min','20K/min',
'30K/min')
xlabel('Temperature (°C)')
ylabel('DTG (wt.%/min)')
grid on

figure
plot(T01,Xi,'b',T02,Xi,'k',T03,Xi,
'r',T04,Xi,'g')
legend('5K/min','15K/min','20K/min',
'30K/min')
xlabel('Temperature (°C)')
ylabel('Weight-loss (wt.%)')
grid on

```

```

figure
plot(T01,dXdt01,'b',T02,dXdt02,'k'
,T03,dXdt03,'r',T04,dXdt04,'g')
legend('5K/min','15K/min','20K/min'
,'30K/min')
xlabel('Temperature (°C)')
ylabel('DTG (wt.%/min)')
grid on

%% Smoothing 2

t01=smooth(t01,0.1,'loess');
t02=smooth(t02,0.1,'loess');
t03=smooth(t03,0.1,'loess');
t04=smooth(t04,0.1,'loess');

T01=smooth(T01,0.1,'loess');
T02=smooth(T02,0.1,'loess');
T03=smooth(T03,0.1,'loess');
T04=smooth(T04,0.1,'loess');

dadt01=smooth(dadt01,0.1,'loess');
dadt02=smooth(dadt02,0.1,'loess');
dadt03=smooth(dadt03,0.1,'loess');
dadt04=smooth(dadt04,0.1,'loess');

dXdt01=smooth(dXdt01,0.1,'loess');
dXdt02=smooth(dXdt02,0.1,'loess');
dXdt03=smooth(dXdt03,0.1,'loess');
dXdt04=smooth(dXdt04,0.1,'loess');

figure
plot(T01,Ai,'b',T02,Ai,'k',T03,Ai,
'r',T04,Ai,'g')
legend('5K/min','15K/min','20K/min'
,'30K/min')
grid on
figure
plot(T01,dadt01,'b',T02,dadt02,'k'
,T03,dadt03,'r',T04,dadt04,'g')
legend('5K/min','15K/min','20K/min'
,'30K/min')
grid on

figure
plot(T01,xi,'b',T02,xi,'k',T03,xi,
'r',T04,xi,'g')
legend('5K/min','15K/min','20K/min'
,'30K/min')
grid on
figure
plot(T01,dXdt01,'b',T02,dXdt02,'k'
,T03,dXdt03,'r',T04,dXdt04,'g')
legend('5K/min','15K/min','20K/min'
,'30K/min')
grid on

%% Activation Energy determination
FWO
T=[T01,T02,T03,T04];

```

```

for a=1:1:51
%a=1:1:length(Ai)
for b=1:1:4
X(b)=(-1)/(T(a,b));
Y(b)=log(Beta(b));

end
fitcst=polyfit(X,Y,1);
M=fitcst(1);
E(a)=-M*(R/1.0516);
end
figure
plot(T01,E);
grid on
figure
plot(Ai,E)
grid on

%% Friedman methode (more
acurate)

T=[T01,T02,T03,T04];
DaDt=[dadt01,dadt02,dadt03,dadt04]
;

for a=1:1:length(Ai)
for b=1:1:4
X(a,b)=1/T(a,b);
Y(a,b)=log(DaDt(a,b));
end
fitcst=polyfit(X,Y,1);
M=fitcst(1);
Efm(a)=-M*R/1;
end

figure
plot(T01,Efm);
grid on

figure
plot(Ai,Efm)
grid on

```

C.4. Heat Transfer in the particle

```

%% Constant parameters
ro=650;
TI=25+273;
TF=800+273;
nu=0.226;
g=9.81;
R=287;
R0=(0.5e-3)/2;
dr=1e-5;
dt=1e-4;

```

```

Beta=100/60;
dT=Beta*dt;
tf=(TF-TI)/Beta;

nt=(tf/dt)+1;

nr=(R0/dr)+1;

%% Initialization
A=zeros(nr-2 ,nr-2);
Tn=zeros(nr-2, 1);
Tn(1:nr-2, 1)=TI;
T=zeros(nr-2,1);
T(1:nr-2, 1)=TI;

%% Maint loop
i=1;
for t=0:dt:tf
    %Initialisation
    Tsys=TI+(t*Beta); %%
    h=2000; %5.69+(0.0098*Tsys);
    % Discretization parameters +
    Matrix coeff
    for j=1:nr-2
        k=0.13+(0.0003*(T(j)-
273));
        Cp=1112+(4.85*(T(j)-273));
        D=(Cp*ro)/k;
        r=dr*j;
        a=dt/(D*(dr^2));
        b=(2*dt)/(r*dr*D);
        c=(h*dr)/k;
        if j==1
            AE=a;
            AW=0;
            AP=1-a;
            A(j,1:2)=[AP AE];
        elseif j==nr-2
            AE=0;
            AW=a-b;
            AP=(1-
(2*a)+b)+((a)/(1+c));
            A(j,j-1:j)=[AW AP];
        else
            AE=a;
            AW=a-b;
            AP=1-(AE+AW);
            A(j,j-1:j+1)=[AW AP
AE];
        end
    end
end

%%Solution of the system of
equations
for n=1:nr-2
    if n==1
        T(n)=(A(n,:) *Tn);
    elseif n==nr-2

```

```

T(n)=(A(n,:) *Tn)+(Tsys*((a*c)/(1+c
)));
        else
            T(n)=(A(n,:) *Tn);
        end
    end
    Tn=T;
    pt=rem(t,5);
    if pt==0
        tt(i)=t;
        TO(i)=Tn(1);
        Ti(:,i)=Tn;

    Ts(i)=((c*Tsys)/(1+c))+((Tn(nr-
2))/(1+c));
        TSYS(i)=Tsys;
        i=i+1;
    end
end

TB=[TO; Ti; Ts];
XX=[TB;TSYS];
AAA=XX(26,:);
BBB=XX(1,:);
CCC=AAA-BBB;
plot(AAA,CCC)
xlabel('Temperature [K]')
ylabel('Temperature Gradient [K]')
grid on

RR=linspace(0,0.25,26);

figure
surf(tt,RR,TB)
xlabel('time in [sec]')
ylabel('radius [mm]')
zlabel('Temperature [K]')

figure
contour(tt,RR,TB)
xlabel('time [sec]')
ylabel('radius [mm]')

C.5. Byproduct yield prediction

Note here that the output from this code is
transferred in excel for final processing

%% initialization

R=8.314;
neq=27;
ns=48;
k=xlsread('Data kinetics','Kin
data','M56:AM58');
Y=xlsread('Data kinetics','Kin
data','M5:AM52');

```



```

X(:,1)=xlsread('Data
kinetics','Kin data','AT5:AT52');
xi(1,:)=xlsread('Data
kinetics','Kin data','M2:AM2');

dT=0.1;
beta=100/60;
dt=dT/beta;
t=0;

Ts=425;

T1=25+273;

Lr=1;
Dr=0.0077;
Dn2=0.02;
Vr=(3.14/4)*(Dr^2)*Lr;
Vn2=7;
Sn2=(3.14/4)*(Dn2^2);
Qn2=Vn2*Sn2;
rt=Vr/Qn2;
Q=(0.6e-3/60);
RT=Vr/Q;

%% Main loop

Tsys=Ts+273;
Tc(1)=25;
j=1;
tr=0;
XR=1;
T=T1;
while XR>0.0001 && t<300
    T=T+dt;
    if T>=Tsys
        T=Tsys;
        tr=tr+dt;
    end
    t=t+dt;
    Tc(j+1)=T-273;

    for x=1:neq

K(j,x)=k(1,x)*(T^k(3,x))*exp((-
k(2,x)/(R*T));
    end

    %Wi=sum (Yi*Ki*xi)
    for y=1:ns
        W(y,j)=0;
        w=0;
        for x=1:neq

w=Y(y,x)*K(j,x)*xi(j,x);
            W(y,j)=W(y,j)+w;
        end
    end
end

for z=1:ns
    xip(z,j)=W(z,j)*dt;
    X(z,j+1)=X(z,j)+xip(z,j);
    if X(z,j)<0
        X(z,j)=0;
        X(z,j+1)=0;
    end
end

for i=1:neq
    if i>=18
        xi(j+1,i)=X(i-6,j);
    elseif (15<=i)&&(i<=17)
        xi(j+1,i)=X(6,j);
    elseif (6<=i)&&(i<=8)
        xi(j+1,i)=X(4,j);
    elseif (10<=i)&&(i<=14)
        xi(j+1,i)=X(i-3,j);
    elseif i==1 || i==4
        xi(j+1,i)=X(1,j);
    elseif i==2 || i==3
        xi(j+1,i)=X(2,j);
    elseif i==5
        xi(j+1,i)=X(3,j);
    elseif i==9
        xi(j+1,i)=X(5,j);
    end
end
% Residual biomass
i=0;
XR=0;
for i=1:13
    XR=XR+X(i,j);
end

j=j+1;
end

```

Appendix D : Thermochemical properties of Cassava Rhizome and Cassava Stalk (source Pattiya et al. 2011 [21])

Analysis	Cassava stalk		Cassava rhizome	
	This work	Literature ^a	This work	Literature ^b
<i>Proximate (wt%, dry basis)</i>				
Volatile matter	79.90%	89.47%	77.75%	81.13%
Fixed carbon	14.09%	6.89%	18.20%	10.39%
Ash	6.01%	3.63%	4.05%	8.49%
Moisture	15.54%	12.21%	8.31%	10.94%
<i>Ultimate (wt%, dry-ash free basis)</i>				
Carbon	51.12%	46.56%	51.59%	No data
Hydrogen	6.87%	8.16%	6.69%	
Nitrogen	0.67%	0.39%	1.27%	
Oxygen	41.34%	44.73%	40.45%	
Sulphur	<0.1	0.17%	<0.1	
<i>Molecular formula</i>	CH _{1.6} O _{0.61}	CH _{2.09} O _{0.72}	CH _{1.54} O _{0.59}	—
<i>Inorganic matter (ppbw, dry biomass basis)</i>				
K	977.39	No data	368.96	No data
Ca	950.92		391.23	
P	559.97		217.08	
Mg	276.68		291.60	
Na	7.82		9.32	
Cl	130.52		51.84	
Cu	0.23		0.20	
<i>Structural analysis (wt%, extractives-free basis)</i>				
Cellulose	35.71%	No data	31.19%	No data
Hemicellulose	41.75%		44.47%	
Lignin	22.54%		24.34%	
Extractives	13.21%		10.80%	
<i>Heating values (MJ kg⁻¹, dry basis)</i>				
Bomb calorimetry	17.58	17.56	23.67	20.10
Calculated HHV	19.49	19.63	19.93	—
Calculated LHV	17.99	17.85	18.47	—